ANALYSIS OF TITANIUM DIOXIDE NANOPARTICLES IN FOODS USING RAMAN SPECTROSCOPIC TECHNIQUES

ANALYSIS OF TITANIUM DIOXIDE NANOPARTICLES IN FOODS USING RAMAN SPECTROSCOPIC TECHNIQUES

A Dissertation Presented

by

JANAM K. PANDYA

Submitted to the Graduate School of the

University of Massachusetts Amherst in partial fulfillment

Of the requirements for the degree of

DOCTOR OF PHILOSOPHY

SEPTEMBER 2020

The Department of Food Science

ANALYSIS OF TITANIUM DIOXIDE NANOPARTICLES IN FOODS USING RAMAN SPECTROSCOPIC TECHNIQUES

A Dissertation Presented

By

JANAM K. PANDYA

Approved as to style and content by:

_____

Lili He, Chair

_____

David J. McClements, Member

_____

Michael Barnes, Member

_____

Eric A. Decker, Department Head

Department of Food Science

DEDICATION

This dissertation is dedicated to my beloved parents Kandarp and Jayshree Pandya for their unconditional love, support, and direction throughout my Ph.D. journey as well as for believing in all my endeavors!

ACKNOWLEDGEMENTS

I would first like to present my deepest gratitude to my Ph.D. advisor, Dr. Lili He. I have been so lucky to have come across many good mentors, advisors, and amazing people in my life so far but Dr. He has been the best I could have ever asked for. I would like to thank her for believing in me and providing me an opportunity to join her lab group. The constant advice that she has provided in the last three and a half years of my Ph.D. journey has made me a better researcher every single day. Dr. He always values and priorities her student's career development opportunities and her tailored approach of supporting and developing students based on their career interest in industry or academia has provided significant direction to my career. I am very grateful to her for allowing me to pursue six months long internship at Nestle as soon as I joined her lab. Moreover, Dr. He has been so patient, optimistic always available, exceptionally responsive, and has always had an optimistic approach toward many hurdles I came across my research. This research has challenged me at so many times, but her support and guidance have always resolved my problems and brought a smile after every meeting with her. She also inspires me constantly to be smart, time efficient and on top of communication, extremely important traits in managing complex and multiple projects. I consider myself so fortunate for the chance to pursue my Ph.D. under her guidance. Additionally, I would also like to thank Dr. McClements and Dr. Barnes for serving on my dissertation committee and providing valuable insights.

Secondly, I would like to recognize my fellow lab members for their continued support and valuable contributions. Without their help, I would not have overcome many research hurdles. The encouraging ideas, perspective and discussion on my research project was extremely valuable. I want to thank Tianxi Yang, Zhiyun Zhang, Brooke Pearson, Bin

Zhao, Michael Hickey, Alex mills, Xinyi Du, Yanqi Qu, Siyue Gao, Joshua Gukowsky, Qin Tu, Haochen Dai, Helen Lin, Lourdes Martinez, Noopur Bapardekar, Yu Ho, Xiaoyan Tan, Jason Yang, Caiping Jiang, Qin Tu and Shengnan Zhan for their direct and indirect contribution to the success of my research. I especially want to thank Zhiyun Zhang and Haochen Dai for their help in high-resolution SEM and TEM images. I had a real privilege to know them and made some of my best friends in the last three and a half years.

Last but not least I want to thank my parents, Kandarp and Jayshree Pandya, and my brother Visaj Pandya for their unconditional support in every possible way in the last six years of my graduate student career. My parents have always believed in whatever steps I have taken in my career and have extended their positive support at every stage. They have always motivated me in difficult times to keep pursuing my dreams. They are the backbone of my life and the purpose of everything that I do and want to do. Without my family, I absolutely would not have reached to this point my career. I also want to thank my landlord and closest friends, Sue and Mitch, with whom I have stayed and shared the last two years of my life. I want to thank them for being excited about every accomplishment I made, listening, and supporting me through tough times especially during Covid-19 and always wishing good for me. They have often stepped into my parents' role while I am away from my parents. I also want to thank my friend Jon Zhang for his support during quarantine times. His friendship has really help ed and supported me during the most challenging time of last one year of my life. At last I want to thank all my friends, extended family and mentors that contributed directly and indirectly to the success of my career. None of this would have been possible without any of them.

ABSTRACT

ANALYSIS OF TITANIUM DIOXIDE NANOPARTICLES IN FOODS USING RAMAN SPECTROSCOPIC TECHNIQUES

SEPTEMBER 2020

JANAM PANDYA, B.E., GUJARAT TECHNOLOGICAL UNIVERSITY

M.S., UNIVERSITY OF MASSACHUSETTS AMHERST

Ph.D., UNIVERSITY OF MASSACHUSETTS AMHERST

Directed by: Dr. Lili He

Titanium dioxide (TiO_2) and its nanoparticles (NPs) are widely used in various applications. Recently, the presence of TiO_2 NPs in food and consumer products raised safety concerns to human health and the environment. Analysis of TiO_2 NPs using traditional techniques such as electron microscopy and dynamic light scattering (DLS) is challenging and time-consuming. The goal of this project is to explore the capability of Raman Spectroscopy in the analysis of TiO_2-NPs and apply this technique for the analysis of TiO_2-NPs in food and environmental samples. Two approaches, i.e. the ligand-based and the mapping-based, were evaluated.

The ligand-based approach utilized the surface enhanced Raman scattering (SERS) property of the TiO_2 NPs as a substrate to enhance the signal of a surface bound ligand, gallocyanin (GLN). This SERS property is only specific to NPs of TiO_2, thus based on the R-value obtained from the ratio of TiO_2 to GLN peak intensities, we hypothesize the R-value can be used to differentiate the NPs from their counterparts. To test this hypothesis, we evaluated various factors, including the size and concentration of the nanoparticles, ligand concentration and experimental parameters such as sample incubation technique to

the R-value. The result shows the size of TiO_2 is the primary factor that determined the R-value. TiO_2 ranges from 65-8 nm had a similar R-value ranged from 2.4 to 3.4 with no statistical difference, however, the R was found significantly higher for 93 nm and 173 nm samples. This result demonstrates the potential of R as a rapid screening method to determine the presence of NPs in TiO_2. Besides size, the results showed the significant impact of particle and ligand concentration on R. On the other hand, pH and ultrasonication did not have any impact. One limitation of this approach is when there was a stronger ligand such as sodium pyrophosphate (SPP) added to disperse the particles, SPP occupies the surface of particles and prevented the interaction of TiO_2 with GLN.

Taking advantage of uniform and stable dispersion using SPP, we evaluated the second approach that is based on Raman mapping in combination with filtration to analyze TiO_2-NPs. We evaluated Raman intensity and map coverage (%) of four different sizes of TiO_2 (173, 93, 41 and 5 nm). The result shows that the 100× magnification was the most capable of detecting the smaller size particles down to 5 nm and as low as 0.0004 g/L. The mapping data revealed the capability of this approach to analyze the size of particles depending on the concentration. At relative higher concentration (e.g. 0.04 g/L), there is a linear correlation between the particle size, its hydrodynamic diameter and % map area covered by the particles. In addition, we observed a linear relationship between the Raman intensities and their particle size, which can be used in distinguishing the particles. At lower concentrations (e.g. 0.0004 g/L), no statistical difference was found in the Raman intensities of particles within nano-rage, although, the larger particles showed significantly higher intensity values.

Both SERS and Raman mapping methods were evaluated to determine the mean particle size and the amount of NPs from commercial E171 and food samples. We evaluated three E171 samples purchased from Amazon.com and three food samples: powdered non-dairy coffee creamer, powdered donuts and chewing gum. The preliminary SEM analysis revealed that one of the E171 samples obtained was rutile polymorph which was marketed as food-grade TiO_2, whereas the chewing gum contained the highest, 69% nanosized particles. Using R obtained from SERS analysis we were able to predict the mean particle size of chewing gum samples, however, due to the lack of R-values from standards between 65 to 200 nm, the SERS approach was not successfully able to estimate the mean particle size of the samples that contained a higher percentage of particles in that range. Consequently, using the correlation established between the map area and Raman intensity with the particle size, we were able to successfully estimate the particle size of TiO_2 particles from both E171 and food samples. We then estimated the amount of NPs from the map area obtained by applying the Raman intensity threshold for the cut-off intensity of 93 nm particles. In all, we developed the novel, rapid, sensitive and economical method to analyze the TiO_2-NPs and successfully demonstrated its application in commercial E171 as well as food samples.

TABLE OF CONTENT

LIST OF TABLES

LIST OF FIGURES

.

CHAPTER 1

INTRODUCTION

1.1. Background

Nanotechnology has grown immensely in last few decades, opening up new and innovative opportunities and bringing solutions to many challenges in various fields. With the advancement in the technology, nanomaterials are synthesized and engineered to achieve unique such as size, surface characteristics, physicochemical properties and functionalities that make them valuable in numerous applications[1]. However, with its increasing applications, many studies report harmful effects of various engineered nanomaterials on the ecosystems and human health[2-5,46]. Titanium Dioxide (TiO_2) is one of the most popular and widely produced engineered nanomaterial (ENP) with a global production of more than 3000 tons per year[6]. TiO_2 is natural sources and assembles in three polymorphs, from which, Anatase and Rutile are most widely used. Titanium Dioxide nanoparticles (TiO_2-NPs) are extensively used as a white pigment in plastic, paper, rubber, paint, toothpaste, sunscreen, pharmaceuticals, food and cosmetics[7]. TiO_2 accounts for two-third of all the pigments produced globally and values about $13 billion[8].

In food, anatase form of TiO_2 is permitted as food additive E171 and considered Generally Recognized as Safe (GRAS). It is used as a white pigment, foods like plant-based milk, coffee creamers, candies, chewing gum, frosting, pudding etc. In addition, it is also used as a flavor enhancer and bulking agent in foods such as beer, wine, mustard, soup, nuts, etc.[9]. The characterization of E171 shows that 36% of the total particles within nano-range[9]. Despite its use in various products, in the last two decades, many studies

demonstrated the potential toxicity of TiO_2 on human health and environment[10-19]. In addition, a toxicology analysis of different structures of TiO_2-NPs reported 100 times more toxicity of anatase than rutile form[20]. Initial research primarily reported the toxicology of TiO_2-NPs with regards to its uptake by inhalation and based on data available then the Internal Agency for Research on Cancer (IARC) concluded that the studies showed sufficient evidence of carcinogenicity in animals and therefore, classifying it as Group 2B carcinogen[21]. However, French food safety agency (ANSES) found toxicological effects of the oral injection of TiO_2-NPs in the recent studies conducted by the organization, banning the selling the food products containing TiO_2 in France, starting January 2020. Although the United States Food and Drug Administration (US FDA) and European Food Safety Agency (EFSA) reports, E171 safe for human consumption, both of these organizations continue to re-evaluate the toxicology of E171 based on new research and evidences[22]. Apart from this, the fate of TiO_2-NPs in environment is concerning as well. Studies have reported elevated levels of TiO_2-NPs in environment water and its impact on ecosystem[23-25].

Although the safety of TiO_2-NPs in foods still remains controversial, concerns amongst food industry and consumers are rising. Owing to its abundance in nature, unique properties and compatibility with most food products, finding a replacement of TiO_2 is extremely difficult. Besides, toxicological effect of the particles depends on many parameters, but most importantly size and concentration therefore, quantification and size characterization is very important. Currently available technologies for size characterization and quantification of TiO_2-NPs are Inductive Couple Plasma (ICP) techniques electron microscopy techniques, Dynamic Light Scattering (DLS) and Flow-

Field Fractionation (FFF). All of these techniques have one or more major disadvantages. The ICP techniques require complex sample preparation and involve hazardous chemicals such as strong inorganic acids. The capital investment and overall cost of analysis of ICP technologies are significantly higher. Similarly, electron microscopic techniques provide high-resolution images which can be analyzed to determine the size and morphology of the particles, but high operational cost, requirement of skilled analysts, complex sample preparation and analysis time limit their use to research laboratories and organizations. DLS is the most commonly used rapid measurement technique, that is inexpensive and requires no sample preparation, but it shows poor accuracy in multimodal particle size distribution as the scattering intensity of the small particles is often masked by the larger particles[26,27]. Aggregation in aqueous solution is a characteristic of TiO_2-NPs and the size characterization using both DLS and FFF requires uniform particle dispersion for the accurate measurement. Additionally, most of these methods are not capable of distinguishing the type of TiO_2 such as anatase, rutile and brookite, which is important as all these forms have different toxicological effects and mechanisms of action. Consequently, there is a potential opportunity for an economically reliable, accurate and rapid screening method that can simultaneously quantify, detect the particle size and identify the type of the TiO_2-NPs.

Raman spectroscopy and Surface-Enhanced Raman Spectroscopy (SERS) is a powerful technique that shown great sensitivity towards nanosized materials. In preliminary research presented by Zhao et al. showed the potential of SERS in simultaneous identification, quantification and size characterization of TiO_2-NPs[28]. However, further research is required to characterize the particles in the nano-range.

Additionally, the physicochemical properties of the particles can be altered by many external factors and understanding the effects of these factors on SERS analysis is necessary for the accurate size characterization of TiO_2-NPs, which is the primary focus of this study. The present study also investigates the implementation of SERS method for detection of NPs in real-time samples such as from lake surface water.

1.2. Objectives

The ***overall objective*** of this study was to evaluate the potential of Raman scattering techniques in the analysis of TiO_2-NPs. The specific objectives of the studies were designed to understand the influence of factors influencing the SERS analysis, evaluating the Raman mapping technique and application of the technology in real time analysis.

Objective 1: Evaluate the factors affecting the SERS analysis of TiO_2-NPs

As demonstrated by Zhao at el., the size of TiO_2-NP_S can be differentiated from larger particles by its SERS effect on the legends bound with it. However, many experimental factors including particle size, particle and legend concentration, dispersion techniques such as pH, ultrasonication and dispersing agents can influence the analysis. Herein, we assess these factors and their impact in the analysis of TiO_2-NPs in terms of the ratio value R of Raman intensity of TiO_2 particles to the SERS intensity of the ligand.

Objective 2: Evaluate the potential of filter-based Raman mapping technique for the analysis of TiO_2-NPs

Raman imaging instrument and its capability of collecting a map consisting of thousands of spectra can be utilized in developing a filter-membrane based technique in the analysis of TiO_2-NPs. The membrane filtration technique allows larger sample quantity which can

further reduce the limit of detection of the analysis making it suitable for environmental analysis. The sensitivity of TiO_2 structure towards Raman scattering can be used to develop ligand-free analysis technique.

Objective 3: Application of Raman mapping technique in the detection of TiO_2-NPs from food and environment samples

Herein, we will evaluate the practical application of the Raman mapping method by evaluating its potential in analyzing TiO_2 anatase NPs from food and rutile NPs from lake water samples.

CHAPTER 2

LITERATURE REVIEW

2.1. Nanoparticles

2.1.1. Nanomaterials and Nanoparticles: Definition and Classification

2.1.1.1. Definition

The nano prefix is derived from the Greek word for dwarf. In general, nanomaterials (NMs) are defined to have at least one dimension in the range of 1 and 10 nanometers (nm). However, different organizations and agencies have difference in opinion in defining NMs[29]. Globally, the International Organization for Standardization (ISO) defines NMs as "material with any external dimensions in the nanoscale or having internal structure or surface structure in the nanoscale"[30]. In the United States, Food and Drug Administration (FDA) has not established regulatory definition of "nanotechnology" "nanomaterials" or "nanoscale" but considers the definition the term that is defined by National Nanotechnology Initiative Program NMs as "materials that have at least one dimension in the range of 1 and 100 nm and exhibit the dimension dependent phenomena"[31]. However, the Environmental Protection Agency (EPA) provides different definitions of NMs and nanoparticles (NPs). According to EPA, "NMs are the diverse class of substances that have structural components smaller than 100 nm in at least one dimension. NMs include NPs, which are particles with at least two dimensions between approximately 1 and 100 nm"[32]. In Europe, the EU states that "a manufactured or natural material that possesses unbound, aggregated or agglomerated particles where external dimensions are between 1–100 nm size range"[33]. Whereas, the British Standards Institution

broadly defines as NMs as “materials with any internal or external structures on the nanoscale dimensions” but specifically describes NPs as “Nano-object with three external nanoscale dimensions.”[34]. Overall, Nanomaterials is a broad terminology with the materials in the nano-range, but nanoparticles are more defined unpolymerized nano-structures and can be considered as a subset of NMs.

2.1.1.2. Classification

Nanomaterials and nanoparticles can be classified similarly in many different ways such as based on their origin, material composition and dimensionality. Based on the origin, the NPs and NMs can be classified into two categories

- Natural: Natural NPs are the nano-size particles or materials that are found naturally in the environment. Regardless of human actions, they are present throughout the earth’s spheres such as atmosphere, hydrosphere lithosphere and biosphere[29]. On the other hand,
- Synthesizes: NMs are intentionally produced through a defined physical, chemical or biological fabrication process. They are often referred to as engineered nanomaterials (ENMs) or nanoparticles (ENPs)

Based on the material composition, the NMs can be classified into four categories:

- Carbon-based: Carbon-based NMs contain carbon and can be further classified as Fullerenes, carbon nanotubes, carbon nanofibers, carbon black, graphene, and carbon onions. They are found in the morphological structure of hollow tubes, ellipsoid and sphere

- Inorganic-based: The inorganic-based NMs are further classified into metal and metal oxide-based nanostructures. This type of NMs are widely engineered from Nobel metals such as gold (Au), silver (Ag), and metal oxides such as titanium dioxide (TiO_2), silicon dioxide (SiO_2) and zinc oxide (ZnO).
- Organic-based: Organic NMs are nanostructures comprised of organic molecules and are biodegradable and non-toxic[35]. Some of the examples of organic NMs are Dendrimers, micelles, liposomes, ferritin, etc. Because of their unique composition and characteristics, organic NMs are widely used for drug delivery applications.
- Composite-based: composite-based NMs are the heterogeneous materials with one phase in the nanoscale dimensions associated with another nanoscale phase or larger molecules. Nanocomposites are found in nature or engineered and comprise of carbon, metal or organic-bases NMs with metal, ceramic or polymer bulk material. Recently, nanocomposites have received a huge amount of interest because of the improved mechanical properties, thermal stability and electrical conductivity[36].

Finally, the NPs can also be classified based on dimensionality, NMs can also be categorized in zero-dimensional (0-D), one-dimensional (1-D), two-dimensional (2-D) and three-dimensional (3-D). Quantum dots, carbon nanotubes, graphene and nanocomposites are examples of 0-D, 1-D, 2-D and 3-D NMs respectively.

2.1.2. Engineered Nanoparticles (ENPs): Properties, Applications and Toxicity

2.1.2.1. Properties

The concept of nanotechnology was first introduced by Physicist Richard Feynman in his talk *There's Plenty of Room at the Bottom* at the annual meeting of American Physical Society in December 1959[37]. With the advancement of technology, in the last few decades, nanotechnology has grown rapidly and has become one of the most emerging grounds, opening up tremendous opportunities in several fields. Nanoparticles are synthesized and engineered for the shape, size and surface properties to achieve unique physiochemical properties and functionalities, making them useful for many diverse applications[1]. Fundamentally, NPs comprise of three layers: the core, the shell material and the surface layer. The core is the center of the NPs and usually referred to NPs itself. The core may play an important role in the functionality or toxicity of the NPs, but it is not the only component that affects the fate of the NPs. The shell is an outer layer of the core and is chemically different material than the core, for example, quantum dots where the core can be one material such as cadmium selenide and the shell is another as zinc sulfide. The surface layer is the outermost layer and is often functionalized with metal ions, surfactants or polymers to deliver targeted fiction[38]. Figure 2.1 shows the graphical representation of typical physicochemical properties of nanoparticles. Many of its distinct characteristics are dependent on particle size and are attributed to its larger surface area. Size and shape are also the essential characteristics as they exert primary control over the distribution of the reactive surface sites responsible for their functionality, particularly in the drug delivery where it is important for its entry in the cell and the interaction with the immune system[39-41]. The size and shape of the nanomaterials also control its aggregation or agglomeration,

an important aspect that may adopt entirely new characteristics as nanocomposites[40]. In aquatic and environmental systems, it plays a critical role in the partitioning of the contaminates trapped by the aggregation[42]. Though the aggregation behavior of the NPs can also be affected on the surface chemistry including charge, coating and binding of a functional group. Surface functionalization and coating techniques are commonly used in targeted drug delivery[43].

2.1.2.2. Applications

Due to the attractive and exclusive characteristics attributed to their small size, the NPs are widely engineered and functionalized to perform a targeted function. ENPs have a wide range of applications in diverse fields like biological, medical, foods, personal care, drug delivery and engineering, just to name a few. ENPs are also used in consumer goods such as tennis, golf and bowling balls, in the fabrication of high-performance tires, cosmetics and pharmaceutical products[44]. With the advancement and innovation of the

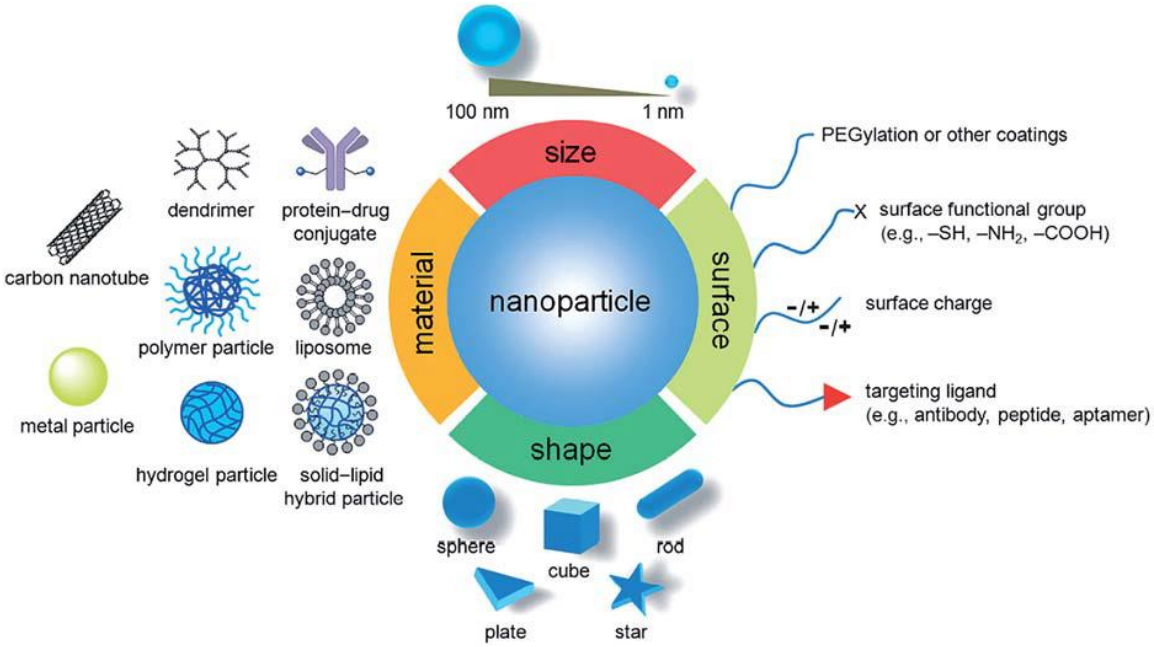

Figure 2.1 Characteristic Physiochemical Properties of Nanoparticles[1]

technology, the scope of ENPs applications is widening rapidly and by 2024 the global nanotechnology market is expected to exceed US$ 125 billion[45]. Table 2.1 summarizes various applications of different ENPs.

Table 2.1 Application of Engineered Nanoparticles[44]

Engineered Nanoparticles (ENPs)	Products/Applications
Carbon nanotubes (CNTs)	Electronic devices, field emission devices, and composite materials, numerous biological and medical applications, as adsorbent material for the removal of pollutants from water
Carbon nanohorns	Catalyst supports, and drug delivery
Tin oxide (SnO_2)	Transparent conducting coating of glass, gas sensors, solar cell, and heat mirror, gas sensors, catalyst supports
Aluminum oxide (Al_2O_3)	Batteries, adsorbent, grinding, catalysis, polishing abrasives
Cerium oxide (CeO_2)	Abrasive materials of chemical−mechanical polishing (CMP) oxygen sensor, polishing materials, gas sensors, fuel additive
Silicon dioxide (SiO_2)	Pharmaceutical products, vegetable oil refining, ceramics, detergents, adhesives, electronics, chromatography, fireproof glass, fillers, catalysts

Titanium dioxide (TiO_2)	Food coloring, photocatalyst, pigments, an additive in pharmaceuticals and cosmetics, paints, antibacterial and self-cleaning materials, sunscreen, cosmetics, UV-protection, catalysis, self-cleaning window coating, fillers, catalyst supports, and photocatalysts
Zinc oxide (ZnO)	Electrostatic dissipative coating, semiconductor material, chemical sensors and solar cells paints, sunscreen, cosmetics, electrical and optical devices, food packaging, catalysis, diode lasers, chemical absorbent, pigments, optical materials
Zinc sulfide (ZnS)	Electroluminescent devices, solar cells, and phosphors
Iron oxide (Fe_3O_4)	Removal of contaminants, sensors, magnetic resonance imaging, biomanipulation; magnetic storage media magnetic refrigeration magnetic resonance imaging (MRI) DNA detection and drug delivery system and cancer therapy
Metallic copper NPs	Applications in catalysis
Silver NPs	Dental resin composites, coatings of medical equipment, paints, textiles, antibacterial agent, food packaging
Magnesium − aluminum oxide	Sensors, catalysis

Cadmium sulfide (CdS)	Photodetectors, optoelectronics, and for solar cell applications
zerovalent iron (Fe^0)	Water remediation
Gold NPs	Drug delivery applications
Fullerene (C_{60})	Superconductors and for drug delivery, sensors, cosmetics catalyst, polymer modifications, optical and electronic devices, sporting goods, polymers, and biological and medical applications, lubricants

2.1.2.3. Toxicity

However, the same NPs that are valuable and useful in many applications, also have potential to exert adverse toxicological impacts on human health, ecosystem and the environment. Many studies report and describe the mechanism of harmful effects of various engineered nanomaterials on the ecosystems and human health[2-5,46]. Silver nanoparticles (Ag-NPs) and titanium dioxide nanoparticles (TiO_2-NPs) have been studied the most and linked the potential cytotoxicity on human organs as well as increased cardiovascular, reproductive and carcinogenic risks[10,11,47-49]. Ag-NPs have long been used as an anti-microbial substance and its prevalence in the ecosystem is concerning. Many studies have shown that silver can enter the human body in many different ways and can accumulate in various organs like lungs, spleen, kidney, liver, and brain. Contradictory, gold NPs have been found to be non-toxic and relatively safe because of its inert core. Metal oxides such as aluminum oxide, iron oxide and zinc oxide have also been studied

widely for their toxicity. Aluminum oxide, which contributes to 20% of the nano-sized chemicals, has been reported to have dose-dependent genotoxic properties[50]. Whereas, the iron oxide particles remain in cell lysosome and may increase the microvascular permeability and cell lysis; cause inflammation and significantly impair the blood coagulation parameters[51]. Similarly, zinc oxide NPs have also been shown to induce cytotoxicity and elevated cell membrane damage and increased oxidative stress in a cell culture study[52]. The Toxicological effects of TiO_2-NPs have also been researched extensively and have been discussed in detail in section 2.2 of this chapter.

The key in the toxicity of any NP is also its physiological properties and its interaction with the cell. The particle size is a primary contributor to the toxicity. Greater surface area to volume ratio of these particles increases their chemical reactivity significantly and results in increased production of reactive oxygen species (ROS). The production of the ROS causes oxidative stress, inflammation[53]. The smaller size also makes it possible for them to enter the cell. In the cell, the NPs induce cytotoxicity by generating intracellular ROS and damaging the proteins, cell membranes and DNA. A study conducted titanium dioxide nanoparticles reported that the ROS activity for the 30 nm particles was the highest, constant between 30 and 100 nm and decreased between 30 and 10 nm[54]. The same study also found that the crystalline phase of TiO_2 also affects the ROS[54]. The amorphous phase was found to be generating more ROS than anatase of rutile because of possible surface defects as active sites. The shape of the particles also affects the toxicity level of the NPs. The rod-shaped Fe2O3 NPs were found to be producing higher cytotoxicity than sphere-shaped particles in a murine macrophage cell line. In addition to the size and shape, surface charge also affect the cellular uptake of the particles and their

interaction with biomolecules. For example, a study conducted on three similarly sized iron oxide particles with different charges were found to have different toxicities on human hepatoma cell line[55].

NPs have been used in various industries and their use is increasing exponentially and so is their exposure to humans. Therefore, accurate detection and characterization of the NPs in the ecosystem, especially food and environment is extremely important for the safety of the humans and the environment.

2.2. Titanium Dioxide and its Nanoparticles

2.2.1. Background

Titanium dioxide (TiO_2) also known as Titania is an inorganic compound that naturally occurs in the oxide form and sourced from ilmenite, rutile and anatase. It is an odorless and tasteless white powder. TiO_2 is non-reactive, non-flammable, heat-stable and poorly soluble in most solvents including water, organic solvents, hydrochloric acid and dilute sulfuric acid. It has excellent physicochemical properties, such as good fatigue strength, resistance to corrosion, machinability, biocompatibility, whitening and photocatalysis, as well as excellent optical performance and electrical properties[56]. Pure TiO_2 assembles in three polymorphs, i.e., anatase, rutile and brookite however, an additional fourth form, amorphous TiO_2 has also be described. Anatase and rutile assume tetragonal while brookite assumes orthorhombic crystalline structure[57]. Figure 2.2 shows structures of all three forms of TiO_2. Thermodynamically, rutile is the most stable phase while anatase and brookite are metastable and readily transform to rutile when heated[58]. Both anatase and rutile forms of TiO_2 are produced in varying particle-size fractions and widely used in the commercial products compared to brookite because of the difficulties

encountered in obtaining it in a pure phase. Most of the TiO_2 is manufactured and purified from ilmenite and rutile mineral sand via chloride process which preliminary yield rutile. However, food grade TiO_2, is manufactured from sulfuric acid-based method which can yield anatase, rutile or mixture of both depending on the reaction condition. According to an estimate, TiO_2 accounts for two-third of all the pigments produced globally valuing at about US$13.2 billion[8].

Whereas, TiO_2-NPs are synthesized either by solution based methods such ass including sol gel method, hydrothermal procedure and electrochemical procedure or by gas phase procedures including chemical vapor deposition and physical vapor deposition. Amongst all, the sol gel method is most widely used as it provides utilizes low processing temperatures and provides product homogeneity and control over particle size and shape[59]. TiO_2-NPs are mostly found to be in the metastable anatase form due to low-energy. TiO_2-NPs are mostly known for their photolytic activity due to its extremely small size. However, unlike other NPs, the TiO_2-NPs tend to agglomerate and are often coated with silicon or aluminum to achieve better dispersion. TiO_2-NPs are one of the most popular and widely produced ENPs with a global production of more than 3000 tons/year and expected to increase significantly by 2025[6]. In recent years, TiO_2-NPs and its extensive use have raised many questions about its safety and toxicity to humans.

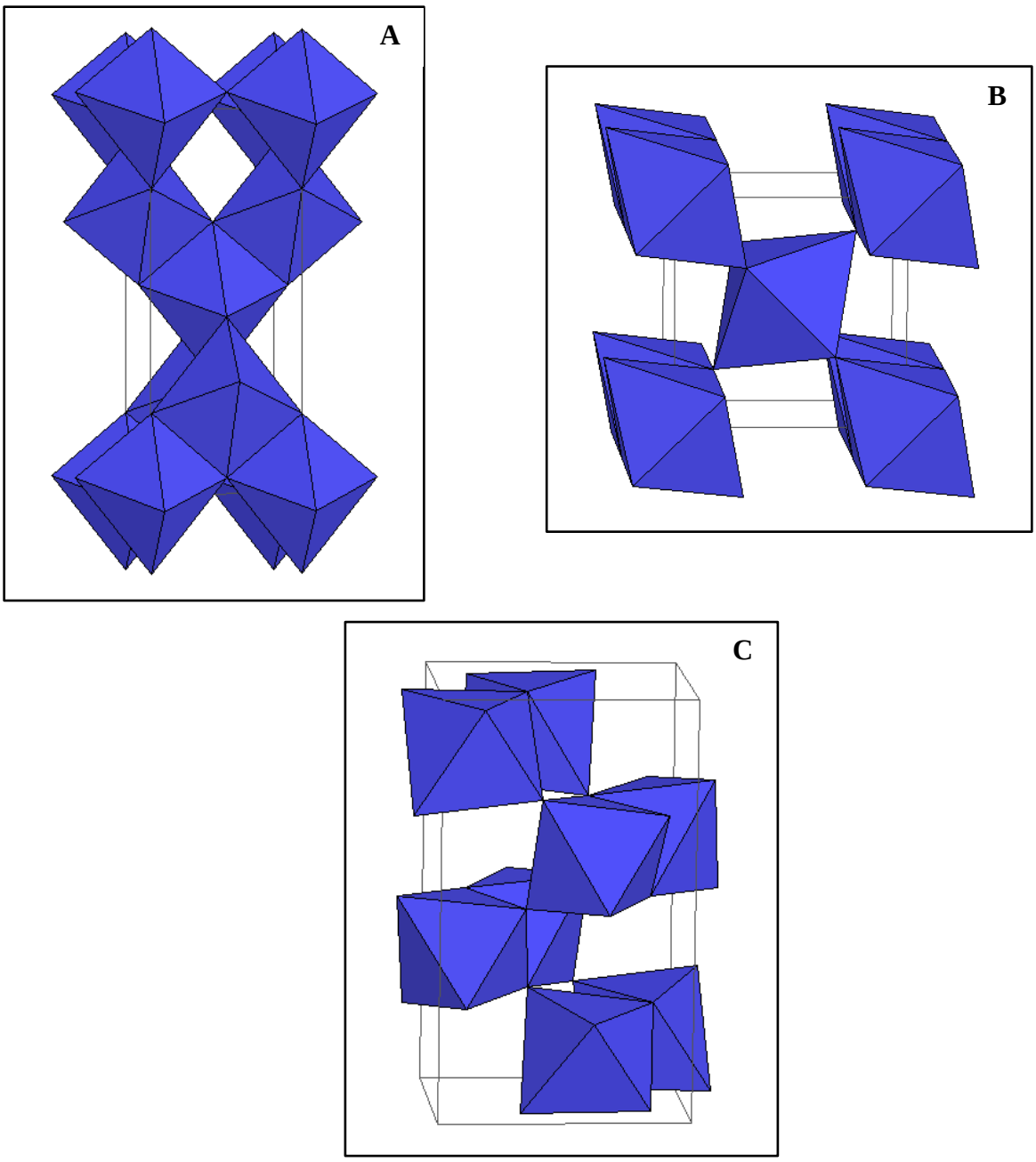

Figure 2.2 The crystal Structure of (A) anatase, (B) rutile and (C) brookite forms of TiO_2 [1]

2.2.2. Application and Toxicity

2.2.2.1. Application

TiO_2 and its NPs, mainly in rutile and anatase forms, are used in a number of applications serving many different purposes. It is widely used as a bulking agent and white pigment because of its brightness, high refractive index, and resistance to discoloration. About 70% of total TiO_2 produced is used as a pigment in paint however, it is also used as a white colorant in food, personal care products such as cosmetics and toothpaste, plastic, paper, rubber, pharmaceuticals, etc.[7]. In food, TiO_2 anatase is preliminarily used as food additive E171. Anatase is considered Generally Recognized as Safe (GRAS) is the only form that is allowed to be used in the food grade applications. According to FDA, the food grade TiO_2 (E171) should be 99% pure and can be used up to 1% by weight of the food[60]. As a white pigment, TiO_2 enhances the white color of certain foods such as dairy and non-dairy products such as coffee creamers, plant based milk, yogurt and ice-creams, candies, puddings, frostings and toothpaste. It is also used as a flavor enhancer in nonwhite products such as nuts, seeds, soups, dried vegetables, mustard, beer and wine[9].

On the other hand, the TiO_2-NPs possess the photolytic activity and widely used as a sunblock sunscreen to obtain the protection against UV light. In addition, the TiO_2-NPs are also used in photodegradation of organic pollutants and water splitting to generate hydrogen for fuel[61]. Apart from that, TiO_2 nanostructures have recently gained interest in potential applications as an anode in lithium-ion batteries and gas sensors[59]. Other applications of the TiO_2-NPs also include self-cleaning glasses, construction and building material, anti-microbial, biomedical, wood preservative and textile. Figure 4.3 highlights key fields of application of TiO_2-NPs.

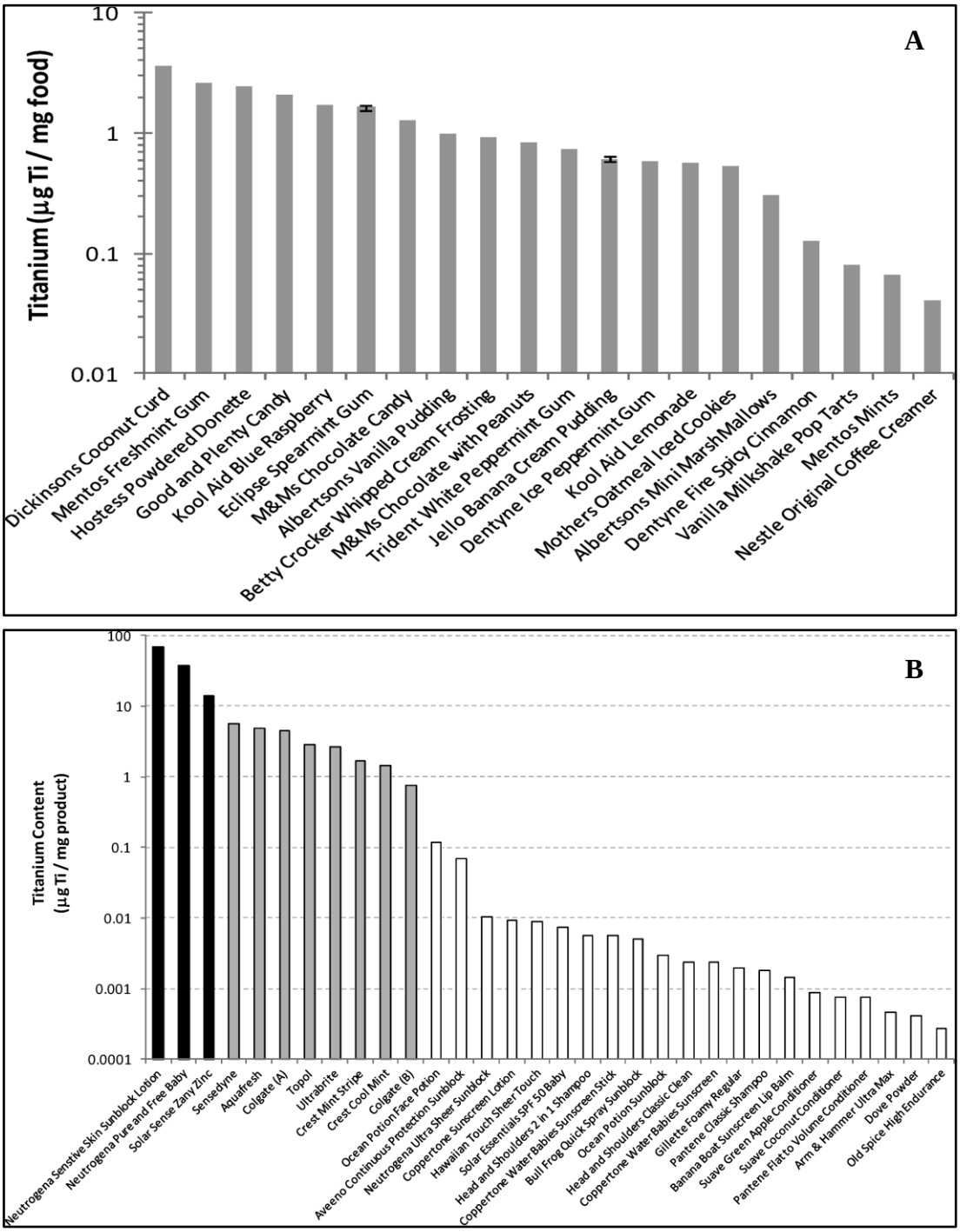

Figure 2.3 Titanium content (µg of Ti/ mg of product) in (A) food products and (B) personal care products[7]

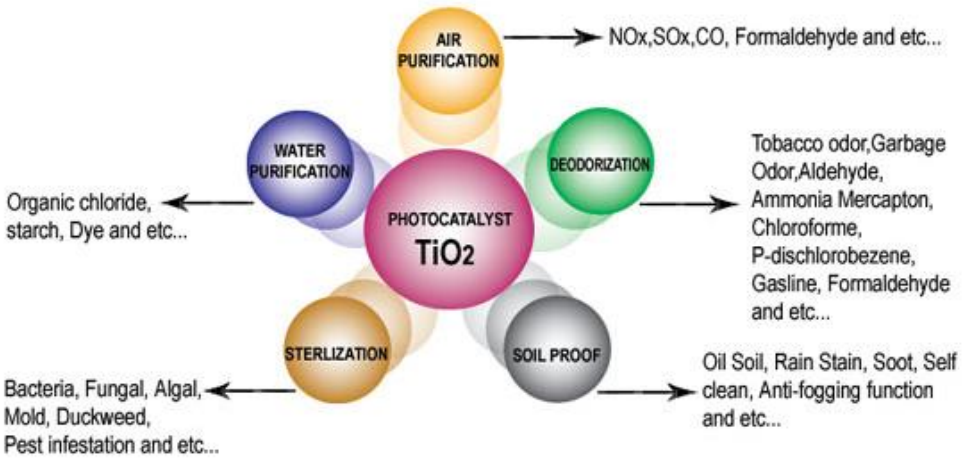

Figure 2.4 Photocatalytic Application of TiO_2-NPs[62]

2.2.2.2. Toxicity

Traditionally, TiO_2 has been considered as non-toxic material and has been used freely in applications including foods. However, in the last two decades, the research began to demonstrate the potential toxicity and carcinogenicity of the NPs. In February 2006, The International Agency for Research on Cancer (IARC) classified TiO_2 as a Group 2B carcinogen i.e. possibly carcinogenic to humans[21]. Following to that, Canada's Workplace Hazardous Materials Information System (WHMIS) also classified it as carcinogen under class D2A[63]. Currently, the titanium content in food products ranges from <0.1 ppm to 14 ppm but in personal care products such as sunscreens, it's level increases as much as 10% by mass[64]. The characterization of the ingredient TiO_2 used in consumer products revealed that about 36% of total particles were in the nano-range[9]. This raised the concern of its use especially in consumer products, amongst consumers, industry and government across the world.

Anatase form of TiO_2 is preliminary used as food additive and a toxicology analysis conducted on different structures of TiO_2 revealed that the anatase is 100 times more toxic

than the rutile form[20]. The study also showed that the anatase generated six times more ROS than rutile form when exposed to UV irradiation[65]. Also, anatase NPs showed stronger adjuvant activity than rutile in an allergy model based on the intranasal sensitization of mice with ovalbumin[66]. Recently, France announced the ban on selling the food products containing TiO_2 starting January 2020, based on the opinion by French food safety agency (ANSES). The agency studied the toxicological effect of the oral injection of TiO_2-NPs and the report recommended reducing the TiO_2 exposure to the consumers, workers and the environment[22,67]. Contradictory, The European Food Safety Agency (EFSA) re-evaluated E171 as food additive in 2016 and 2018 and concluded that based on the available literature, TiO_2 does not pose any concerns respect to carcinogenic activity and genotoxicity and considering it safe for human consumption[22].

In recent years there is been increase in the number of publications studying toxicological effects of TiO_2-NPs. Initially, the toxicology of TiO_2-NPs was studied mainly with regards to its uptake by inhalation. But In past three years, more than 100 studies investigate the toxicity of TiO_2-NPs in different animal models with respect to oral delivery. Most of them show strong evidence of various toxicities and adverse health effects. TiO_2-NPs have been reported to be accumulated in multiple organs such as heart, brain, spleen, lung, leaver and kidney, and exhibiting developmental and genetic toxicity[11,12]. A study conducted on Drosophila melanogaster (fruit flies) resulted in adverse effects on reproductive dynamics, repetitive breeding and increased genotoxicity[13]. Apart from fruit flies, developmental and genotoxicity of TiO_2 were also reported in zebrafish[14-16]. In another study reported on rats, food grade TiO_2 containing diet promoted colon microinflammation and accelerated the growth of aberrant crypt foci, thereby showing

carcinogenic activity[10]. Research in rats points out that liver may also be the target organ of TiO_2-NPs induced toxicity[17,18]. Moreover, Morgan et al. provide evidence of reproductive toxicity provoked by TiO_2NPs in adult male rats[19]. The mechanism of toxicity may be attributed to some of the following reasons: Reactive Oxygen Species (ROS) produced by TiO_2-NPs, cell wall damage caused by cell attachments, due to electrostatic force from the larger surface area or due to the attachment to intracellular organelles and biological macromolecules[2]. The NPs can also interact with the DNA and other genetic material within the cell and thereby inducing genotoxicity[68].

ENPs including TiO_2-NPs are also an emerging class of environmental contamination that has to drown attention of the researchers. The industrial revolution and exploration of a new area of NPs application have increased the risk of their fate in the environment, significantly affecting the ecosystem. A recent study quantifying the total amount of TiO_2-NPs in the surface water from Lake Taihu, China, showed alarmingly elevated levels[23]. Widespread use of TiO_2-NPs may pose a threat of combine exposure of it with other pollutants and intensify the toxicity[24]. A study investigating the toxicity TiO_2-NPs in presence of bisphenol A (BPA) found increased oxidative stress, and micronuclei formation as a result of synergistic effect[25]. High concentrations of the NPs in the environmental water may also induce genotoxicity in aquatic life such as freshwater fish and algae. However, more research is still needed to be conducted to further investigate the presence and environmental implications of TIO_2-NPs.

2.3. Current Technology in Analyzing TiO_2-NPs in Food and Environment

Although countries like France have already banned the use of TiO_2 in food products, EU and USA are still investigating the scientific evidence and there are

significant challenges that restrict the investigation and affirmative actions on its usage in consumer products. The consumers demand cleaner and safer products which means the elimination of TiO_2 from the food products however, for the industry and government there are some major challenges. One of them being, finding a suitable replacement for TiO_2. Because of its abundance in nature, unique properties and compatibility with most food products, finding a replacement for TiO_2 is extremely difficult. In addition, toxicological effect of the TiO_2-NPs depends on many parameters, but most importantly size and concentration therefore, quantification and size characterization is very important. Currently available analytical techniques and method for the quantification and size characterization of TiO_2-NPs is discussed below.

2.3.1. Analytical Techniques for Quantification of TiO_2-NPs

Currently used analytical technologies for quantification of TiO_2 are Inductive Coupled Plasma Mass Spectrometry (ICP-MS) and Inductive Coupled Plasma Optical Emission Spectrometry (ICP-OES) and Single Particle Inductive Coupled Plasma Mass Spectrometry (SP-ICP-MS). From all, ICP-MS is widely considered as gold standard method and used for the analysis of many elements including Ti. Many studies have reported using ICP-MS for reliable quantification of Ti and the analysis protocol is widely available[6,9,20,23]. However, the quantification of Ti using these analytical techniques requires complex sample preparation. TiO_2 is chemically stable in solid phases and not in ionic form so, to convert the TiO_2 in the elemental form that can be detected by the instrument, nitric acid (HNO_3), hydrochloric acid (HCL), hydrofluoric acid (HF), sulfuric acid (H_2SO_4), hydrogen peroxide (H_2O_2) and their combinations are used[6]. Often time microwave digestion is used to achieve higher reproducibility of the results. Nevertheless,

these techniques can only quantify the amount in the form of total Ti and cannot differentiate the NPs. Therefore, in order to analyze NPs, ICP-MS is usually hyphened with techniques such as Flow Field Fractionation (FFF) or Hydrodynamic Chromatography (HDC), but these techniques are unable to deal with low NPs concentration[69]. However, a recent advancement in the technology, SP-ICP-MS is been reported to overcome many of these challenges[6,23,69-72]. SP-ICP-MS operates on the basis of traditional ICP-MS but in a "single-particle" mode, where nanoparticles are introduced individually into the instrument and then recording the time-resolved analysis (TRA) intensity within each short dwell time[69]. However, the chemicals used in the ICP-MS analysis are not green and environment friendly and pose significant hazards to human health and environment. In addition, highly trained professionals are required for accurate sample preparation and operation of these instruments. Overall analysis cost is also much higher using these technologies because of higher capital investment, specific facility requirements and the usage of ultra-pure reagents.

2.3.2. Analytical Techniques for Size Characterization of TiO_2-NPs

Along with quantification, size characterization is a crucial factor contributing to the toxicity of the TiO_2-NPs. Weir et al. first characterize the food grade TiO_2 E171 and reported that it contained at least 36% particles with one or more dimensions in the nano range (<100 nm)[7,22]. With the current urgency of eliminating TiO_2 from consumer products, a reliable and rapid size characterization technique can bring up a solution that can be beneficial to both industry and consumers, i.e. removal of the NPs from E171. In the latest report in 2019, EFSA from EU stated not to consider E171 potential carcinogen

and ban its use in the food products and mentioned working on the physio-chemical characterization including size of E171 before coming to any conclusion[22].

Many studies have been reported characterizing the TiO_2-NPs from food and environment using different analytical techniques[6,7,9,20,23,69-71,73]. The current technology used for size characterization of TiO_2-NPs includes Microscopic, light scattering, flow fractionation, and spectrometry based methods[74]. The most commonly used microscopic techniques include Scanning Electron Microscopy (SEM) and Transmission Electron Microscopy (TEM). For example, Peters et al. and weir et al. used SEM to characterize the NPs in E171 and foods such as chewing gum[7,9]. SEM and TEM provide high-resolution images that not only help to determine the size of the individual particle but also help understanding its morphology and other characteristic behavior such as aggregation. However, high capital investment and operational cost, requirement of skilled analysts, complex sample preparation and analysis time (especially in case of TEM) limit their use to research laboratories and organizations. A very small sample size is used for SEM and TEM measurements which often may not provide the accurate representation of the entire sample. Dynamic light scattering (DLS) is another most commonly used rapid measurement technique that measures the Brownian motion of the NPs in the suspension and relates its viscosity to the size. Although the sample preparation is minimal and the analysis time is in minutes, as an indirect detection method, DLS shows poor accuracy in multimodal particle size distribution as the scattering intensity of the small particles is often masked by the larger particles[26,27]. Flow-Field Fractionation (FFF) another technique that utilizes external field perpendicularly applied to the laminar flow with a parabolic velocity profile of the sample which results in particle concentration according to their

size[75]. However, aggregation in aqueous solution is a characteristic of inorganic NPs and the size characterization using both DLS and FFF requires uniform particle dispersion for the accurate measurement.

Although conventional ICP-MS detects the elemental Ti and cannot differentiate the NPs, studies have reported the size characterization of TiO_2-NPs from environmental water samples using ICP-MS coupled with FFF and HDC. However, these methods are not accurate enough with lower concentration samples. Above all, SP-ICP-MS is being pushed as a gold standard method for NPs characterization in recent years. SP-ICP-MS characterizes the NPs based on the intensity difference of a single particle when injected in the system by comparing it with the intensity of the standard with particular particle size. However, there are certain disadvantages limits its potential. One of the major limitations its size detection limits. A recent study published by Lee et al. reported the detection limit of SP-ICP-MS only up to 20 nm for TiO_2-NPs[69]. Additionally, the sample preparation for the analysis is extremely critical and optimum dilution is required to be attained to achieve individual monitoring of a single NP[76]. It is also critical to remove any matrices, as they heavily interfere with the signal. Furthermore, to achieve reliable, precise and accurate characterization and quantification of the NPs, state of the art instrumentation such as quadrupole instruments with collision cell for kinetic energy discrimination, ICP-SFMS with mass resolution up to about 10 000, the quadrupole based MS/ MS technique (ICP-QQQ), etc. are necessary. These instruments require extremely high capital investment and also have high operating cost, which might serve as a valuable asset for a research organization or laboratory but is not economically sustainable for TiO_2 manufacturers or the food industry just to characterize the particle size of E171. Other

miscellaneous methods such as X-ray diffraction (XRD), electron microscope coupled with energy disruptive spectrometer (EDS) have also been reported for the characterization ingredient TiO_2-NPs from lake water[23,77].

Nevertheless, most of the methods discussed above are not capable enough to distinguish the type of the TiO_2 such as anatase, rutile and brookite, which is important as all these forms have different toxicological effects and mechanism of action. Consequently, there is a potential opportunity for an economically reliable, accurate and rapid screening method that can simultaneously quantify, detect the particle size and identify the type of the TiO_2-NPs. Surface-Enhanced Raman Spectroscopy (SERS) is a novel emerging technique that is ultra-sensitive to nano-rage. The next sub-section discusses the potential of SERS in characterizing NPs in detail

2.4. Raman and Surface-Enhanced Raman Spectroscopy

2.4.1. Raman Spectroscopy

Raman spectroscopy is a vibrational spectroscopic technique first introduced by Indian physics Dr. C.V. Raman in 1928[78]. Basically, it is an inelastic scattering of light where incident photons interact hit the molecules, most scattered elastically, called Rayleigh scattering. But when the photon interacts with the molecule, it either gains or loses the energy and scatters inelastically. The incident photon scattered with energy gain is called anti-stokes scattering and scattering of low energy photon is termed as Stokes scattering[79]. Figure 2.5 illustrates this phenomenon. The change in the energy of inelastic scattering of the photon is termed as Raman scattering whereas the frequency change is called Raman shift. The intensity of the Raman scattering at each Raman shift constitutes Raman spectra. The Raman shifts are dependent on the chemical bonds or the functional

groups of the molecules involved in the scattering. Therefore, the Raman spectra can provide a “fingerprint” or “barcode” of a specific molecule that helps in identification and quantitative analysis of a substance. Dr. C.V. Raman was awarded a Nobel prize in Physics for the invention in 1930. Raman scattering has a high molecular specificity, making it an excellent technique for material analysis however, it is a rare phenomenon, with a very low probability of Raman scattered photon, approximately 1 in 10^{880}. For this reason, Raman spectroscopy did not see any major developments until 1960 where the invention of laser expended the scope of the experiments. Between 1970 to 2000, advancement in the rapid detection techniques and nanotechnology introduced the concept of surface-enhanced Raman spectroscopy (SERS).

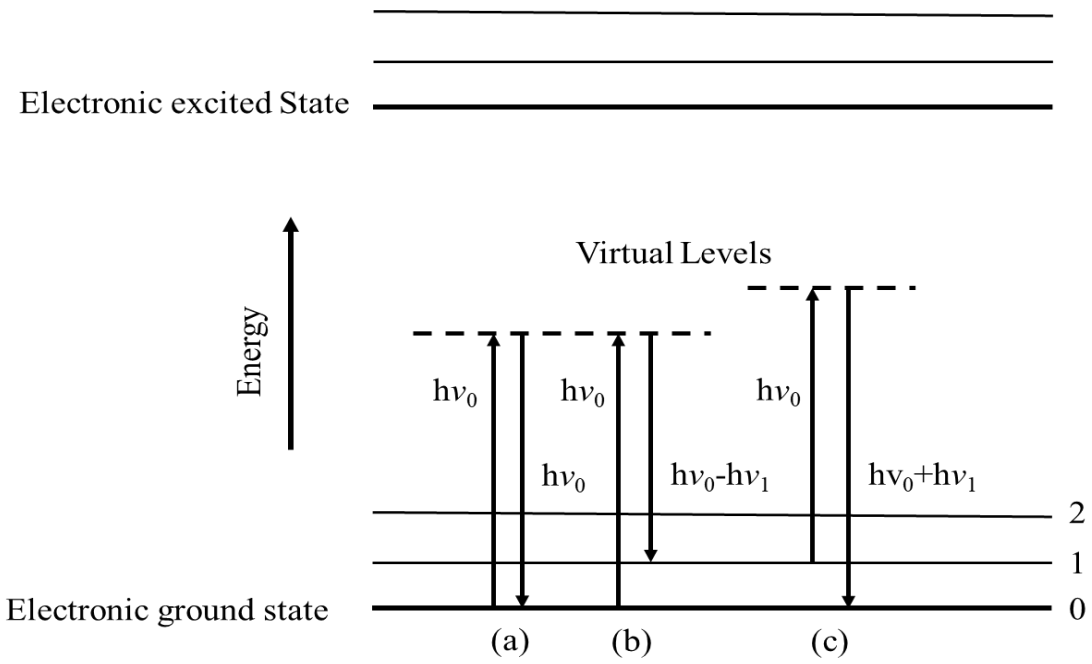

Figure 2.5 Energy-level diagram showing the states involved in Raman scattering (a) Rayleigh scattering (b) Stokes Raman spectroscopy (C) Anti-Stokes Scattering

2.4.2. Surface-Enhanced Raman Spectroscopy

Surface-Enhanced Raman Spectroscopy (SERS) is the recent advancement of the Raman spectroscopy that provides significant enhancement to the Raman shifts of the molecule, making it detectable even at lower concentration. In 1974, Fleischman et al. proposed the SERS phenomena for the very first time, when they observed enhanced pyridine signals when it was absorbed on to the roughed silver surface[81]. Since then, SERS has received significant amount of research interest and many potential applications have been explored. Although the mechanism of SERS is very complicated and not fully understood yet, it is observed that the signal improvement is mostly obtained by electromagnetic enhancement and chemical effects in some cases. SERS additionally requires the presence of SERS substrates which are typically metal nanostructures as an integral component[82]. Where, the interaction is not only between light and analyte molecules but also with nanostructures which provides a signal enhancement up to 10^{11} depending on the nature of the target analyte and the SERS substrate[82,83]. This type of effect is usually provided by electromagnetic waves that are generated when the incident light excites the electrons of the metal substrate. When the analyte is placed in the proximity of these electromagnetic waves, it experiences enhanced electromagnetic field and produces an enhanced Raman scattering. Alternatively, the chemical enhancement is the effect of the charge transfer which occurs when the molecule is absorbed on a metal surface, providing signal enhancement[84]. Compared to the electromagnetic enhancement, the charge transfer mechanism only provides up to 100 times signal enhancement[85]. Figure

2.6 illustrates the concept of SERS, whereas table 2.2 shows Raman/SES peak assignments of the molecular or functional group[86].

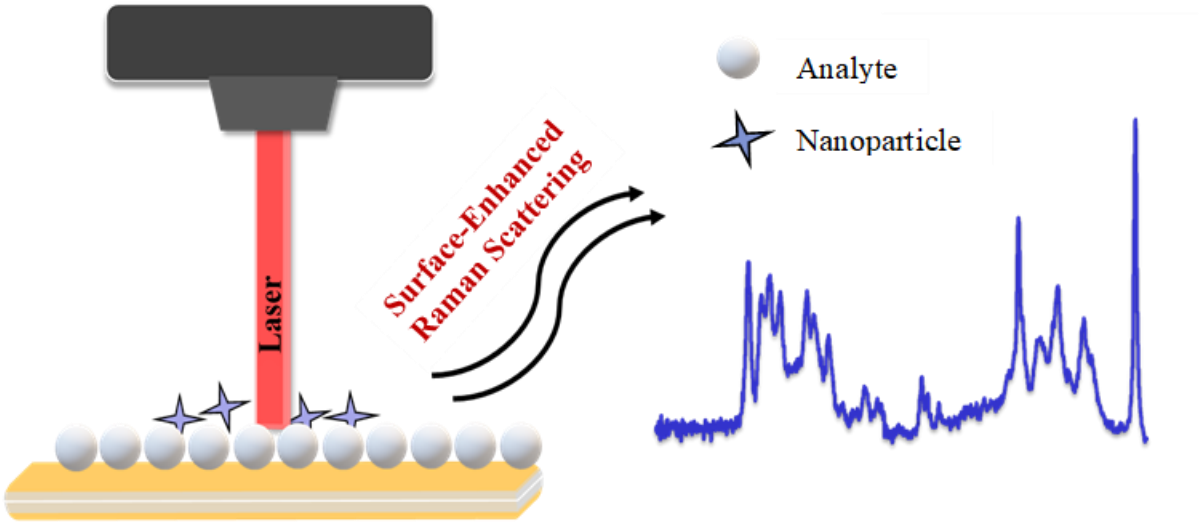

Figure 2.6 Illustration of Surface-Enhanced Raman Scattering

Table 2.2 Raman Peak Assignment Based on the Vibrations of Chemical Bonds and Functional Groups[86]

Raman Peak (cm-1)	Chemical Bonds or Functional Groups
143-148	TiO_2 Anatase
240-275	Au-Cl, Au-S, Au-N, or Au–C vibrations, AuNP aggregation
445-450	TiO_2 Rutile
460	Proteins
469	Hydroxyquinoline
545	Glutathione (N-C-C), cysteine, nucleic acids

651-659	Glutathione (C-S), cysteine, C-S
669	Oxidized glutathione (C-S, C-S, N-H, amide IV), porphyrin ring
731-739	NAD (A ring), hydroxyquinoline, proteins, C-S
799	Glutathione (COO-), NAD
874	Glutathione (C-C), enzymatically bound NADP+, proteins
902	Glutathione (C-C), proteins
912	RNA
920-944	Oxidized glutathione (C-COO-), NADH (N), chlorophyll a, proteins
952	Oxidized glutathione (C-COO-), proteins
979-980	RNA, NADP+ (P), proteins
1022-1026	NAD+ (N ring)
1030-1034	NAD (N ring), enzymatically bound or unbound NADP+, glutathione (C-N), phenylalanine
1037-1038	Proteins
1125	Glutathione (N-C, C-C), proteins
1157-1166	β-carotene, carotenoids, quinoid rings, proteins, tyrosine
1169-1174	Proteins, enzymatically bound NADH (A)
1175	Proteins, Oxidized glutathione (C-CN, NH3+), tyrosine, phenylalanine, hydroxyquinoline
1192	Phosphate of DNA/RNA
1203	C-C6H5 stretch
1214	Oxidized glutathione (Amide III, III', C-O, CH2), hydroxyquinoline, β-carotene, DNA/RNA

1224	Proteins (i.e., reductase enzymes, amide III), DNA/RNA
1244-1246	Glutathione (amide III), NADH (N, A), proteins
1250-1253	Glutathione (amide III), β-carotene, hydroxyquinoline, NADP+, DNA/RNA, proteins
1264	Glutathione (amide III), hydroxyquinoline, nucleobases (T, A), proteins (amide III or =C-H)
1267	Hydroxyquinoline, proteins
1278	Oxidized glutathione (Amide III, III', C-O, CH2), proteins (i.e. reductase enzymes)
1282	Proteins (i.e., reductase enzymes), Amide III, glycine, proline
1288-1304	Chlorophyll a, nucleobases, amide III
1340-1344	NAD+ (A ring), chlorophyll a, proteins
1410	Glutathione (COO-), enzymatically bound NADP+ (A/R, N)
1445-1449	C-H2, proteins
1476-1484	Hydroxyquinoline, NAD (A ring), proteins (i.e., reductase enzymes)
1491-1495	Chlorophyll a, Oxidized glutathione (CH2, N-H, CN), NAD (A ring), nucleobases, proteins (i.e., reductase enzymes)
1517-1527	β-carotene, carotenoids, chlorophyll a, porphyrin rings, proteins (i.e., reductase enzymes)
1544-1554	NAD (A ring), chlorophyll a, amide II, tryptophan
1559-1562	Amide II
1565-1569	Hydroxyquinoline, amide II, tryptophan, COO-, nucleobases
1584-1591	NADP+ (A/R, N), NAD (N ring), proteins (i.e., reductase enzymes)

1594-1597	Hydroxyquinoline, NAD+ (N ring), proteins
1604	Oxidized glutathione (NH3+), proteins (i.e., reductase enzymes)
1623	Glutathione (amide I, I'), NAD+ or NADP+ (N), proteins (i.e., reductase enzymes, amide I)
2125-2146	Au (0)–CN^-

Recent advancements in this technology and development of innovative nanostructures as SERS substrate now allowed users to detect an analyte within a few minutes and with very little on no sample preparation time. Since Raman scattering results from the vibration of the chemical bonds or functional group, it is an excellent fingerprinting tool for each molecule present in the analyte, making it highly selective. In many applications, SERS is a direct and nondestructive tool that can detect the targeted analyte with minimal or no sample preparation[87]. Moreover, SERS is considered a highly sensitive analytical method that is capable of detecting even a single molecule and with the detection limit up to parts per billion (ppb) or parts per trillion (ppt) levels[88]. In spite, Raman microscope is easy to operate with very short analysis and data collection time period and does not require highly trained personals to operate. The Raman microscope is available as benchtop instrument, portable as well as handheld device and shows compatibility with many other analytical techniques such as headspace analysis, filtration methods and immunological assays[89-91]. In addition, the portable version of the technology is also capable of *in situ* identification and detection of toxins, food additives, bacteria etc.[92,93]. These unique advantages of SERS make it much more powerful and advantageous compared to other vibrational spectroscopic techniques such as infrared (NIR). Therefore,

the application of SERS is increasing in food and pharmaceutical testing with a particular focus on chemical contaminates, adulterants[83,94,95].

2.4.3. SERS and Nanoparticles

Metal nanostructures, as discussed above, are considered powerful SERS substrates. Metal nanostructures such as Ag, Au, Cu, and TiO_2 exhibit strong Raman signals and also provide significant signal enhancement to the analyte signals when placed in the proximity of the NPs. Many studies have shown successful application of Raman spectroscopy in detection of ENPs in food and environment[95-98]. Nanoparticles in the suspension or aggregated form are also widely used as SERS substrate in detection of microbes, pesticides, food additives, toxins or other contaminants with NPs with higher sensitivity and lower limit of detection[95,99-102]. The signal enhancement of the NPs depends upon many physiochemical properties of the NPs but most importantly, on the size and shape[103]. Within the nano-range, when the particles are too small, the effective conductivity and light scattering properties, which are needed for SERS enhancement, diminish and as the size increase, the SERS effect increases as it depends on the number of electrons available[104]. Nevertheless, the signals from the nano-sized particles are higher compared to the larger size particles.

Previous studies have shown that both anatase and rutile polymorphs of TiO_2-NPs are sensitive to the Raman spectroscopy and show strong and distinct Raman shifts[105]. Hence, TiO_2-Nps has been used as a SERS substrate in many studies to detect the targeted analyte[106-109]. However, very few to no studies have considered SERS as a tool for size-characterization of the NPs, specifically TiO_2-NPs. Zhao et al. recently presented the potential of SERS in characterization of TiO_2-NPs in a preliminary study[28]. This study

demonstrated that, due to the advantage of greater SERS effect of NPs on a ligand, it was possible to differentiate the TiO_2 particles within and outside of the nano-range. However, further research is required to characterize the particles in the nano-range. Additionally, the physiochemical properties of the particles can be altered by many external factors and understanding the effects of these factors on SERS analysis is necessary for the accurate size characterization of TiO_2-NPs, which is the primary focus of this study. The present study also investigates the implementation of SERS method for detection of NPs in real-time samples such as from lake surface water.

CHAPTER 3

Factors Affecting the SERS Analysis of Titanium Dioxide Nanoparticles

Abstract

Titanium dioxide and its nanoparticles are widely used in different applications and in recent times, its safety to human health and environment is a rising concern. Herein, we evaluated the potential of Surface-Enhanced Raman Spectroscopy (SERS) as an analytical tool in the analysis of TiO_2-NPs. We first demonstrated that Raman spectroscopy can easily distinguish between different polymorphs of TiO_2 such as rutile and anatase. Also, Gallocyanin (GLN) assisted SERS method was also able to easily distinguish between the nano-sized particles from the larger particles based on R-value obtained from the ratio of TiO_2 to GLN peak intensities. Furthermore, we evaluated the factors affecting the SERS analysis of the NPs to better understand its sensitivity within the nano-range. We found that the size and concentration of the nanoparticles, ligand concentration and experimental parameters such as sample incubation technique and point selection for the measurement could have major influence on the SERS analysis. Furthermore, numerous dispersion techniques were assessed to evaluate its potential in dispersing the TiO_2-NPs and effect on the SERS analysis. We found that probe sonication method in combination with dispersing agents produced most stable and disperse suspension however, due to the charge-transfer effect it prevented the interaction of TiO_2 with GLN.

3.1. Introduction

Titanium dioxide (TiO_2) and its nanoparticles (NPs) are widely used in numerous applications serving various functions[8,56]. Due to its inexpensive cost, abundant availability, unique properties and advancement in nanotechnology, the market of TO_2 nanomaterials is seeing an exponential growth[6,21,63]. It's anatase form, E171 is considered as GRAS and used in food and pharmaceutical products as a white color, bulking agent and flavoring agent [18]. However, in the recent year, researchers have demonstrated its potential toxicity and have been categorized as potential carcinogens in many countries[,21,63]. Especially, its application in food and consumer products raises a significant concern because at least 36% of the E171 has been reported nano-sized[9]. Therefore, size characterization of the TiO_2-NPs is significantly important to ensure its elimination for the safety of human health and environment.

Surface Enhanced Raman Spectroscopy (SERS) is considered a powerful analytical technique in detection of food and environment contaminants due to its high selectivity and specificity[100,110]. SERS possesses strong sensitivity towards NPs and many researchers have demonstrated the potential of SERS in the characterization of metal nanoparticles[111-114]. The previous research published by Zhao et.al demonstrated a novel approach in analyzing TiO_2-NPs using SERS. It utilizes the ratio value (R) between the Raman intensity of the TiO_2 peak and the SERS intensity of the ligand bound to TiO_2 particles. The SERS intensity of the ligand relies on the size of the NPs thereby, providing a distinct R for different particle sizes within and outside the nano-range[28]. Although their research demonstrates a proof of concept of SERS application in the detection of the TiO_2-NPs,

different particle sizes in the nano-range requires further investigation. Moreover, NPs behavior can be altered by their intrinsic properties and many experimental factors. Hence, understanding the impact of these factors on the SERS analysis is necessary for accurate size characterization of TiO_2-NPs.

The overall goal of this study was to examine in detail, the potential of SERS as a tool to analyze nanoparticles specifically, TiO_2-NPs and evaluating the challenges in the analysis by understanding the factors affecting the NPs behavior and its sensitivity to SERS. Since SERS has a great sensitivity in the nano-range and the enhancement of the ligand signals entirely depends on the size of the particles surrounded by it, agglomeration may play an important role in the analysis. Moreover, other factors such as size and concentration of the NPs, ligand concentration, sample preparation and SERS analysis technique may cause significant influence on the accurate measurement. We first examined the performance of the method previously developed by Zhao et al. using GLN as a ligand. We chose GLN as a ligand instead of Myricetin (MYC) because the overall signal intensity of MYC was found to be weak especially at lower concentrations and GLN showed stronger sensitivity towards SERS. We then evaluated factors affecting the SERS analysis one by one. We then examined the effect of different dispersion techniques such as pH adjustment, Ultrasonication and dispersing agents for their ability to disperse TiO_2-NPs and influence on SERS measurement. We took this approach to better understand the effect of size, concentration and measurement techniques on R-value.

3.2. Materials and Method

3.2.1. Chemicals

All Titanium dioxide Anatase powder samples of particle sizes 5,30,40,50,100 and 800 nm (nominal size provided by the supplier) were purchased from US Research Nanomaterials Inc. (Houston, TX) and MK Nano (Mississauga, ON). All the other chemicals used during this study such as gallocyanin (GLN), hydrochloric acid (HCL), sodium hydroxide (NaOH) and sodium pyrophosphate ($Na_4P_2O_7$) were purchased Sigma Aldrich (St. Louis, MO). All the chemicals and reagents were prepared with ultrapure water (18.2 MΩ·cm) from Barnstand Smart2Pure Water Purification System (Thermo Scientific, Waltham, MA), except, GLN which was prepared in absolute ethanol purchased from Fisher Scientific (Waltham, MA).

3.2.2. SERS analysis of TiO_2-NPs

The SERS analysis of TiO_2-NPs was conducted by following the protocol as described in fig. 3.1. The TiO_2 particles were first dispersed in ultrapure water with an initial concentration of 0.4 g/L and sonicated for at least 10 minutes using bath sonicator [Branson 2000, Branson Ultrasonic, Danbury, CT] and/or probe sonicator [Fisher Scientific, Waltham, MA]. The dilutions were made by diluting the stock solution with ultrapure water and sonicating prior to use. GLN stock solution of 1 mM concentration was prepared in ethanol and diluted to desired concentration prior to use. As illustrated in the schematic diagram, first 100 µL of the TiO_2 suspension was mixed with equal volume of GLN in a 0.5 ml plastic tube (Fisher Scientific, Waltham, MA). The mixture was allowed to incubate for 30 minutes at room temperature with gentle shaking, followed by centrifuging at 6000 G for 5 minutes in Sorvall centrifuge (Thermo Scientific, Waltham,

MA) and the supernatant was discarded. The particles were redisposed with 10 µM of ultrapure water.

For the measurement of Raman microscope, 2 µL of the sample was dropped on a gold slide (Fisher Scientific, Waltham, MA) and allowed to air-dry. The sample was then analyzed on Raman microscope (DXR, Thermo Scientific, Waltham, MA) equipped with a 780 nm laser. All the analyses were performed using a 20X microscope and 5.0 mW laser power. The slit aperture and acquisition time was set at 50 µm and 2 seconds respectively. The data was collected and analyzed using OMNIC 9.7 software (Thermo Scientific). For each measurement, three replicates were collected to ensure repeatability. At least 10 spots were randomly selected for each replicate and the spectrum was collected in the rage of 100 to 2000 cm^{-1}. Discriminant analysis on TQ Analyst 9.7 software (Thermo Scientific) was performed to average the spectra and to obtain the statistical spectrum.

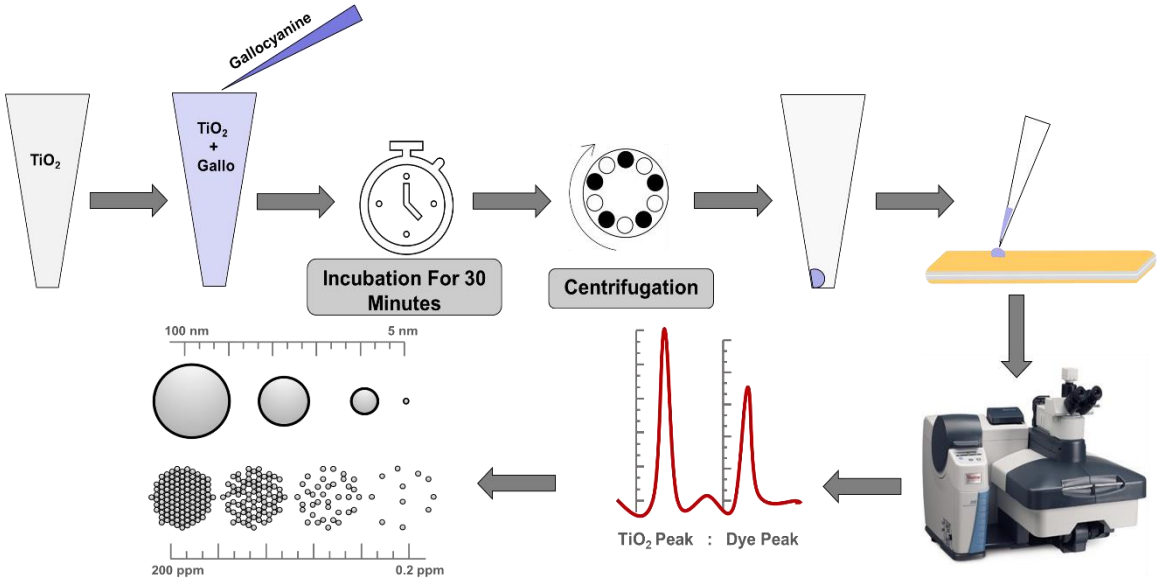

Figure 3.1 Schematic Diagram of the Sample Preparation for the Size Characterization of TiO_2-NPs Under Raman Microscope

3.2.2.1. Point Selection

The selection of the analysis points is very important in achieving good reproducibility of the results. Once all the samples are prepared, placed on gold slide and air-dried, the TiO_2 aggregate can be clearly seen under the Raman microscope for the higher sample concentration. But for the lower concentration, it can be easily mistaken with dust particles or other impurities on the slide. Therefore, correct selection of points is very important to obtain accurate and reproducible results. Figure 3.2 shows an example of point selection and corresponding spectrum of 93 nm particles for both 0.2 and 0.0002 g/L concentration. All the analysis was conducted using 20X microscopic objective. It is very important to have clean and scratch less gold slide to achieve good repeatability of the signals with lower standard deviation. Selection of correct spot generates reproducible singles for both higher and lower concentrations.

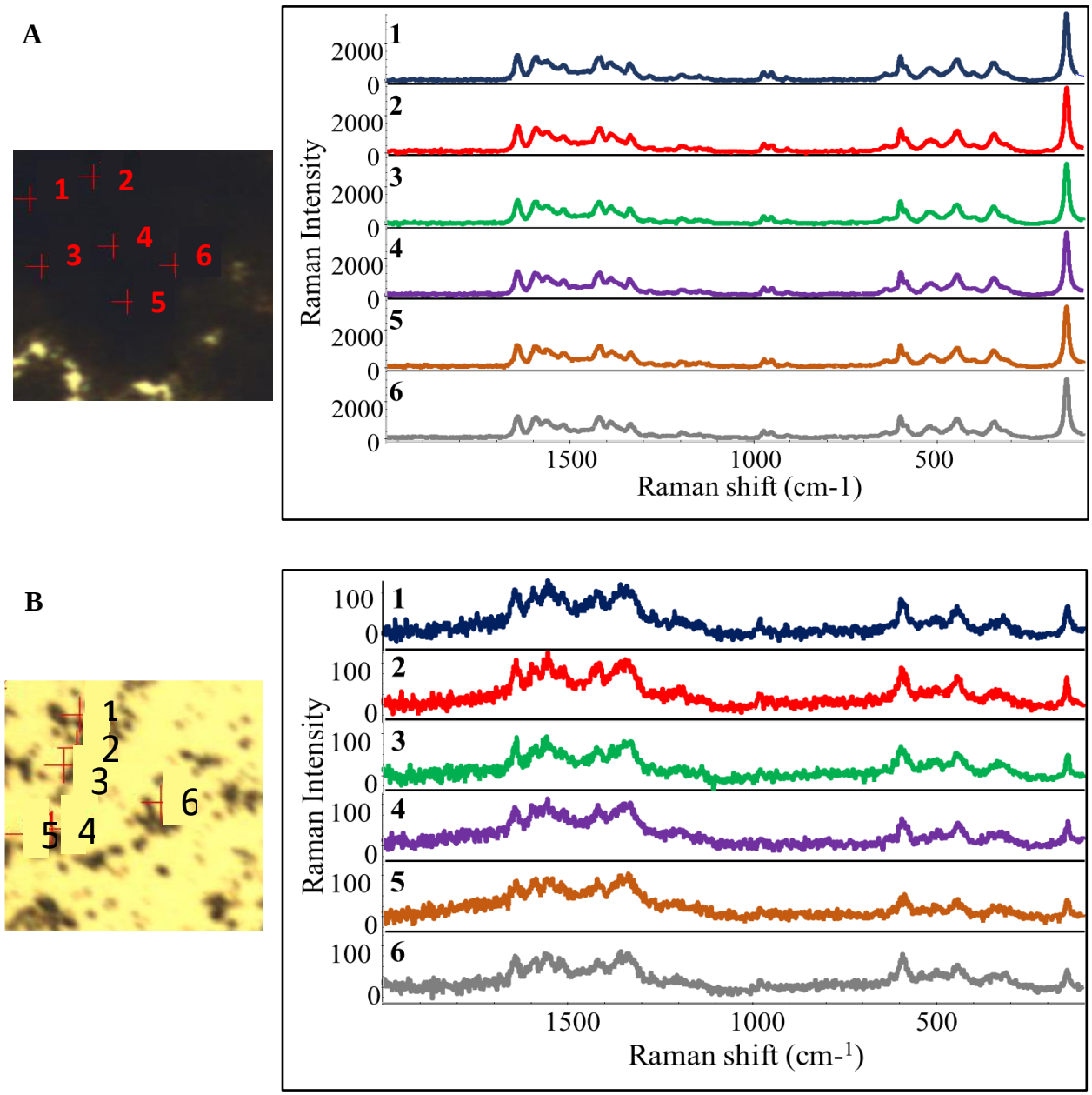

Figure 3.2 Point selection under Raman microscope for the analysis of TiO_2-NPs for (A) 0.2 g/L and (B) 0.0002 g/L concentration of the NPs

3.2.3. Experimental Design

Table 3.1 shows the summary of all the experiments performed. All the TiO_2 particles were first characterized by TEM to confirm the supplier specifications. In order to understand all the factors that can influence the size characterization, the first set of experiments were designed to understand the influence of the experimental parameters (case 1-3) such as selection of points, ligand concentration (5,10 and 20 µM) and NPs concentration (0.2, 0.02, 0.002 and 0.0002 g/L). Once the experimental parameters were optimized, the next set of experiments investigated the effect of agglomeration and dispersion techniques on the SERS analysis of NPs. TiO_2-NPs with different particle sizes were first analyzed under Raman microscope as well as DLS. All the samples were bath sonicated for 10 minutes before the analysis, to avoid large agglomerates. These experiments were critical in building the correlation between the aggregation state of NPs and the SERS measurement. Many researchers have examined various methods to understand the NPs aggregation and dispersion[115-117]. We evaluated some of the most effective dispersion strategies and such as electrostatic stabilization by pH adjustment, ultrasonication and dispersing salts such as sodium pyrophosphate in SERS analysis of NPs. Electrostatic stabilization increases the particle charge of NPs which increases the particle-particle repulsive forces, thereby suppressing the agglomeration. Different concentrations of TiO_2 dispersion have a pH value of ~5.6. The influence of both acidic (3.0) and basic pH (10.0) was investigated. The samples were prepared by dispersing the NPs in ultrapure water and the pH was adjusted adding NaOH and HCL. Ultrasonication is one of the common techniques used for dispersion. The dispersion here is achieved by the application of external force to overcome weak van der Waals altercation between

particles. However, the type and duration of the treatment affect the efficiency of the dispersion. In this study, we investigated bath and probe sonication techniques. The bath sonication samples were prepared by simply sonicating in an ultrasonic bath sonicator for 10 minutes at room temperature. For the probe sonication, the samples were initially dispersed in a bath sonicator for 5 minutes followed by 10 minutes of probe sonication at 50%. TiO_2-NPs dispersion and its effect on SERS analysis were also examined by using dispersing agent, sodium pyrophosphate. The pyrophosphate ions get adsorbed on the TiO_2 particles and improve particle dispersion due to the change in the surface charge. The effect of the dispersing agents in combination with probe sonication was also examined. TiO_2 particles were dispersed in 0.05 M $Na4P_2O_7$ solution followed by bath sonication and/or probe sonication.

All the samples were prepared and analyzed on Raman microscope by the protocol described above. The spectra were collected and analyzed using OMNIC and TQ Analyst software. Size measurement on DLS was also performed for each case for understanding the agglomeration status of NPs at each stage and its effect on the SERS measurement.

Table 3.1 Summery of Experiments Performed

Case	Objective	Particle Size (nm)*	Particle Concentration (g/L)	Solvents and Chemicals Used
1	Initial size characterization of TiO_2-NPs	173, 93 and 65	0.2	Water, GLN

2	Point selection under Raman microscope	93	0.2 and 0.0002	Water, GLN
3	Determine the effect of particle size	173, 93, 65, 41, 29 and 8	0.2	Water, GLN
4	Determine the effect of ligand concentration	41 and 93	0.2	Water, GLN
5	Determine the effect of gentle vs vigorous shaking	41	0.2	Water, GLN
6	Determine the effect of particle concentration	93, 41, 29 and 8	0.2, 0.02, 0.002 and 0.0002	Water, GLN
7	Effect of pH	65	0.2	Water, GLN, HCL, NaOH
8	Effect of ultrasonication	65	0.2	Water, GLN,
9	Effect of dispersing agent + probe sonication on particle dispersion and SERS analysis	65, 29	0.2	Water, GLN, SPP
*The particle size mentioned here was obtained from SEM/TEM analysis. Please refer to section 3.3.1 for more information.				

3.2.4. DLS, SEM, TEM and Statistical Analysis

Initial size characterization of all the particles was performed by Scanning Electron Microscopy (SEM) (JEOL JSM-6320F) and Transmission Electron Microscopy (TEM)

(JEOL JEM-2000FX). The SEM analysis was performed by placing the powder samples onto a silicone base. For TEM analysis, the samples were prepared by dropping 10 µL of the TiO_2 solution in water (0.2 g/L, pH 2, adjusted by HCL) on to the copper grid coated by carbon grid. The grid was dried overnight at room temperature and before the analysis. Three clear and high-resolution images were captured. Statistical analysis of the size distribution was conducted using ImageJ software. More than 30 particles were counted for each image. All the Dynamic Light Scattering (DLS) measurements in this study were performed after appropriate ultrasonic treatment to achieve uniform dispersion. All the samples were diluted appropriately to achieve the attenuation number between 6 and 8 in order to obtain accurate measurements. About 1 ml of the sample was analyzed with Nano-ZS Zetasizer (Malvern Instruments, Malvern, UK) and the measurements were recorded.

3.3. Results and Discussion

3.3.1. SEM and TEM Measurement

The particle size of the TiO_2-NPs samples was first analyzed by SEM. As shown in figure 3.3 and table 3.2, the particle size of 30, 40 and 100 nm sample was found to be 29, 41 and 93 nm respectively. These numbers were more or less consistent with the numbers provided by the supplier. However, the particles with a claimed size of 800 and 50 nm showed an actual size of 173 and 65 nm respectively. The 5 nm particles were very aggregated and could not be analyzed by SEM (Figure 3.3 (F)), therefor TEM analysis was conducted by dispersing the particles with acidic pH in a suspension. The particle size obtained for a 5 nm sample from TEM was 8 nm (Figure 3.4). In addition, the SEM images also revealed that particles were agglomerated in a uniform arrangement. Particle size data obtained by TEM was further taken into consideration while performing the experiments.

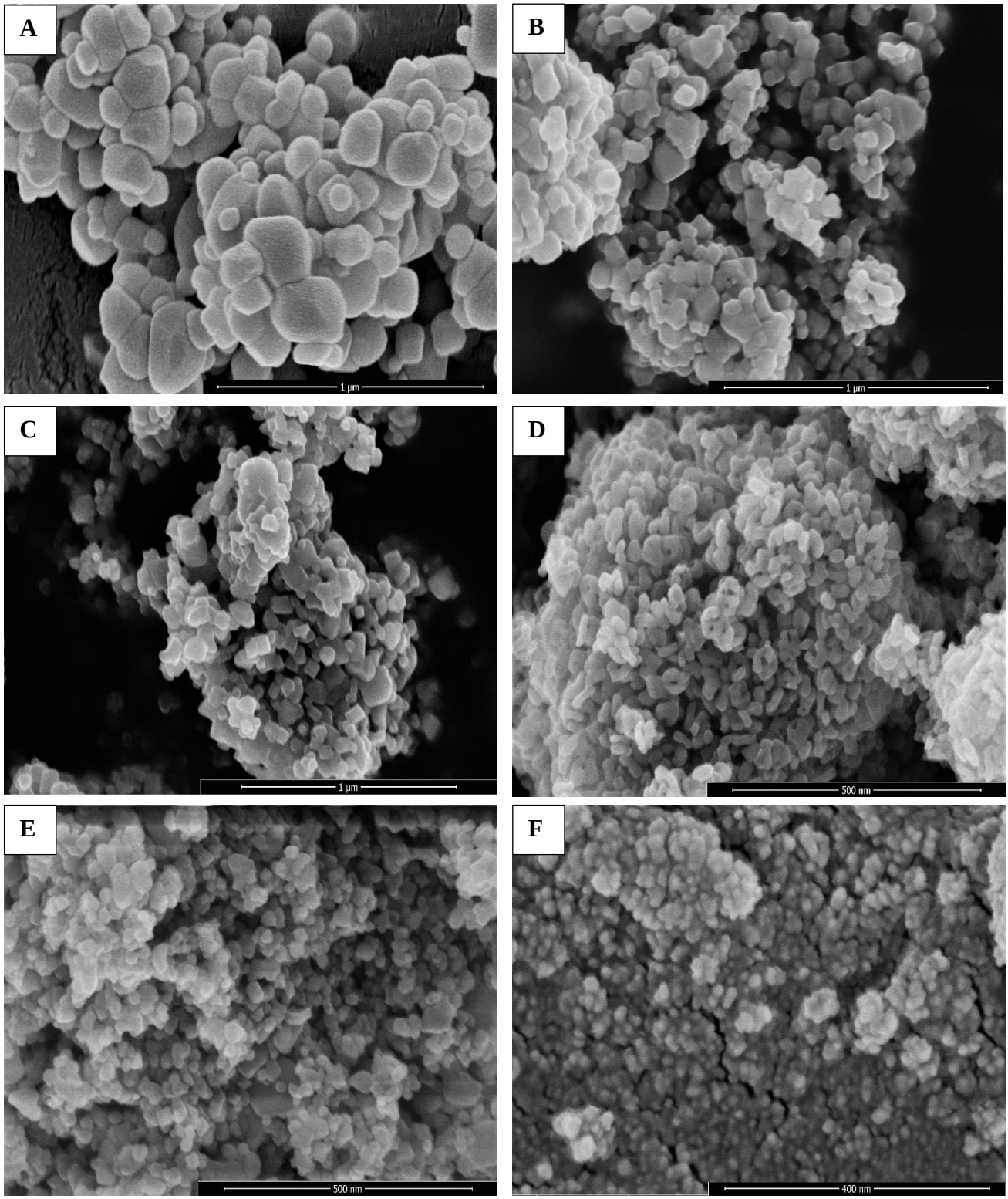

Figure 3.3 Scanning Electron Microscopic Images of (A) 200 nm (B) 100 nm (C) 50 nm (D) 40nm (E) 30 nm (F) 5 nm Particles.

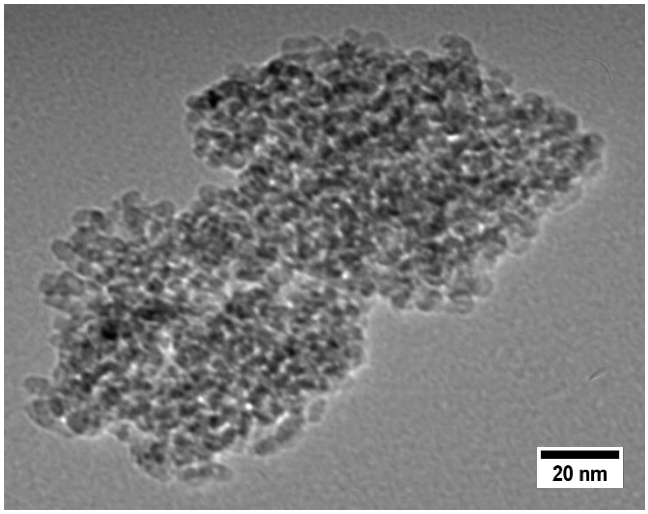

Figure 3.4 Transmission Electron Microscopic Image of 5 nm Particles

Table 3.2 Particle Size Obtained by SEM/TEM and Hydrodynamic Diameter Obtained by DLS Corresponding to Supplier Particle Size Claim

Supplier Size Claim (nm)	SEM/TEM Analysis (nm)	DLS Measurements (nm)
800	173±66	319±12
100	92±28	795±15
50	65±28	3793±482
40	41±7	1039±57
30	29±7	895±77
5	8±2	1523±102

3.3.2. Raman Spectroscopy of TiO_2-NPs

The samples were prepared by placing the 2 µL of 0.2 g/L dispersed anatase and rutile particles on the gold slide and allowed to air-dry. The slide was then placed under the Raman microscope and the data was collected using the same parameter mentioned in section 3.3.2. Figure 3.5 shows the characteristic Raman signature of TiO_2 anatase, rutile and a mixture of both. As seen in the figure, anatase shows the characteristic Raman shifts at 144, 396, 514 and 636 cm^{-1}, whereas, rutile showed the peaks at 607 and 450 cm^{-1}. These results are consistent with that is reported other researchers[28,105,118]. Characteristic peaks of both anatase and rutile can be easily identified in the mixture sample. Hence, anatase and rutile can be easily distinguished based on their intrinsic Raman signatures. Similar results were also achieved by other researchers[28,119] previously.

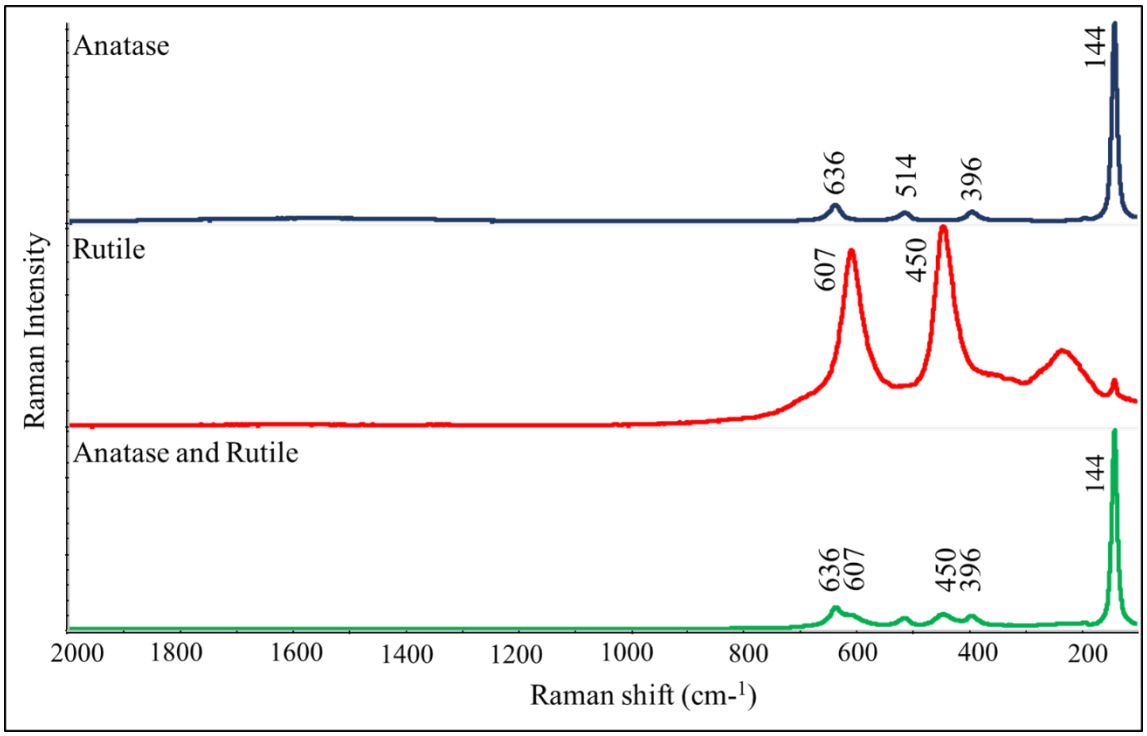

Figure 3.5 Raman spectra and peak assignment of TiO_2 anatase, rutile and a mixture of both types

3.3.3. Size characterization of TiO_2-NPs using SERS

Size characterization of TiO_2-NPs using Surface Enhanced Raman Spectroscopy (SERS) utilizes the approach of fingerprinting the NPs as well as the signal enhancement of ligand bound to the NPs, based on the size of the NPs. SERS is an advancement of the Raman spectroscopy, where the presence of SERS substrates, typically metal nanostructures, provides the enhancement to the Raman signals of the analyte[94]. Although the signal improvement is mainly due to the large electromagnetic enhancement called "hot spots" produced by the NPs, the SERS activity critically depends on the parameters like size, shape and arrangement of the NPs[83].

Since the basis of this study depends on this hypothesis and the signal enhancement of the ligand, GLN, depends on the size of the TiO_2-NPs it's bound to, this enhancement can therefore be utilized to determine the size of the NPs. GLN is phenoxazine dye with three benzene rings and numerous unsaturated bonds, which provides high bonding affinity with TiO_2-NPs and stronger SERS effect due to its molecular structure. Figure 3.6 shows characteristic Raman signature of TiO_2 anatase, GLN and SERS signature of anatase bound GLN. Anatase exhibits characteristic Raman peaks at 144, 396, 514 and 636 cm^{-1}[128]. Whereas GLN shows its peaks at 1639, 1590, 1557, 1514, 1416 and 1333 cm^{-1}. The spectrum of TiO_2 bound GLN clearly indicates the presence of both TiO_2 at GLN peaks, which shows that GLN was able to bound to TiO_2 due to charge transfer and obtained the SERS effect from the NPs. This SERS signals produced by GLN bound to TiO_2-NPs in this study is stronger than ligands reported in previous studies[119]. Here, the ratio R between the Raman intensity of the characteristic peak of TiO_2 at 144 $cm^{-1}$and the SERS intensity

of the characteristic peak of GLN at 1639 cm^{-1} can be obtained. Notably, This R-value obtained should be distinct to different particle sizes within and outside nano-range[28].

To examine the SERS effect of particles on the ligand and the R-value, three particle sizes were chosen: within nano-range (65 nm), cut-off (93 nm) and outside nano-range (200 nm). The sample preparation, measurements on Raman microscope, data collection and data analysis were conducted by following the protocol described in section 3.3.2. Figure 3.7 shows the SERS spectra of 173, 93 and 65 nm anatase particles and their respective R-value. Here, the TiO_2 and GLN concentrations are 0.2 g/L and 10 µM respectively. The intensity of the TiO_2 peak at 144 cm^{-1} is significantly higher for the 173 nm particles and decreases in the nano-range. This could be attributed to the aggregation and arrangement of the particles on the gold slide upon drying. Moreover, the TiO_2 peak intensity changes with the TiO_2 concentration and can be used to quantify the amount of TiO_2. However, if the concentration is fixed, it can also be used to differentiate the NPs from larger particles. Contradictory, the SERS intensity of GLN peak at 1639 cm^{-1} is the lowest for the 173 nm particles. The intensity increases and is the highest for the 93 nm particles and decreases again for the 65 nm particles but is still higher than 173 nm particles. The increase in the GLN intensity is a result of the SERS effect from the TiO_2 that it is bound to. The SERS enhancement largely depends on the size of the NPs and the optimum enhancement size range is different for different types of NPs. When particles are smaller with respect to the wavelength of the excitation light, effective conductivity and the electronic scattering is reduced, affecting the SERS enhancement[120]. But, when the particle size increases within the nonorange, the SERS enhancement increases as it depends on the number of electron available[104]. In TiO_2-GLN, the SERS enhancement increased

when the particle size increased from 65 to 93 nm. Njoki et. al also observed that the SERS enhancement of the gold NPs on 4-mercaptobenzoic acid (MBA) increased when the particles sized increased from 50 to 90 nm[121]. As the Raman and SERS intensities of both anatase and GLN changes with the particle size, its effect can be better understood from the ratio value R obtained from equation 3.1. The R-value as seen in the insert A of figure 3.6, is significantly lower and distinct for the particles in the nano-range. This shows the ability of SERS in distinguishing the nanoscale particles from larger particles.

$$\frac{Intensity\ of\ TiO2\ peak\ at\ 144\ cm^{-1}}{Intensity\ of\ the\ GLN\ peak\ at\ 1639\ cm^{-1}} \qquad \text{(Equation 3.1)}$$

Although this method can clearly distinguish the NPs from larger particles, the effect of the different particle sizes in the nano-range on R requires further investigation. The behavior of the NPs can be altered by some external factors as well as the physicochemical properties of the NPs and understanding the effects of these factors on the R is necessary for more accurate size characterization of TiO_2-NPs using SERS. While the shape of the TiO_2-NPs used in this study was found to be inconsistent, other experimental factors and the inherent property of NPs such as agglomeration could impact the accuracy of the measurement and have been investigated.

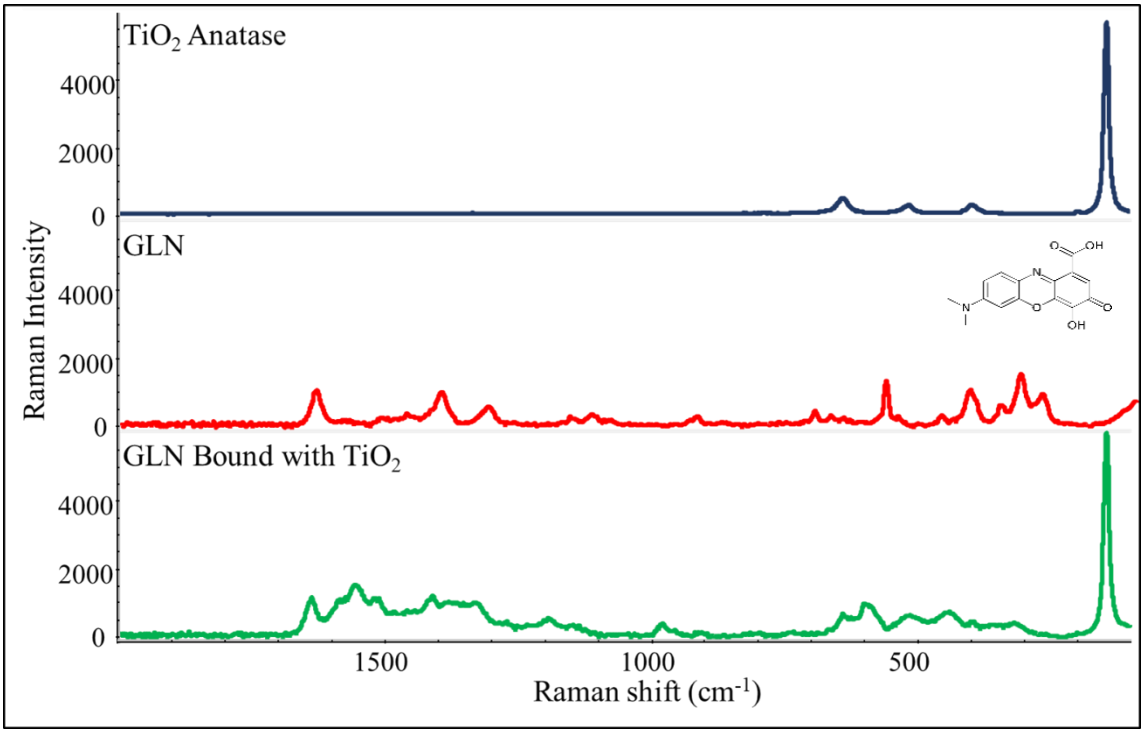

Figure 3.6 Raman spectrum of TiO_2 anatase, gallocyanin and SERS spectrum of anatase bound gallocyanin

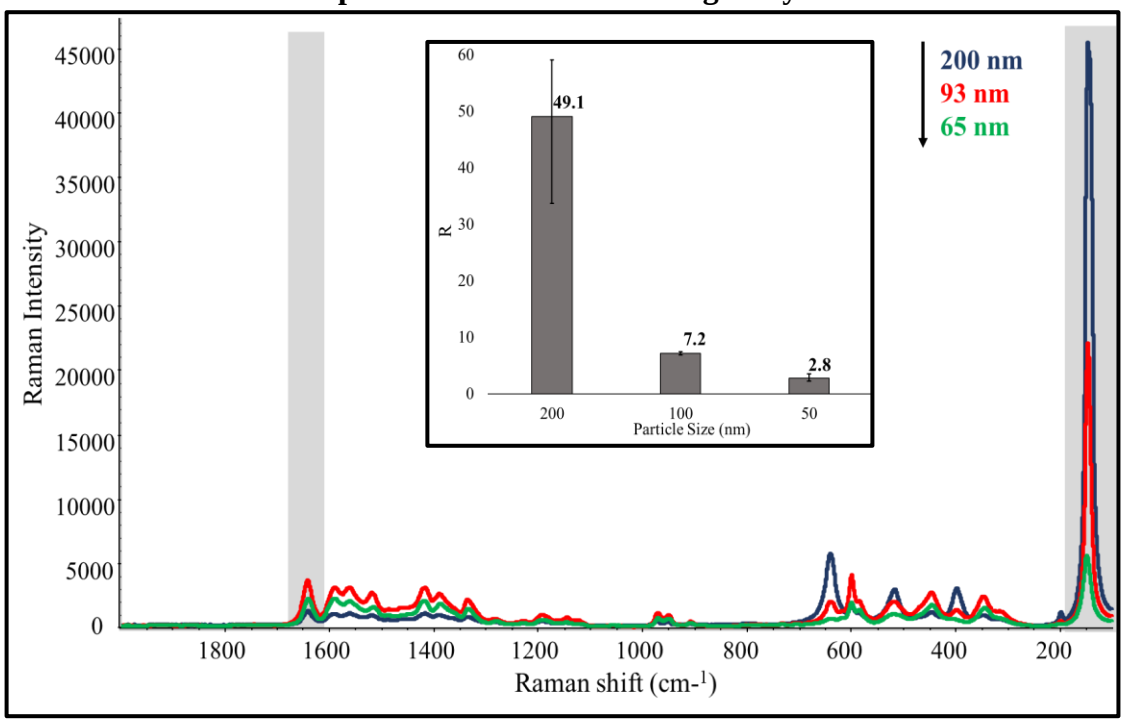

Figure 3.7 SERS spectra of 200, 93 and 65 nm TiO_2 particles. Insert A displays the R value associated each sample

3.3.4. Factors affecting SERS analysis of TiO_2-NPs

SERS showed promising results in distinguishing the NPs from larger particles. However, characterizing the particles in the nano-range can be challenging because of the unique physicochemical properties of the NPs. Therefore, the effect of these properties along with some experimental conditions needs to be evaluated to further explore the potential of SERS as an analytical tool for size characterization of TiO_2-NPs. The effect on the SERS analysis was evaluated in terms of the ratio value R. The factors first were characterized under primary and secondary factors. The primary factors included size, concentration of the particles and the concentration of the ligand. The secondary factors included pH, sonication treatment and the effect of dispersing agents.

3.3.4.1. Size

After examining the potential of SERS in clearly distinguishing the NPs from the larger particles, the next set of experiments examined the sizes under the nano range. The size characterization of the nanoscale particles is considered challenging and has only been achieved with electron microscopy and SP-ICP-MS. However, even using these techniques, TiO_2-Nps smaller than 20 nm is extremely difficult or impossible to characterize. The impact of the size on SERS analysis of TiO_2-NPs was analyzed in terms of the R-value. Figure 3.7 shows the changes in R with the size of the particles, regardless of variations in the concentration of the NPs and ligand. The particle size presented here is obtained from the TEM analysis of the sample and not from the supplier specifications. Figure 3.8(A) shows the cumulative R-value for the particle ranging from 173 nm to 8 nm, considering major variables affecting R, such as particle size, particle concentration and ligand concentration. The effect of each of the variables on R is discussed separately in

next section. From the figure, it can be identified that R decreases with the decreases in the size from 173 nm to 65 nm ($p<0.05$). However, for particles 65, 41, 29 and 8 nm, no significant difference in the value of R was found (One-way ANOVA, $p>0.05$). In other words, particles within the nano-range showed statistically similar R-values. This might be attributed to the unique properties of the NPs such as agglomeration. TiO_2-NPs are not soluble in the water but dispersed through sonication therefore, as explained by Derjaguin-Landau-Verwey-Overbeek (DLVO) theory, their smaller size and larger surface area allow them to interact with each other[122]. This particle-particle interaction not only increases their hydrodynamic diameter but also reduces the surface area for the ligand to bound to, which might affect the overall SERS enhancement from the NPs. In addition, the concentration of the ligand and the NPs can also saturate the system, saturating the signals, therefore the effect of their concentration on R needed to be investigated.

According to the definition by the European Union, the material containing particles in unbound, agglomerated or aggregation state and containing at least 50% particles with dimensions within 1 to 100 nm are classified as nanomaterials[142]. To evaluate the sensitivity of R to a mixture of particle sizes, we mixed the 41 nm particles with 93 nm particles at different proportions. The result (Figure 3.8 (B)) shows the R decreased with the decreasing proportion of 40 nm particles. As low as 10% of 40 nm particles can be detected based on the R. As the R between 8 and 65 nm is statistically insignificant, this method is potentially useful for screening for the nanoparticles in this range. However, the current limitation of this method is the lack of data between 65 and 100 nm due to the unavailability of the nanoparticle standards in this range.

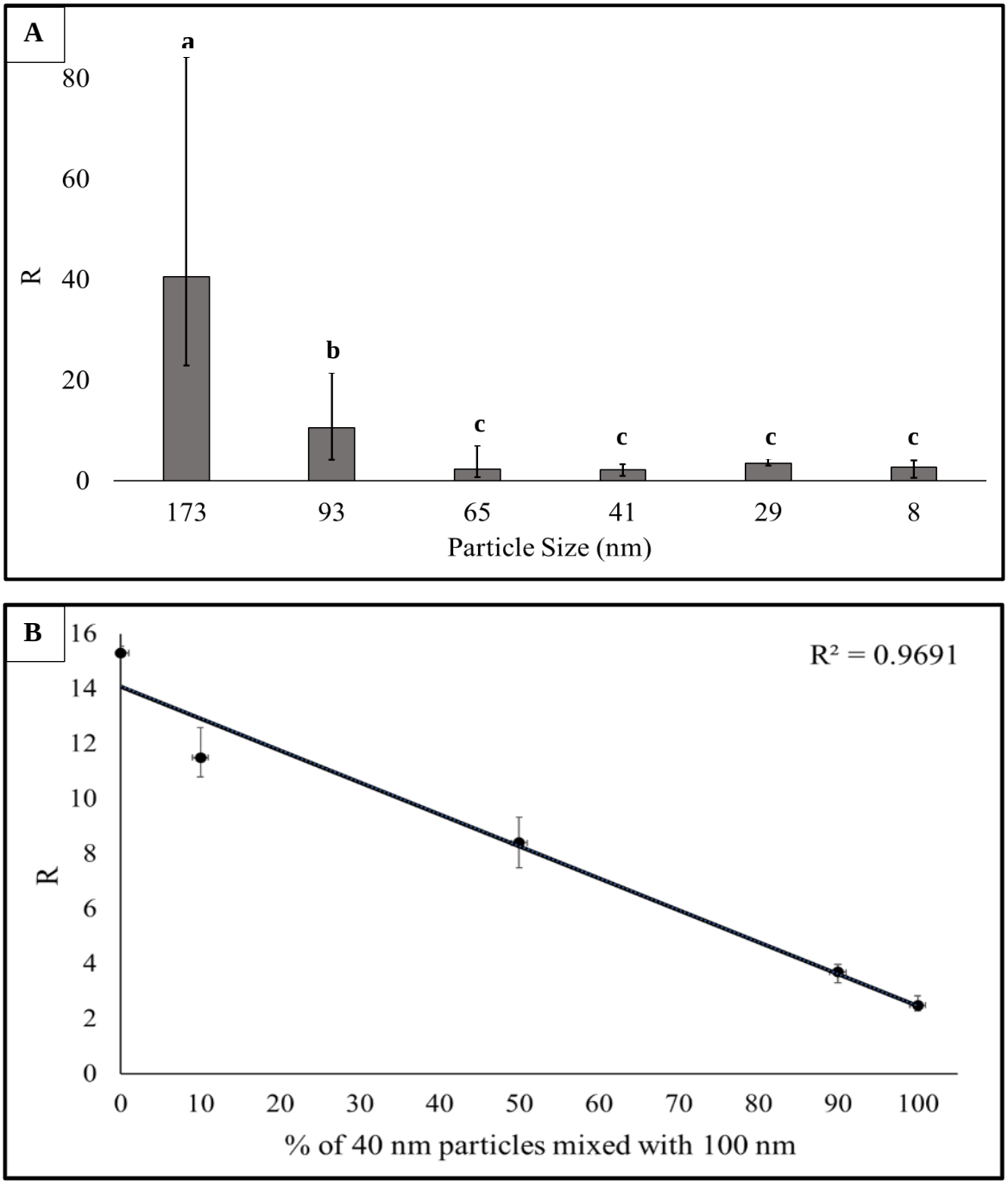

Figure 3.8 (A) Cumulative R value considering all the variable affecting R. Similar alphabets on each bar means no significant difference in the R value ($p>0.05$) (B) Linear relation between R and % of 40 nm particles mixed with 93 nm

3.3.4.2. Ligand Concentration

Three GLN concentrations 5,10, 20 and 50 µM were tested. Figure 3.9 shows the effect of different GLN concentration on the R of 40 and 93 nm TIO_2-NPs. The NPs concentration is kept constant at 0.2 g/L. Both 40 and 93 nm particles showed similar effects. The SERS intensity increased from 5 µM to 10 µM but the signal reaches the saturation at 10 µM and did not increase when the concentration was increased to 20 or even 50 µM. On the other hand, the intensity of the TiO_2 peak decreased with increasing in the GLN concentration. The decreases in TiO_2 intensity with increasing GNL concentration is a result of the surface layer of GLN on TiO_2-NPs. The thickness of the GLN layer around the NPs may increase with the increase of the GLN concentration, which limits the interaction of the photon with TiO_2. This data also suggests that, although the SERS effect is mainly dependent on the NPs, the ligand concentration plays an important role. Therefore, the GLN concentration was optimized to 5 µM in order to avoid surface saturation and to obtain the satisfactory R-value (>1). Besides, binding of GLN to the TiO_2-NPs requires about 30 minutes and vigorous shaking and rotation. Gentle shaking or less incubation time could result in insufficient binding, resulting in higher R, especially for the sample with higher particle concentration. Figure 3.10 shows the comparison of the R-value of 0.2 g/L 40 nm particle sample prepared with gentle and vigorous shaking. Vigorous shaking kept the particles suspended in the solution and provided opportunities to bind with the dye. On the other hand, the samples prepared with gentle shaking had particles sedimented at the bottom creating less surface area for the dye to bound, resulting in the lower SERS intensity, thereby increasing the R.

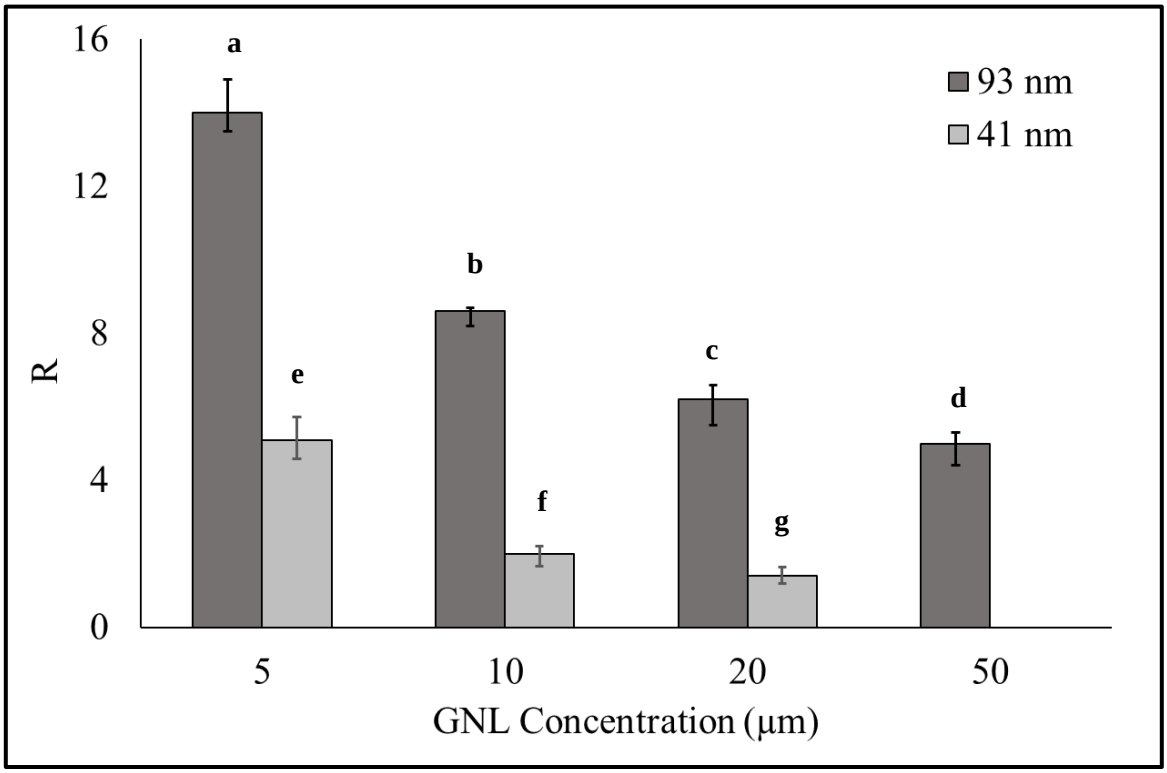

Figure 3.9 SERS Spectra of 0.2 g/L 93 nm and 41 nm particles prepared with 50, 20, 10 and 5 µM GLN. Different alphabets on each bar represents significant difference in the R value ($p<0.05$)

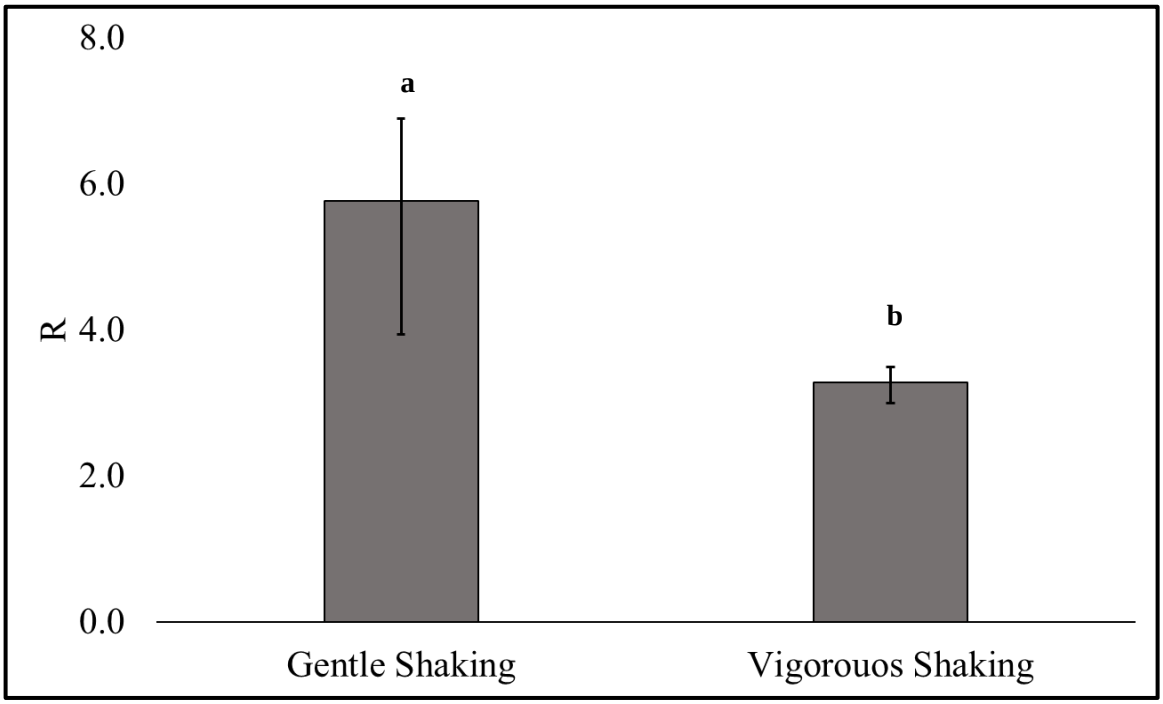

Figure 3.10 Effect of gentle shaking vs vigorous shaking on R. Different alphabets on each bar represents significant difference in the R value ($p<0.05$)

3.3.4.3. Particle Concentration

The investigation of the effect of particle concentration on R is very significant as it can help determines the limit of detection of the method. Four different TiO_2-NPs concentration with a logarithmic reduction from 0.2 g/L to 0.0002 g/L were analyzed to examine its impact on R. Four particle sizes were chosen to understand the effect of concentration on R across the nano range: 93, 41,29 and 8 nm. The same analysis protocol was followed as discussed above and GLN concentration was kept constant at 5 µM. Each sample was bath sonicated for 10 minutes and prepared by vigorous shaking upon mixing with GLN to avoid particle sedimentation. Figure 3.11 depicts the effect of different concentration for different particles on R. The R-value for the 93 nm sample is significantly higher for the 0.2 g/L sample ($p<0.05$) which decreases and is statistically indifferent to the lower concentrations (0.02, 0.002 and 0.0002 g/L) ($p>0.05$). GLN concentration may affect the inconsistency in the R-value across the concentration range. At higher concentration for larger size particles, 5 µM concentration may be insufficient. Increasing the GLN concentration from 5 to 10 µM resulted in statistically constant R (8.3) for the 93 nm particles across the concentration range (data not shown). Contradictory, for 41 and 29 nm samples, the R-value remains constant across the concentration range ($p>0.05$). Neither size of the concentration of the NPs impact the R for these samples. Zhao et. al. conducted similar experiments on 200, 100 and 30 nm particles using Myricetin as a ligand and demonstrated the constant R for 0.2 and 0.02 g/L concentrations[28]. Furthermore, in the present study, the analysis of the 8 nm particles was found to be difficult for the lower concentration because of the extremely small particle size. For the higher concentration (0.2 g/L) the R for the 8 nm particles was found statistically similar to that of other particles

in the nano-rage however, for the lower concentration, the spot identification on the microscope is challenging, which reduces the accuracy of the measurement. Overall, based on the present data the conclusion can be drawn that the R is independent of the concentration for the particles however, optimization of the correct GLN concentration is necessary to obtain accurate results. Moreover, accurate and reproducible results were difficult to achieve for the 8 nm particles, due to its extremely small size.

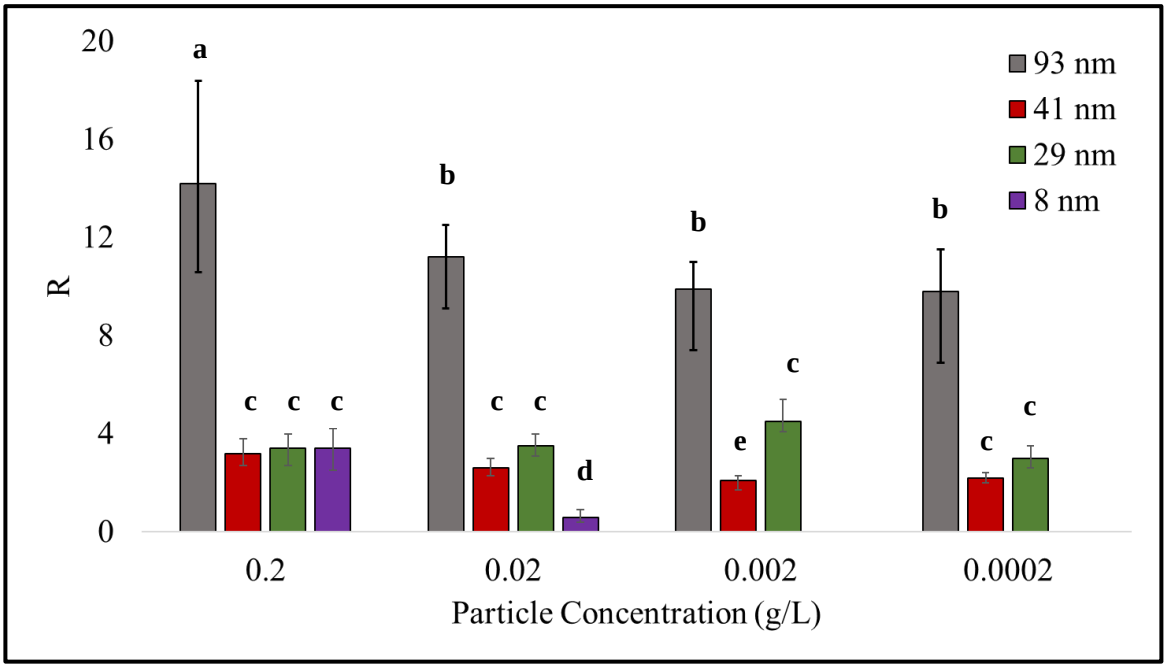

Figure 3.11 The impact of concentration for the various size of TiO_2-NPs on R. Different alphabets on each bar represents significant difference in the R value ($p<0.05$).

3.3.4.4. pH

TiO_2-NPs are insoluble in water and remain in the dispersed form. However, due to their smaller size and strong particle-particle interaction, they easily form agglomerate and sediment down. In the present study, the SERS intensity of the particles relies on two aspects: the SERS effect gained from the NPs and the aggregation of the particles on the slide. When particles are aggregated on the slide, it concentrates the particles in one place thereby allowing maximum number of particles to be detected under a laser spot. Therefore, the aggregation is favored upon addition of the ligand in the NP suspension. However, the initial agglomeration of the particles increases its hydrodynamic diameter and reduces the surface area for the ligand to bound to. Due to this, the SERS effect of the NPs on ligand may get affected, affecting the overall R. Hence, aggregation may play critical role in the SERS analysis of the NPs. Moreover, as discussed in the previous sections, R for the particles within nano-range was found to be statistically similar. Therefore, the impact of agglomeration on R needs to be evaluated to better understand its role in SERS analysis of TiO_2-NPs. Three different types of stabilization techniques were applied to study the dispersion effects on R. Charging the particles by changing the pH, Ultrasonication and using dispersing agents.

The dispersion ability of the particles can be altered by changing the pH of the suspension. Changing the pH of a solution changes the surface charge of the particles which could promote dispersion of aggregation depending on the types of the particles and its isoelectric pH. Isoelectric pH is the point where the particles have zero surface change. But at lower or higher pH the particles possess positive or negative surface change respectively. The negative or positive surface charge creates strong electrostatic repulsive forces,

suppressing the aggregation. The repulsion is strong enough to overcome the weak van der Waals bond between the particles, however, when the surface charge becomes close to zero, it weakens and allows the particles to form aggregates. The isoelectric pH of the TiO_2 around 5.8[123]. Therefore, reducing or increasing the pH away from 5.8 should charge the particles, promoting dispersion. Jiang et al. reported that pH lower than 4.2 or higher than 8.2 may allow the maximum dispersion[122]. The effect of the pH was examined on 65 nm particles. The particles (0.2 g/L) were fist dispersed in water by following the standard protocol. The pH was adjusted to approximately 2 and 10 using HCL and NaOH respectively. The particle size analysis was performed immediately using DLS to determine the effect of pH on size distribution. The SERS analysis was also performed simultaneously to examine its influence on R and the results are shown in figure 3.12. The DLS data shows that the pH treatment was able to reduce the hydrodynamic diameter of the particles compared to the control, with basic pH (pH 10) being more effective than acidic pH. Nonetheless, this approach was considerably ineffective, and the particles were still found largely aggregated. The standard deviation of the measurement was considerably higher and size distribution of the pH treated particles was wide-ranging (data not are shown). This indicated the limitation of DLS in the accurate measurement of the particle size in the largely agglomerated system. The results obtained here are different than those reported by Jiang et al., where the researchers were able to lower the size of the TiO_2-NPs considerably by pH adjustment[122]. In the SERS analysis, no significant difference in the R was observed for the pH adjusted samples compared to the control ($P<0.05$). Both DLS and SERS results suggest that the particle stabilization using pH adjustment did not have any effect on the SERS analysis of the TiO_2-NPs. It remains

unclear if large agglomeration plays any role in the SERS measurement therefore, other dispersion techniques were investigated.

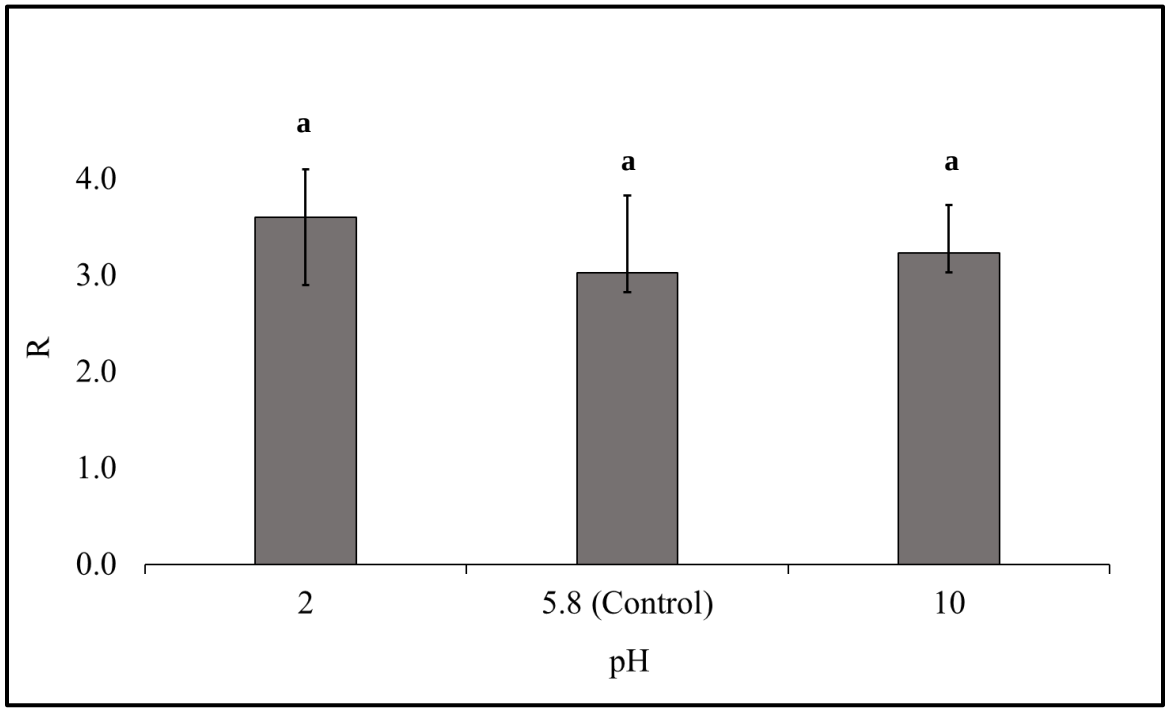

Figure 3.12 Effect of pH adjustment of 0.2 g/L, 6 5 nm particles on R. Similar alphabets on each bar means no significant difference in the R value (p>0.05).

3.3.4.5. Ultrasonication

Ultrasonication is the most commonly used effective technique to disperse the nanomaterials or particles in a suspension[117]. Ultrasonication creates cavitation by pulling apart the liquid, which can impose enough shear pressure to overcome weak forces of particle agglomeration[122]. Probe and bath sonication are the most commonly used ultrasonication methods. Bath sonication creates active cavitation zones whereas probe sonication creates a single zone of high concentration of cavities[122]. Some researchers have shown the effectiveness of the probe sonication in comparison with bath sonication for dispersing the NPs[117,122,124]. However, it has also been demonstrated that probe sonication could also promote further agglomeration[124]. The formation of a single zone of cavity formation and destruction during probe sonication can further enhance particle-particle interaction and promote agglomeration by kinetic coagulation[122]. Therefore, the effectiveness of both probe and bath sonication on the SERS measurement was examined on the 65 nm particles. The initial sample preparation (control) for all the analysis included 10 minutes bath sonication step for the preparation for NPs suspension. The probe sonicated sample was first dispersed by bath sonication for 5 minutes and then probe sonicated for 10 minutes. Both samples were then mixed with the GLN and analyzed on Raman microscope using standard protocol. The particle size analysis also was performed using DLS to determine the effectiveness of sonication on dispersion. As shown in figure 3.13, no significant difference in the DLS size measurement between both treatments was found. Similarly, R for the probe sonicated sample was found slightly lower than the probe sonicated sample but no statistical difference between both measurements was found ($p>0.05$). These results indicate that there was no considerable change in the hydrodynamic

diameter of both particles was observed between probe and bath sonicated samples. Therefore, no significant difference in the SERS analysis can be expected. However, some researchers have also found that ultrasonication in combination with dispersing agents was most successful in effectively dispersing the NPs[122,125]. Therefore, the next set of experiments examined the effectiveness of the combined stabilization technique on SERS analysis.

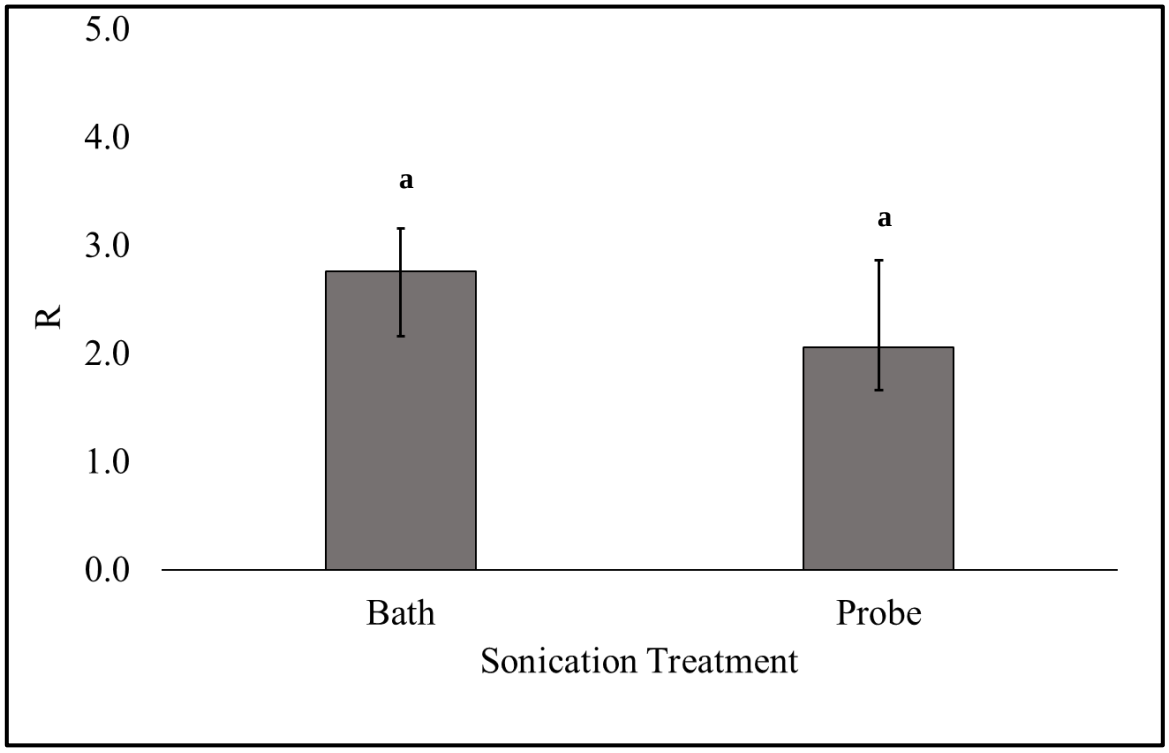

Figure 3.13 Effect of sonication treatment on 0.2 g/L, 6 5 nm particles on R. Similar alphabets on each bar means no significant difference in the R value (p>0.05).

3.3.4.6. Dispersing Agents

Another electrostatic stabilization technique used for the NPs dispersion is using the dispersing agents. Similar to pH, the dispersing salts can control the surface charge of the NPs by dissociating into charged ions when dissolved in the solution. These ions are absorbed by the ionic particles such as TiO_2, increasing the surface charge of the particles. Many chemical compounds and their salts have been used as dispersing agents in achieving uniform dispersion of the NPs. Polyethyleneimine (PEI 600), ammonium polymethacrylate (Darvan C), Triton X100 and salts containing pyrophosphate such as sodium pyrophosphate (SPP) have been used by other researchers as a dispersing agent in combination with ultrasonication[122,125]. We examined the effectiveness of SPP in combination probe sonication on TiO_2-NPs. The 65 nm particles were first dispersed in 0.001 M SPP solution and dispersed using a bath or probe sonicator for 10 minutes. The Particle size of both samples was measured by DLS. The absorption of pyrophosphate ions onto TiO_2 surface changed the surface charge and showed significant decrease in the particle size for both probe and bath sonicated samples compared to the control. Probe sonicated samples with SPP demonstrated the lowest hydrodynamic diameter of 191 nm whereas bath sonicated samples with SPP indicated 670 nm (Figure 3.14 (A)). In addition, a similar test was also performed with 29 and 93 nm particles and the stability of the dispersion was assessed. The results showed that probe sonication in presence of SPP was more effective for 29 nm particles compared to bath sonication. However, for the larger size, for example, 93 nm, both probe and bath sonicated treatments did not have significant difference. Also, small size particles (29 and 65 nm) produced smaller hydrodynamic diameter suspension compared to larger particles (93 nm) was more had smaller

hydrodynamic diameter compared to bath sonication. We also assessed the stability of the suspension. Both bath and probe sonicated samples in presence of SPP showed excellent stability with no statistical difference in the particle size over four days ($P<0.05$). This data indicates that dispersing agents such as SPP provides more effective particle stabilization for nano-sized particles compared to any other approaches. Furthermore, the combination of two dispersion strategies such as sonication and electrostatic stabilization further reduced the hydrodynamic diameter producing most stable dispersed suspension.

The samples prepared with SPP were then mixed with GLN and analyzed on Raman microscope to examine its effect on R. Unfortunately, the absorption of the pyrophosphate ions onto the TiO_2 surface did not allow the ligand to bind with the particles. Therefore, no SERS peak from GLN was observed (Figure 3.15). Additionally, SPP is not a SERS active compound so even though it was absorbed onto the TiO_2 surface, it did not produce any SERS peak. These results show the specificity of GLN toward TiO_2 particles and its importance in the analysis of the NPs. Although the simultaneous treatment of probe sonication and electrostatic stabilization resulted in the most stable and dispersed suspension, the application of this strategy in SERS analysis using GLN as a ligand is not successful.

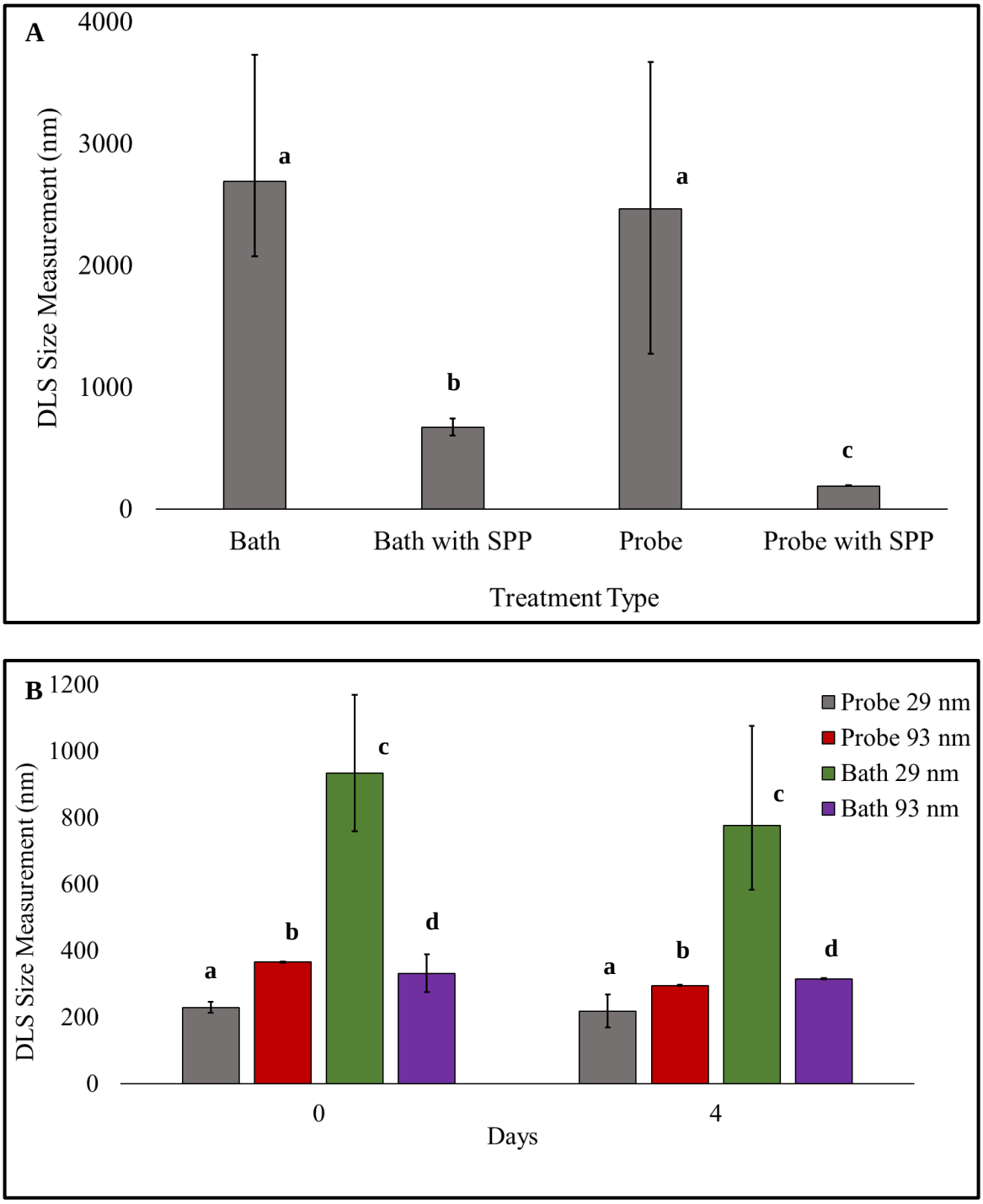

Figure 3.14 (A) DLS Particle size measurements of probe and bath sonicated 65 nm particles (0.2 g/L) with and without SPP, (B) Stability of both probe and bath sonicated 29 and 93 nm (0.2 g/L) particles in presence of SPP over four days. Similar alphabets on each bar means no significant difference in the R value ($p>0.05$). For figure (B the statistical analysis for each treatment was performed separately.

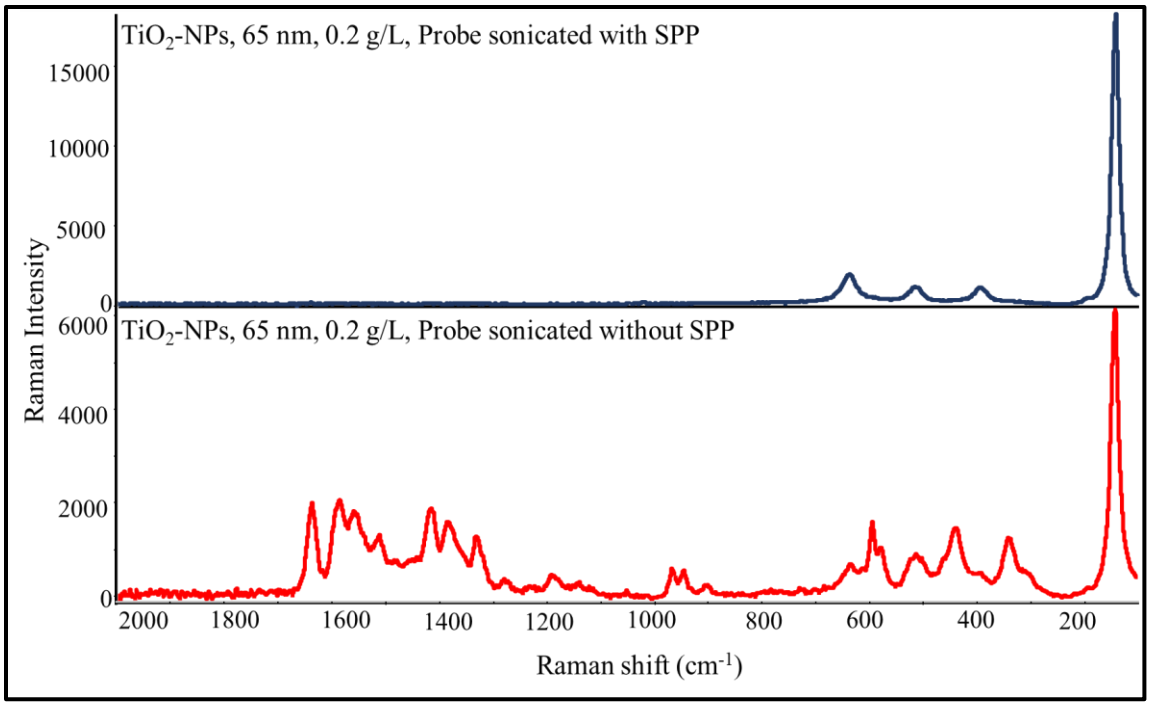

Figure 3.15 SERS Spectra of 65 nm, 0.2 g/L TiO_2 particles dispersed by probe sonication with and without SPP

3.4. Conclusion

In conclusion, in the present study, we assed SERS and an analytical tool in the size characterization of TiO_2-NPs and evaluated the factors affecting the analysis. We demonstrated that SERS is a powerful tool with selectivity and sensitivity in identifying different TiO_2 polymorphs such as anatase and rutile. We also proved its sensitivity in rapid and easy discrimination of the Nano-size particles from larger particles from the ratio value generated from the peak intensities of TiO_2 to GLN. Additionally, we also showed the effect of numerous parameters on the SERS measurement of TiO_2-NPs such as size and concentration of the particles, concentration of the ligand and experimental parameters such as point selection and incubation method. Various strategies of dispersion of NPs in the aqueous solution was evaluated. Methods such as pH adjustment and ultrasonication did not show any significant effect on particle dispersion as well as SERS analysis. However, the use of a dispersing agent, sodium pyrophosphate in combination with probe sonication resulted in significantly improved and stable dispersion. But this strategy was not successful in the SERS analysis as the GLN was not able to attach with the TiO_2 because of the surface modification by the absorption of the pyrophosphate ions. This method could not successfully differentiate the different sizes of the particles within the nano-range. Which could be a cause of the particle agglomeration or the equivalent enhancement SERS enhancement from the particles. Nevertheless, we noticed that the intensity of the TiO_2 peaks varies with the particle size therefore, further analytical strategies based on the TiO_2 peak for a fixed concentration, using Raman mapping should be explored.

CHAPTER 4

Evaluating the Potential of Filter-Based Raman Mapping for the Analysis of TiO_2-NPs

Abstract

In this chapter, we evaluated the potential of Raman mapping technique in combination with membrane filtration as a rapid scanning tool to analyze TiO_2-NPs. Raman imaging instrument is the latest and advanced technique capable of collecting thousands of spectra within a few minutes. We collected the map of four different sizes of TiO_2, 173,93,41 and 5 nm samples after dispersing using probe sonicator with sodium pyrophosphate as a dispersing agent. Our study found that the 100X magnification was the most capable of detecting the smaller size particles up to 5 nm up to the concentration as low as 0.0004 g/L. Moreover, we demonstrated the positive linear correlation between particle size, its hydrodynamic diameter and % map area covered by the particles. Besides, we established the linear relationship between the Raman intensities corresponding to their particle size at 0.04 g/L, which can be used in distinguishing the particles. At lower concentrations, no statistical difference was found in the Raman intensities of particles within nano-rage, although, the larger particles showed significantly higher intensity values.

4.1. Introduction

New and advanced technologies is been developed in the detection and characterization of nanomaterials. Amongst all, Raman spectroscopy and different techniques associated with it such as Spontaneous Raman Spectroscopy, Surface Enhanced Raman Spectroscopy, Resonance Raman Scattering and Coherent Raman are emerging as rapid and ultra-sensitive tool with diverse applications because of its capability to detect up to a single molecule[126]. One more addition to the recent advancement in the area of Raman scattering is Raman Imaging and Mapping. Raman imaging techniques has seen substantial interest as it allows a sample distribution map and label free imaging of chemical compounds and microorganisms[126]. The advanced Raman Imaging instrument provides impressively short spectrum collection time, collecting thousands of spectra in just a few minutes.

Raman mapping has been found effective in many applications. Its application in food and agriculture includes Polyacetylenes in vegetables, pathogen detection, bacterial identification, food composition analysis, protein evaluation, adulterant detection etc.[127]. Many researchers have shown its application in label-free mapping of bacteria[128-130]. Additionally, its application in medical research includes mapping the neurotic plaques in the brain of Alzheimer's patients and the diagnosis of cancer[131,132]. Research has also demonstrated its application in biomedical and drug delivery by label-free imaging of drug delivery and intracellular uptake of nanocarriers[126,131,132]. Several researchers have also explored mapping of nanoparticle using Raman imaging techniques[133,134]. However, to the best of our knowledge, Raman mapping approach in identification and size characterization of the nanoparticles has not to be explored.

Titanium dioxide nanoparticles (TiO_2-NPs) are widely used in many applications including food and consumer products. With the recent research exploring its potential toxicity, size characterization of TiO_2-NPs becomes increasingly important. The structure of the TiO_2 particles is highly sensitive and can be detected using a simple Raman technique without the requirement of signal enhancement from the substrate. Moreover, Raman scattering of the metal particles is heavily influenced by their particle size, especially within the nano-range. Considering these advantages, the objective of this study was to evaluate the potential of filter-based Raman mapping technique in the analysis of TiO_2-NPs.

We assessed the samples with particle size ranging from 8 to 173 nm and concentration from 0.04 to 0.0004 g/L to evaluate the potential of Raman mapping in the analysis of TiO_2-NPs based on the Raman intensities generated by the particles. The membrane filtration technique was used to filer and concentrate the particles. TiO_2-NPs are dispersed in aqueous solutions and form large agglomerates. However, using the combination of ultrasonication and dispersing agents, their hydrodynamic diameter can be efficiently controlled, allowing them to retain on a 100 nm filter membrane. The agglomeration and formation of a monolayer on a filter membrane provide size dependent enhancement to the Raman signals from the particles. Also, the filtration technique can permit large sample volume which can significantly push the detection limit making it suitable for environmental applications.

4.2. Materials and Methods

4.2.1. Materials

Titanium dioxide Anatase powder samples of particle sizes 8,41,93 and 173 nm (Size obtained from TEM analysis) were purchased from US Research Nanomaterials Inc. (Houston, TX) and MK Nano (Mississauga, ON) were used in this study. Sodium pyrophosphate (SPP, $Na_4P_2O_7$), purchased Sigma Aldrich (St. Louis, MO) was used for particle dispersion. All the chemicals and reagents were prepared with ultrapure water (18.2 MΩ·cm) from Barnstand Smart2Pure Water Purification System (Thermo Scientific, Waltham, MA). Hydrophilic Polytetrafluoroethylene (PTFE) filter membrane with 0.1 µm pore size and 25 mm diameter were purchased from Millipore Sigma (Burlington, MA).

4.2.2. Sample Preparation

Titanium dioxide suspensions, 0.4 g/L, were prepared in 0.005 M SPP solution made in ultrapure water. The samples were first sonicated in a bath sonicator [Branson 2000, Branson Ultrasonic, Danbury, CT] for five minutes to initially disperse the particles and break the large lumps. To break the agglomerates and uniformly disperse the particles, the TiO_2 suspension was then sonicated using a probe sonicator (Fisher Scientific, Waltham, MA) for 10 minutes at 75% Amplitude. The particle size of each sample was analyzed using DLS. For the Raman measurements, sample dilutions of desired concentrations (0.04, 0.004 and 0.0004 g/L) were prepared with 0.005 M SPP solutions and properly mixed. One milliliter of each sample was then filtered at negative 50 kPa pressure on 0.1 µm PTFE filter membrane using the filtration system (Millipore Sigma, Burlington, MA) with a chemical duty vacuum pump (Model WP6111560, Millipore Sigma, Burlington, MA). The filtration assembly with a 13 mm holder was used therefore the sample was filtered in the

13 nm area. However, a 25 nm filter membrane was used to fit onto the filtration system base and to ensure accurate filtration without any air gaps. The filter membraned was allowed to air-dry for 5-10 minutes and fixed on a glass slide using double sided tape for the analysis under Raman microscope. Figure 4.1 illustrated the components of the membrane filtration system used for the present study.

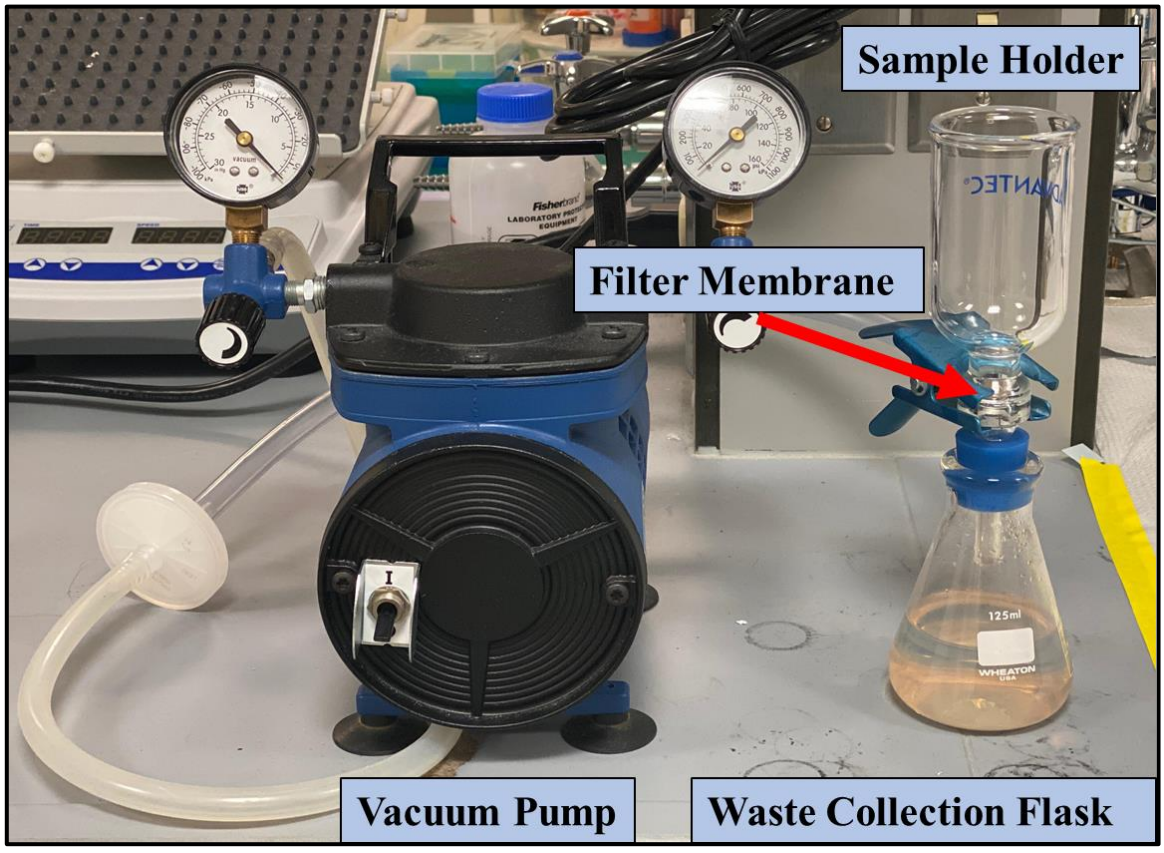

Figure 4.1 Components of a vacuum membrane filtration system

4.2.3. Raman Mapping of TiO_2-NPs

The Samples filtered on a filter membrane were analyzed on a Raman imaging microscope (DXRxi, Thermo Scientific, Waltham, MA) equipped with a 780 nm laser. The Raman instrument used in this study was different than the one used in the previous experiments. DXRxi Raman microscope is the most advanced and most recent version equipped with rapid mapping and imaging techniques. The instrument is capable of collecting thousands of spectra within a few minutes and therefore is preferred for the mapping of an area containing analyte on a filter membrane. All the analysis were performed using 20 and 100X microscope lenses and 10.0 mW laser power. The slit aperture and acquisition time was set at 50 µm and 0.05 seconds respectively. The data was collected and analyzed using OMNICxi software (Thermo Scientific). At least 15 spots were randomly selected for each replicate. The mapping image was analyzed using the peak height tool and adjusting the intensity threshold bar in the analysis mode on the OMNICxi software. Discriminant analysis on TQ Analyst 9.7 software (Thermo Scientific) was performed to average the spectra and to obtain the statistical spectrum.

4.2.4. DLS and Statistical Analysis

All the Dynamic Light Scattering (DLS) measurements during this study were performed after probe sonication treatment of each suspension prepared in SPP solution. All the samples were diluted appropriately to achieve the attenuation number between 6 and 8 in order to obtain accurate measurements. About 1 ml of the sample was analyzed with Nano-ZS Zetasizer (Malvern Instruments, Malvern, UK) and the measurements were recorded. Each analysis was performed in triplicates and mean values with error as standard deviation was reported.

4.3. Results and Discussion

Before, measurement of Raman imaging microscope, the hydrodynamic diameter for each sample was measured by DLS. Table 4.1 presents the compilation of size data obtained from supplier, electron microscopy and DLS with standard deviations. The DLS data of the particles dispersed with SPP and probe sonicated shows significantly lower numbers than presented in Table 3.2. Although the hydrodynamic diameter of each sample is statically different (1-way ANOVA, $p<0.05$), their size range from approximately 200 to 350 nm. Based on this results 0.1 µm pore size of the membrane was chosen for the filtration step to allow maximum particle retention. PTFE membrane was selected because of its low background noise during Raman measurement and excellent compatibility with various chemicals and solvents. Vacuum filtration technique was chosen over syringe filtration to obtain accurate and rapid filtration. Moreover, vacuum filtration can also handle large sample size to analyze lower concentration samples in environmental applications. Membrane diameter of 25 nm was chosen to fit on the filtration base however, however, filtration was carried out using a 13 mm holder to obtain filtration accuracy and avoided any air-gaps.

Table 4.1 Hydrodynamic diameter of particles prepared in 0.005 M SPP solution and dispersed with probe sonication. Different alphabets mean statistically different results ($p<0.05$)

Supplier Size Claim (nm)	SEM/TEM Analysis (nm)	DLS Measurements (nm)
5	8±2	360±6[a]
40	41±7	325±8[b]
100	92±28	289±1[d]
800	173±66	192±4[e]

4.3.1. Raman Mapping of TiO_2 particles

Each sample prepared by the protocol described above was analyzed using Raman imaging microscope. Each sample was properly focused in such a way that the collected mosaic area was in proper focus. Unfocused areas produce low or no signal intensity therefore, the membrane was carefully placed on to the double-sided taped slide such that the surface was leveled, and the wrinkles were minimized. For all samples, the map was collected for approximately 400-450 µm of the area. Important measurement parameters such as laser power, exposure time and pixel step-size were optimized such a way that optimum signals for each sample were obtained with the lowest analysis time. The laser power of 10.0 mW, exposure time of 0.05 seconds and analysis step-size of 5 µm pixels was selected to obtain each analysis time around 5 minutes. Figure 4.2 (A) and (B) shows the map of the negative control and the membrane with 93 nm TiO_2-NPs, 0.04 g/L concentration. Figure (C) and (D) shows corresponding Raman spectra of both control and

sample respectively. In the Raman maps obtained in this study, the blue color represents the lowest intensity or absence and red represents the highest intensity of the presence of the peak analyzed. The map of negative control shows characteristic signals of PTFE membrane at 285, 382, 731 and 1377 cm^{-1} and absence of the TiO_2 peak. Both TiO_2 and membrane peak can be observed in figure (B). The signature peak of the TiO_2 is found to be a little bit shifted from 144 to 137 cm^{-1}. This could be because of different Raman instruments used in this study. Instrument component such as optical modules which is responsible for the laser illumination and collection of Raman scattered photons could result in minor peak deviations[135].

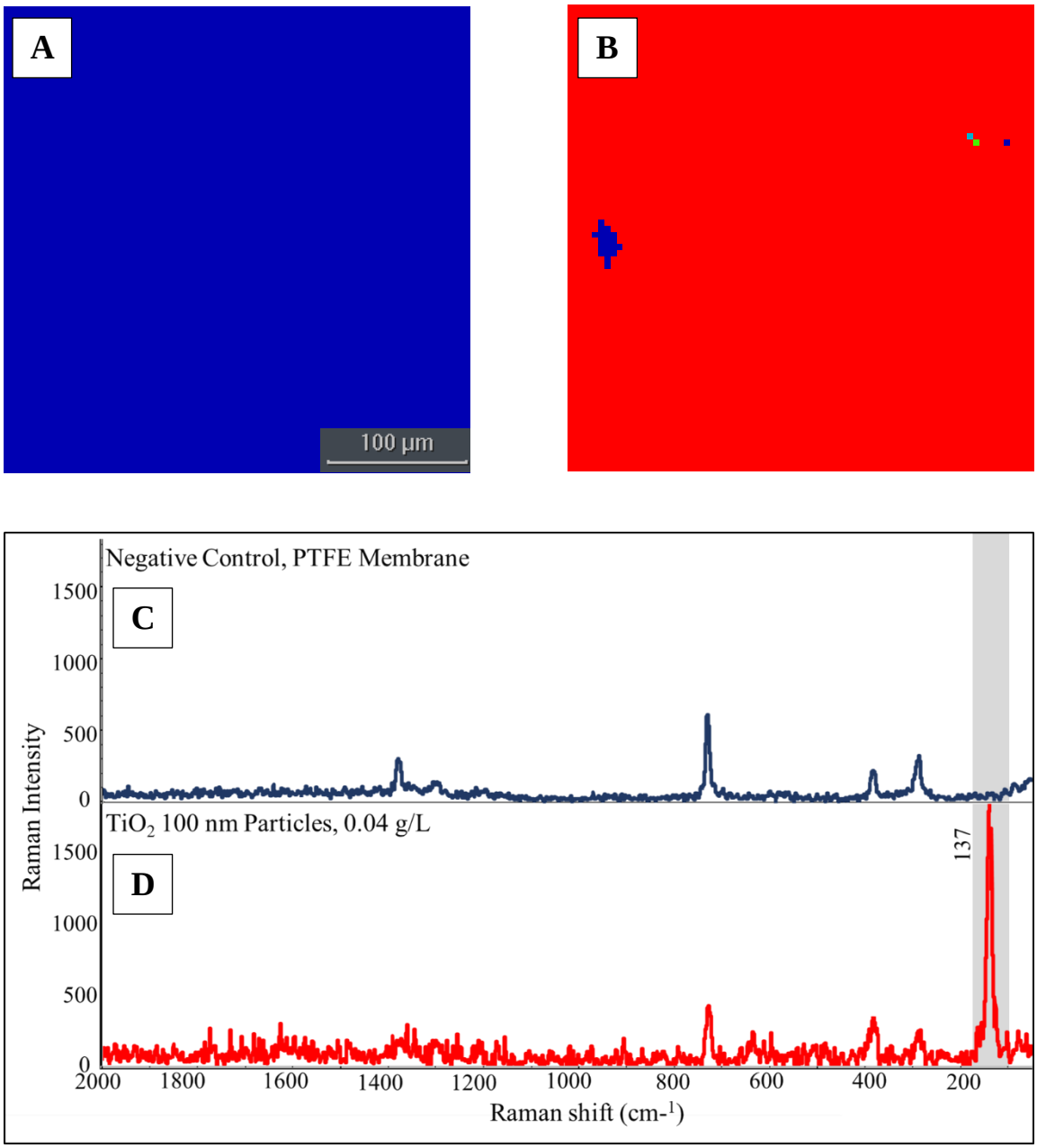

Figure 4.2 (A) and (B) are the Raman map of negative control and are 93 nm, 0.04 g/L TiO_2-NPs respectively. Figure (C) and (D) shows the corresponding Raman spectra of negative control and TiO_2 particles respectively.

4.3.2. Objective Lens

The next set of experiments were performed with both 20X and 100X objective lens to identify the difference in the measurements and preferred lens that can efficiently analyze nano-sized and larger particles. Three different concentrations for each sample, 0.04, 0.004 and 0.0004 g/L were analyzed. Figure 4.3 (A) through (L) depicts Raman maps of different concentrations of 173 and 8 nm particles. Figure (A) to (C) and (D) to (F) are the maps of 173 nm particles containing three different concentrations mentioned above and analyzed using 20X and 100X objectives respectively. As shown in the figures and table 4.2, at 0.04 and 0.004 g/L concentrations, the entire map area was covered by the particles however, at 0.0004 g/L concentration, 100X objective was able to detect particles more efficiently than 20X. Similarly, for the 8 nm particles, no differences in the map results were observed between two different objectives at higher concentrations (Image (G) and (J)). However, for 0.004 g/L concentration, the number of particles detected by the 100X was significantly higher than 20X ((H) and (K)) and no particles were detected by the 20X objective at even lover concentration of 0.0004 g/L. But, the 100X objective was still able to detect the particles ((I) and (L)).

For mapping under Raman imagining microscope, the sample is required to be in focus to achieve optimum distance for the laser to interact with the analyte. Laser illumination on and light collection from the sample in Raman spectrometer involves components such as mirrors, fiber-optic probes, detector and microscopic objectives. In addition to the acquisition time and laser power, the performance of Raman measurements depends on optical parameters such as the optimum angle of collection and optical throughput[135]. The light collection efficiency of the microscope is directly related to the Numeric Aperture

(NA) of the objective. NA is the size of the conical beam of the light passing through the lens[136]. Hence, the objective with higher NA has higher solid angle of light collection. As the magnification increases, NA increases and reaches 0.95 at the very most in practical cases. The NA of the 20X and 100X objectives used in this study were 0.40 and 0.90 respectively. At higher magnification and NA, the beam comes to the focus as very short working distance and over a wide angle[135]. Therefore, the illumination profile of the sample analyzed through 20X and 100X is completely different effecting the overall analysis. Our results showed that analysis of larger particles such as 173 nm through different microscope objectives produced almost similar analysis. But the smaller particles, for example, 8 nm, showed better results at higher NA as a result of better focus and illumination profile. From the Raman maps in figure 4.3 and table 4.2, no significant difference in the % area covered by the particles was observed at higher concentrations for 20X and 100X magnification. However, as the concentration and particle size decreased, 100X was able to detect particles more efficiently. Similarly, no significant changes were observed in the peak intensity of either particle at higher concentrations (0.04 g/L) while analyzed at different magnification (Figure 4.4 (A)). But as seen in figure 4.4 (B), significant increase in the peak intensity for both particles was observed at 0.0004 g/L concentration at 100X magnification. Therefore, from this study it can be concluded that 100X magnification is more efficient in analyzing lower size and concentration of TiO_2 particles, which is very important for the analysis of NPs in food and environment application. Hence, the Raman map was collected using a 100X objective in the rest of the study. The differences observed in the peak intensities and map area between the particles regardless of the objective is discussed in the following section.

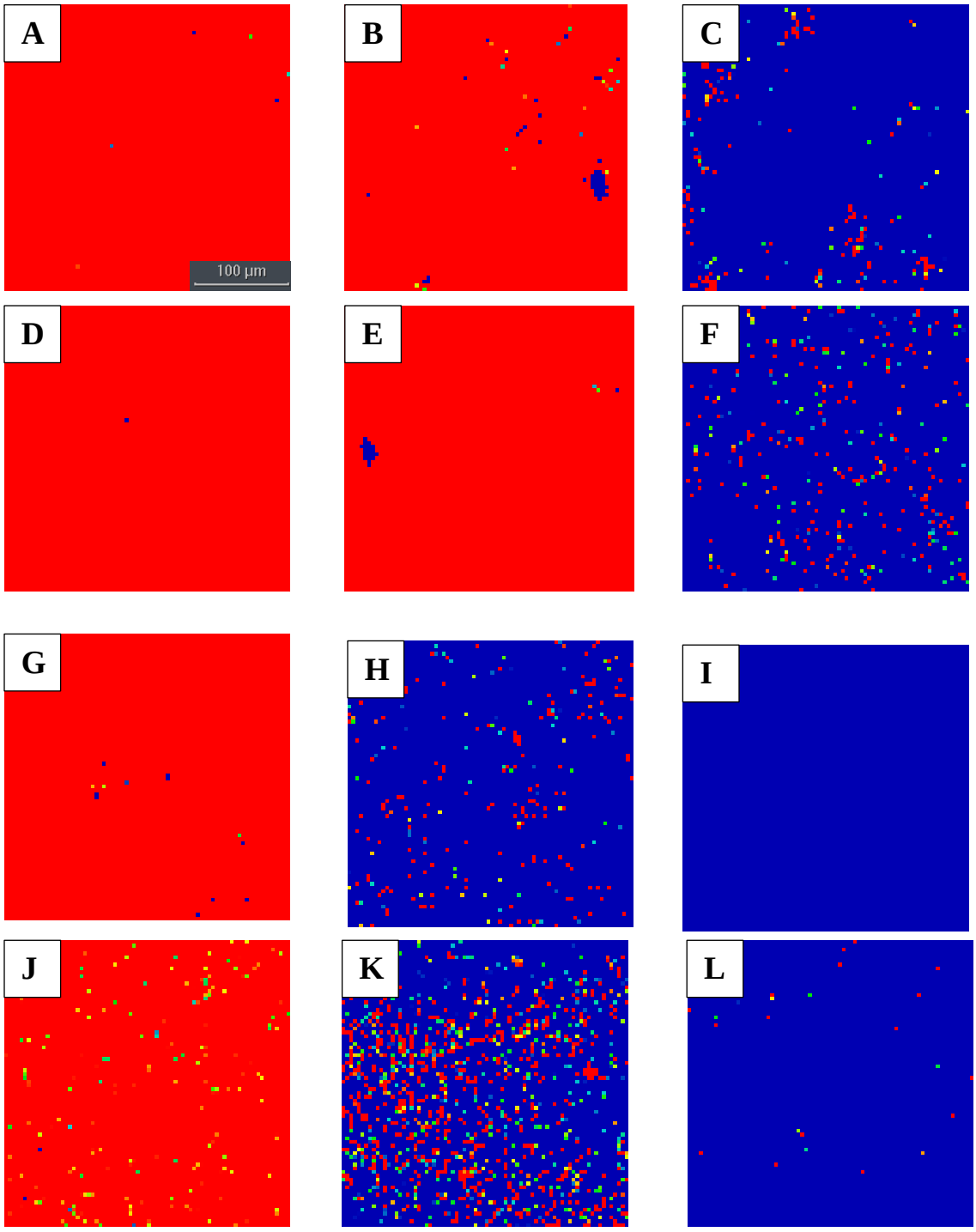

Figure 4.3 (A), (B) and (C) are the maps of 93 nm TiO_2-NPs 0.04, 0.004 and 0.0004 g/L concentrations respectively, collected from 20X objective. (D), (E) and (F) are the map of same particles collected from 100X objective respectively. (G), (H) and (I) are the map of 8 nm TiO_2-NPs of 0.04, 0.004 and 0.0004 g/L concentrations collected from 20X objective. (J), (K) and (L) are the map of same particles collected from 100X objective respectively.

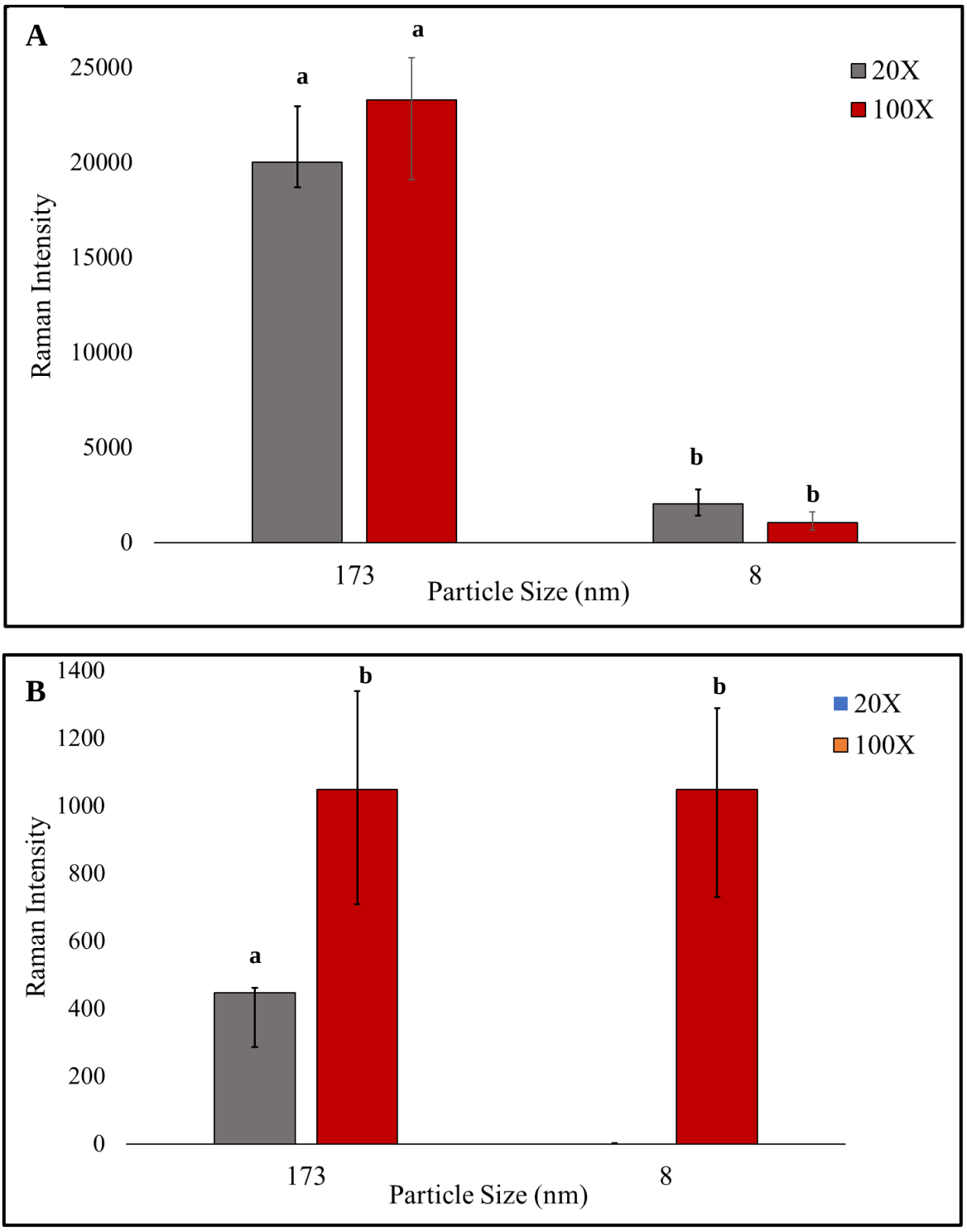

Figure 4.4 Raman intensity of peak at 137 cm^{-1} for 173 nm and 8 nm TiO_2 particles analyzed using 20X and 100X magnification for concentrations (A) 0.04 g/L and (B) 0.0004 g/L. Similar alphabets on each bar means no significant difference in the Raman intensity ($p>0.05$).

Table 4.2 Percentage of Map area covered by different concentrations of 173 and 8 nm particles when analyzed using 20X and 100X microscope objectives

Concentration of Particles (g/L)	Map Area Covered by Particles (%)			
	TiO_2 Particles, 173 nm		TiO_2-NPs, 8 nm	
	20X	100X	20X	100X
0.04	100	100	99.8	97.5
0.004	98.6	98.2	4.3	20.0
0.0004	3.4	5.8	0.0	0.5

4.3.3. Raman Mapping of Different Sizes of TiO_2 particles

TiO_2 suspensions of size 8, 41, 93 and 173 and three concentrations 0.04, 0.004 and 0.0004 g/L were prepared by the sample preparation protocol described in section 4.2.2. The Raman maps for each sample were collected using the 100X objective and the analysis parameters described in section 4.2.3. Table 4.3 shows the % of map area covered by different sizes and concentrations of TiO_2 particles. The significant reduction can be noticed in the map area covered by the particles within the nano-range when the concentration is decreased from 0.04 to 0.004 g/L, but no change is observed for 173 nm particles. One of the possible reasons behind that could be understood from looking at the particle size measurement data obtained from TEM and DLS (Table 4.1). The particle size measured by TEM and hydrodynamic diameter obtained my DLS indicate that 173nm particles were dispersed evenly without any agglomeration. On the other hand, all the other particles, including 93 nm sample were found to be aggregated resulting in larger hydrodynamic diameter than their true size. The uniformly dispersed and larger size of 173

nm particles covers almost the entire membrane surface even at 0.004 g/L concentrations. However, the other particles that are smaller in size and are agglomerated cover significantly less area. We also found a linear correlation between the actual particle size obtained from TEM, hydrodynamic diameter from DLS and % area covered by particles. As the particle size decreased, the hydrodynamic diameter increased, therefore, the % map area decreased (Figure 4.6 (A) and (B)). Besides, the pore size of the membrane used in this study is 100 nm. The larger concentration of the nano-sized particle may block the membrane pores, allowing more particle retention compared to lower concentration. At lower concentrations, the agglomerated particles, if any may pass through the membrane.

Table 4.3 Percentage of Map area covered by different concentrations and sizes of TiO_2 particles

Concentration of Particles (g/L)	Map Area Covered by Particles (%)			
	173 nm	93 nm	41 nm	8 nm
0.04	100^{a}	93.0^{a}	98.9^{a}	97.5^{a}
0.004	$98.0\ 2^{a}$	51.6^{b}	15.3^{d}	4.7^{e}
0.0004	5.8^{a}	3.1^{b}	1.7^{c}	0.5^{c}

Furthermore, we also analyzed the Raman intensities of the map collected from all the particles. Figures 4.7 and 4.8 describes the findings. At 0.04 g/L concentration, all the particles produced distinct Raman intensities and followed linear regression with the coefficient of regression R=0.94. The Raman intensity of the 173 nm was the highest and it reduced with the reduction in the particle size (figure 4.7). However, for lower

concentrations such as 0.004 and 0.0004 ppm, different trends were observed. The Raman intensity decreased with the decrease of the concentration and for 173 nm particles, it was found to be significantly higher than nano-scale particles. But no statistical difference was observed between the Raman intensities of 93,41 and 8 nm particles. The Raman intensities of particles can be affected by many parameters such as size, shape and aggregation status. Additionally, the monolayer arrangement of particles and dispersed particles have a different response when illuminated by a laser. Monolayer aggregation of particles, especially metal particles generates enhancement in the Raman signals, often referred to as SERS enhancement[103,137]. The effect of SERS enhancement of the particles is even dramatically effected by their physiological parameters such as size and shape. Since metal particles such as silver and titanium dioxide are very sensitive to the Raman spectroscopy, it makes it possible to detect them at very low concentrations and up to a single particle. However, at these low levels, the signal enhancement is not as efficient as in aggregated state in the presence of electromagnetic clouds. A similar phenomenon can be seen here. The particle concentration of 0.04 g/L produces monolayer arrangement of the particles providing significant signal enhancement where the effect of different particle sizes is distinctive. Whereas, at lower concentrations of 0.004 and 0.0004 g/L, larger particles can be distinguished from the nanosized particles based on the Raman intensities. Though a smaller difference in the particle size is not distinguishable. Furthermore, from this study, it can also be understood that although particle aggregation on the filter membrane provides uniform and significant signal enhancement, localized aggregation may not have any significant effect on the Raman intensity of a sample.

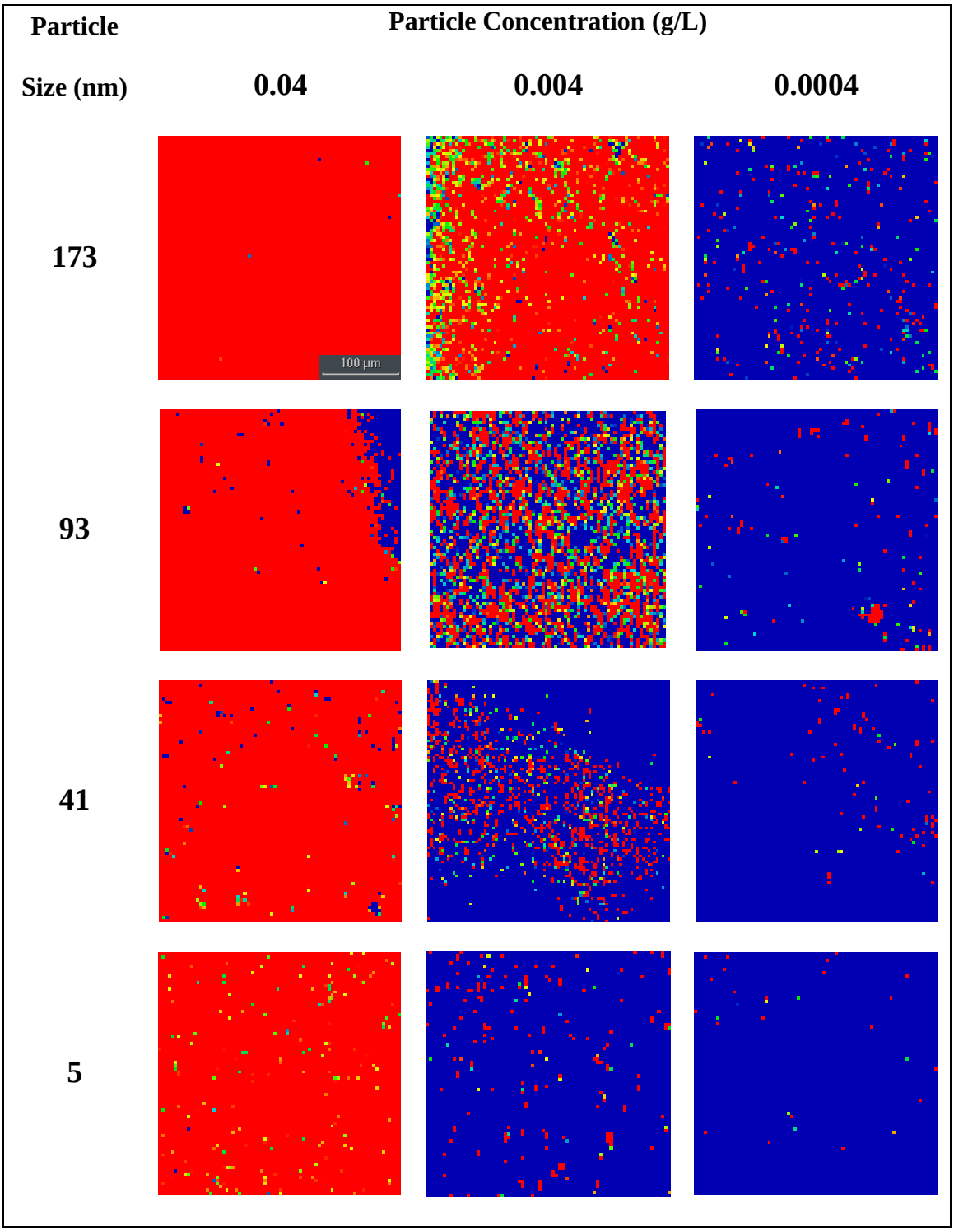

Figure 4.5 Raman maps TiO_2 particles of different size and concentrations

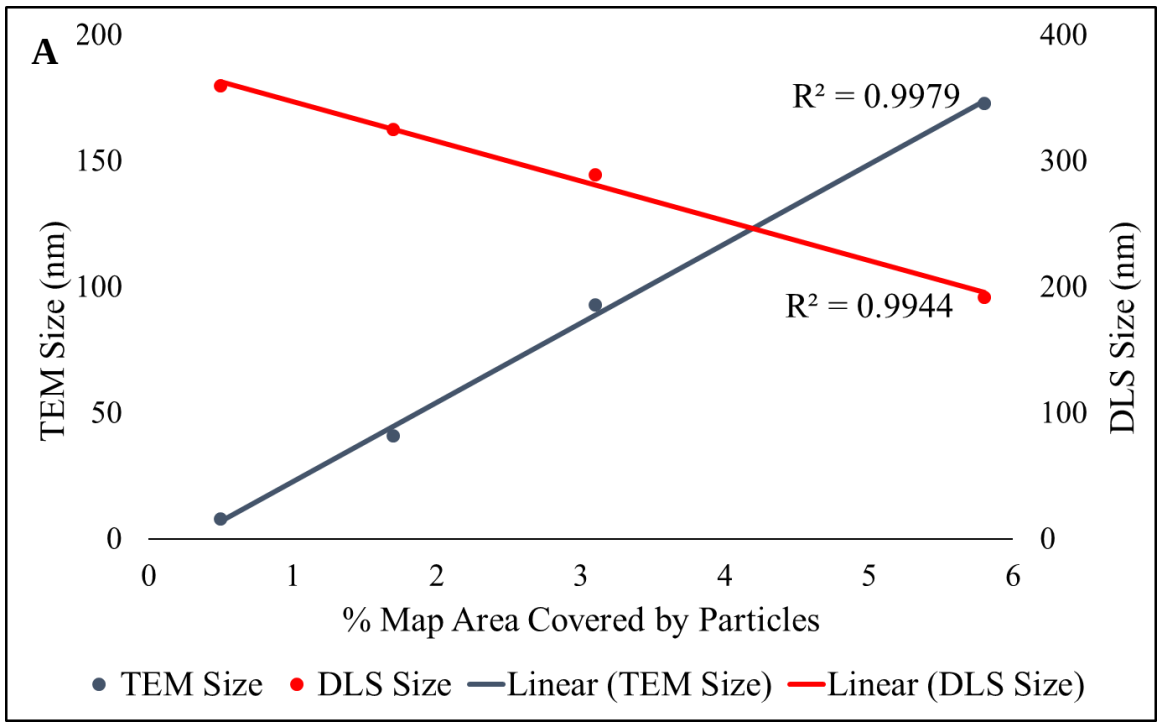

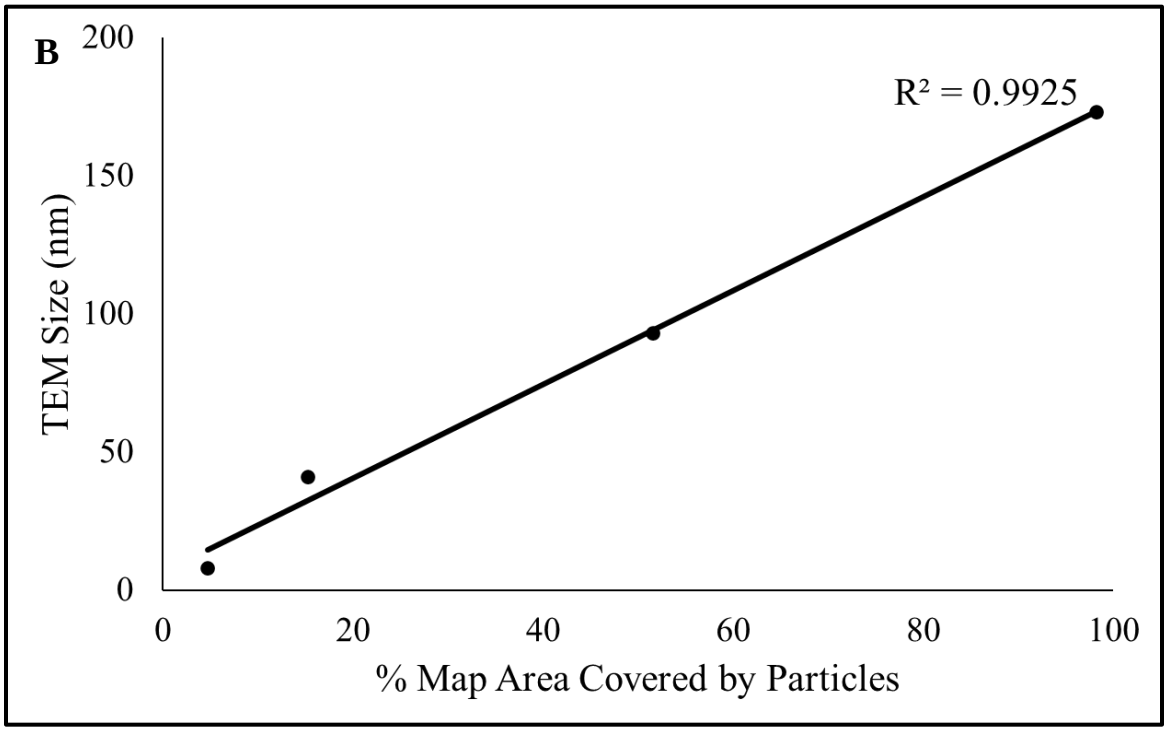

Figure 4.6 (A) Correlation of % map area covered by 0.0004 g/L particles to particle size obtained by TEM and hydrodynamic diameter from DLS (B) Correlation of % map area covered by 0.004 g/L particles to particle size obtained by TEM

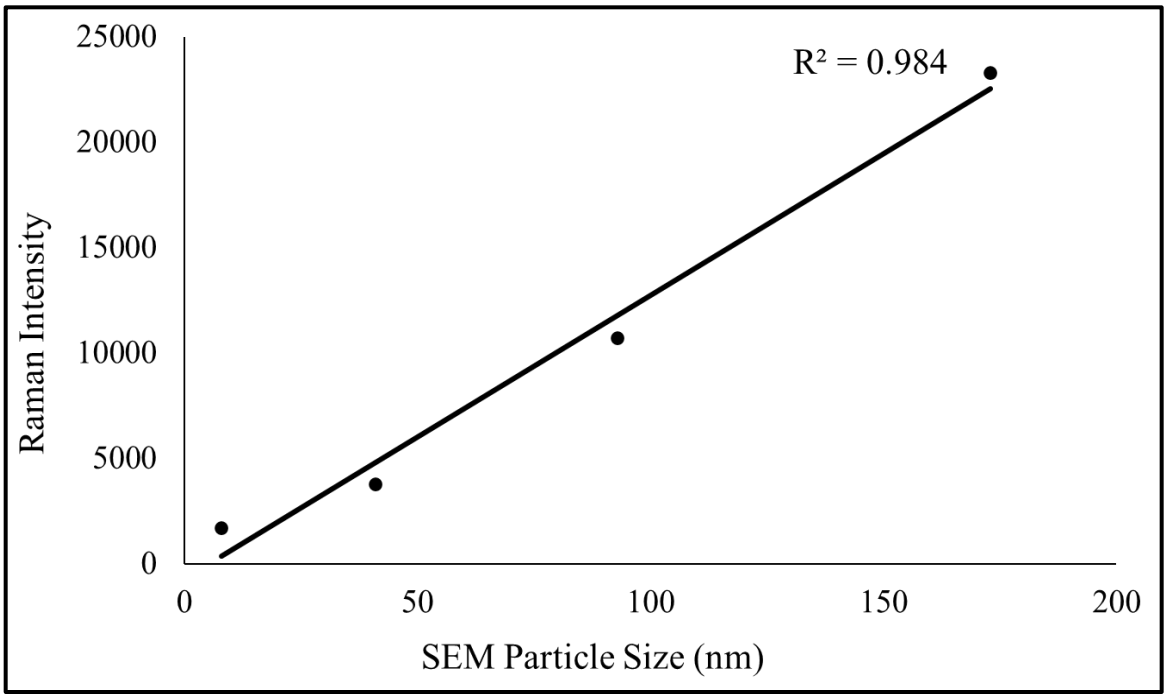

Figure 4.7 Raman intensity of 0.04 g/L TiO_2 particles of different sizes

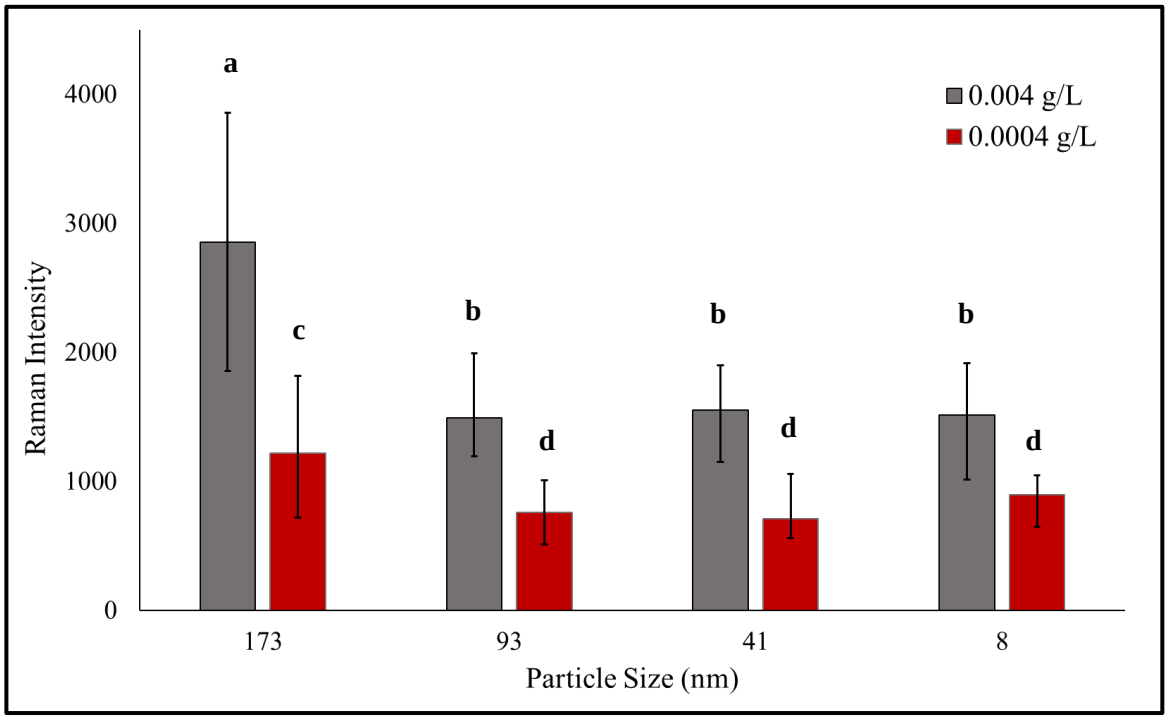

Figure 4.8 Raman intensities of 0.004 and 0.0004 g/L TiO_2 particles of different sizes. Similar alphabets on each bar means no significant difference in the Raman intensity ($p>0.05$).

4.4. Conclusion

The present study evaluated the potential of using Raman mapping technique in the analysis of TiO_2-NPs. We evaluated the effect of magnification, particle size and concentration on the mapping results. We found that 100X magnification was more capable of detecting the smaller size particles up to 5 nm up to the concentration as low as 0.0004 g/L. Moreover, we showed the linear relationship between the particle size, hydrodynamic diameter and the % of map area covered by the particles. Additionally, we examined the correlation between the Raman intensity obtained from the map and the particle size and found linearity at 0.04 g/L concentration, which and be used in distinguishing the particles. At lower concentrations, no statistical difference was found in the Raman intensities of particles within nano-rage although, the larger particles showed significantly higher intensity values. This study also successfully demonstrated the potential of membrane filtration technique in the analysis of TiO_2-NPs. This technique can further be applied in analyzing the lower concentration of TiO_2-NPs from food and environmental samples. Although in this study the lowest concentration examined was 0.0004 g/L, further research is required to determine the limit of detection. The advantage of the filtration method is that the sample size can be increased in the detection of the ultra-low concentration of the particles.

CHAPTER 5

Application of SERS and Raman Mapping Approaches in the Detection of TiO_2-NPs from Food Samples

Abstract

In the present chapter, we validated the SERS and Raman mapping approach in real-world samples. We purchased three E171 samples from Amazon.com and three food samples: coffee creamer, donuts, and chewing gum to assess the performance of the methods developed in the last two chapters in the analysis of the TiO_2-NPs. The preliminary Raman analysis revealed that one of the E171 samples was rutile polymorph therefore, that sample was excluded from further analysis. Preliminary SEM analysis revealed that chewing gum contained the highest amount (69%) of TiO_2-NPs. We then applied the SERS and Raman mapping approach to predict the average particle size and the amount of NPs in each sample. The SERS analysis showed the positive correlation of the mean particle size and R in chewing gum sample and suggested that more standards in the range of 65 to 200 nm are required to accurately determine the average particle size of the sample with a wide range of particle size distribution. We also obtained the Raman maps of the samples and evaluated them by using the map area and Raman intensity models developed in the previous chapter. We were successfully able to predict the mean particle size of each of the samples by using the Raman intensity model at g/L concentration and map area model at 0.0004 g/L concentration. Moreover, we also established the positive correlation between the map area occupied by the NPs and the amount of NPs present in the sample by applying the Raman intensity for 93 nm particles as the cut-off threshold.

5.1 Introduction

The preliminary function of E171 is to providing white color to the food products. FDA regulations allow the use of TiO_2 in foods up to 1% of the total food weight[60]. According to Weir at el., coconut curd, chewing gum, powdered donuts, candies, puddings, frostings, iced-cookies, marshmallows, and coffee creamers are some of the products that contained the most amount of TiO_2[7]. Studies report up to 36% of the TiO_2 particles in these food products may have at least one dimension less than 100 nm[9]. The quantification method of the TiO_2 from food samples is well established however, the size characterization is challenging due to its smaller particle size. In recent years, there has been significant interest in characterizing TiO_2 particles used in food products as several studies report its potential toxicological effects. Researchers have attempted to characterize the particle size of bulk E171 as well as TiO_2 extracted from food and consumer products[9,7,64,138,139-141]. Various advanced technologies have been used but all of these technologies pose significant limitations that hinder its application in a real manufacturing environment such as for TiO_2 manufactures or quality control in the food industry.

Various types of ICP techniques such as Single Particle (SP-ICP-MS), Quadrupole-ICP-MS (ICP-QMS), Tandem (ICP-MS/MS), Sector Field ICP-MS (ICP-SFMS) and asymmetric flow field-flow fractionation ICP-MS (A-ICP-MS) have shown the potential in the detection of TiO_2-NPs[140]. Though the studies characterizing TiO_2 particles from foods have mostly demonstrated the use of SP-ICP-MS. It is a powerful technique that can detect up to a single particle however the studies have shown its size detection limit in the range of 20-50 nm[9,140]. Scanning Electron Microscopy or Transmission Electron Microscopy coupled with Energy Dispersive X-ray Spectroscopy (SEM-EDS and TEM-

EDS) is another method that has been used in the analysis of TiO_2-NPs. Although this technology requires high capital investment, has a higher operating cost and the analysis is very time-consuming which limits its application to research laboratories.

On the other hand, as explained in earlier chapters, Raman spectroscopy has various advantages, the most important being, its sensitivity in the nano range. In this chapter, we applied the two approaches: SERS and Raman mapping that we developed in previous chapters to analyze the TiO_2-NPs from ingredient E171 as well from food products. We purchased E171 samples from three different manufacturers and three food products containing TiO_2 such as chewing gum, donuts, and coffee creamer from the supermarket. We chose these products as they are widely consumed and contains a significant amount of TiO_2. The analysis of E171 followed a similar protocol as described in the previous chapter but the food products were first digested to remove the matrix interference. All the analysis was conducted as 0.04, 0.004, and 0.0004 g/L concentration. The average particle size of the sample was determined from the R-value calculated from the SERS analysis. The percentage map area covered by the particles was determined from the Raman maps and particle size was correlated for each sample.

5.2. Materials and Methods

5.2.1. Materials

Three food-grade titanium dioxide (E171) samples were purchased from different suppliers on Amazon.com (Seattle, WA). Three food product samples: Hostess Donuts, Coffee mate original powdered coffee creamer and Dentyne Ice Peppermint chewing gum were purchase from a local Target store (Hadley, MA). Sodium pyrophosphate (SPP, $Na_4P_2O_7$), hydrogen peroxide (≥30% w/w) and gallocyanin (GLN) were purchased from Sigma Aldrich (St. Louis, MO). Concentrated nitric acid and absolute ethanol were purchased from Fisher Scientific (Waltham, MA). All the chemicals and reagents were prepared with ultrapure water (18.2 MΩ·cm) from Barnstand Smart2Pure Water Purification System (Thermo Scientific, Waltham, MA). Hydrophilic Polytetrafluoroethylene (PTFE) filter membrane with 0.1 µm pore size and 25 mm diameter were purchased from Millipore Sigma (Burlington, MA).

5.2.2. Sample Preparation

E171 samples were prepared by following the similar sample preparation protocol described in section 3.2.2 and 4.2.2 of previous chapters. The food samples were first digested to extract TiO_2 particles. The samples in the amount of 0.1 to 0.5 g were first weighed in the 15 ml borosilicate glass tube (Fisherbrand, Fisher Scientific, Waltham, MA). The surface coatings of donuts and chewing gum accounts for the most amount of TiO_2 therefore, their surface was scrapped for the analysis. The samples were then digested with 3 ml of nitric acid at 115^o C for 40 minutes in the heating block (Fisher Scientific, Waltham, MA). The samples were then completely cooled before adding 0.5 ml of hydrogen peroxide. The samples were heated at 115^o C for an additional 20 minutes to

complete the digestion. Once cooled the supernatant was carefully discarded and precipitated TiO_2 was pipetted out in 1 ml of water. The particles were washed by centrifuging at 6000 G for 3 minutes and the supernatant was discarded. They were washed again with ethanol by centrifuging to remove fat-soluble compounds if there were any. The particle was then diluted with an appropriate amount of ultrapure water or 0.005 M SPP solution to achieve the desire working concentration.

The samples for SERS experiments were diluted with ultrapure water and sonicated in bath sonicator [Branson 2000, Branson Ultrasonic, Danbury, CT] for 10 minutes to achieve uniform dispersion. The rest of the sample preparation method followed the similar protocol described in section 3.2.2. The samples for Raman mapping experiments were diluted in 0.05 M SPP solution, then bath sonicated for five minutes and probe sonicated (Fisher Scientific, Waltham, MA) for 10 minutes at 75% Amplitude. To obtain the desire working concentration of 0.04, 0.004, and 0.0004 g/L, the dilutions were made based on the TiO_2 concentration estimation obtained for each product from Weir et al[7]. One milliliter of each sample was then filtered through a 0.1 µm PTFE filter membrane using a vacuum filtration system. Once completely air dried, the Raman map was collected using the protocol described in section 4.2.3.

5.2.3. SERS Analysis and Raman Mapping

SERS analysis was performed using the protocol described in section 3.2.2. For all the E171 samples and particles extracted from food, the analysis was performed at 0.04 g/L concertation of particles and 5 µM concentration of GLN. The R-value was obtained by taking the ratio of the peak intensities of TiO_2 at 144 cm^{-1} to GLN at 1639 cm^{-1}. The Raman mapping was conducted using the experimental parameter described in 4.2.3. The maps

were obtained using a 100X magnification lens at concentrations 0.04, 0.004, and 0.0004 g/L. The data were analyzed to obtain the % map area occupied by the particles and Raman intensity for each sample.

5.2.4. SEM and Statistical Analysis

Reference particle size characterization of E171 particles as well as particles extracted from food products was performed by Scanning Electron Microscopy (SEM) (JEOL JSM-6320F). The SEM analysis for E171 samples was performed by placing the powder samples onto a silicone base. For the size characterization from food samples, the samples were digested first to extract the particles using the protocol described in section 5.2.2. Once the particles were washed, they were dropped on the glass slide and allowed to dry for at least 48 hours before performing SEM analysis. Three clear and high-resolution images were captured. Statistical analysis of the size distribution was conducted using ImageJ software. More than 30 particles were measured for each image and distributed in four different size categories: <60 nm, 60-100 nm, 100-200 nm, and >200 nm.

5.3. Results and Discussion

5.3.1. SEM Analysis

5.3.1.1. E171 Samples

Three E171 samples, S1, S2, and S3 were analyzed on SEM. Figure 5.1 A through C shows the SEM images obtained for three E171 samples. The ImageJ analysis of the images revealed that one sample contained more than 37% NPs whereas the other two samples contained <7% NPs. Notably, Sample 1 was marketed as a nano-free product, which actually contained more than 37% nanosized particles. However, it is worth noting that only 2.6% of particles in Sample 1 and none in Sample 2 were identified in the range

of ≤ 60 nm (Table 5.1) in which the standards were analyzed. The majority of NPs in sample 1 was found to be between 60-100 nm. Figure 5.2 shows the particle size distribution of all three E171 samples.

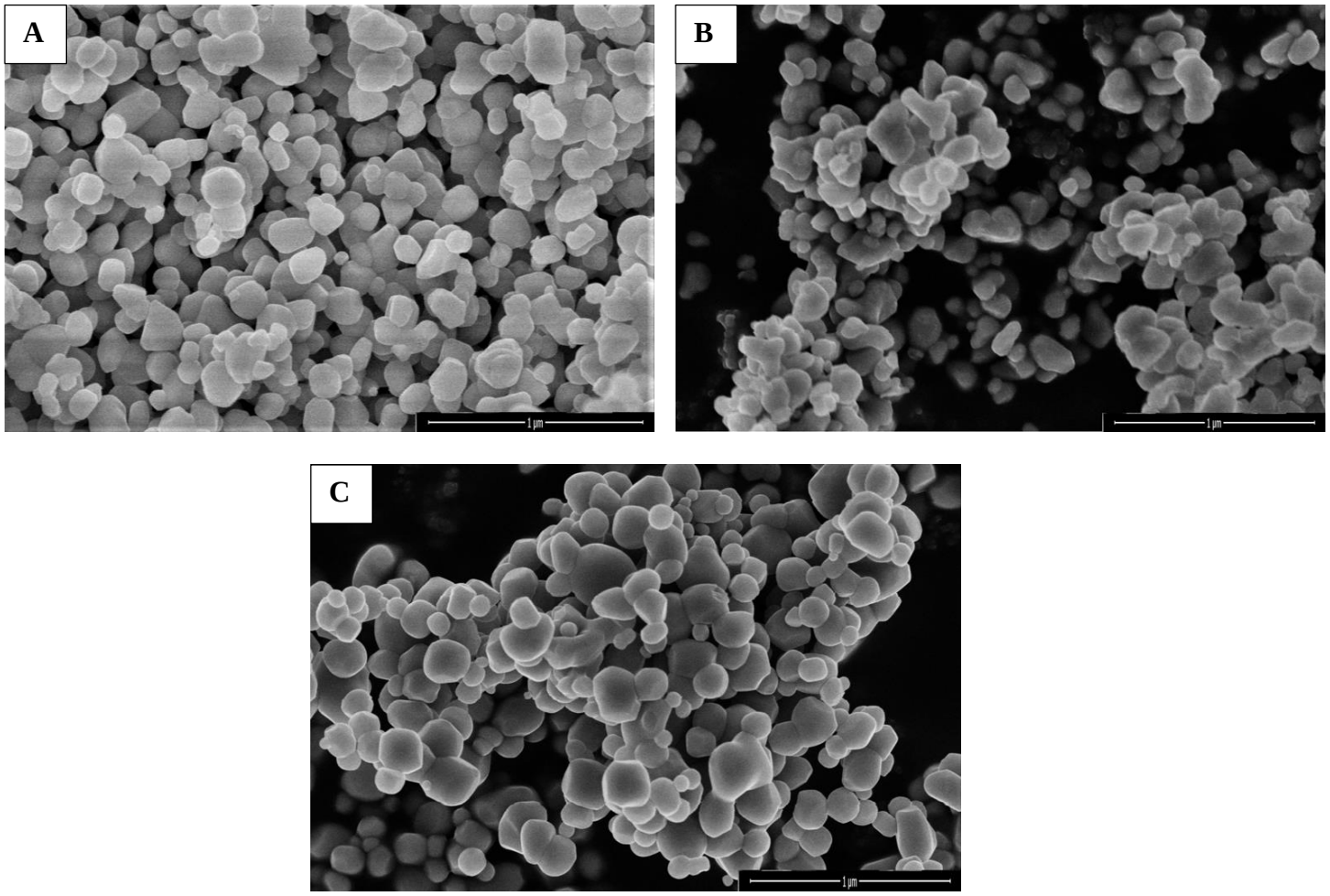

Figure 5.1 Scanning Electron Microscopic Images of (A) S1 (B) S2 and (C) S3 of food grade TiO_2

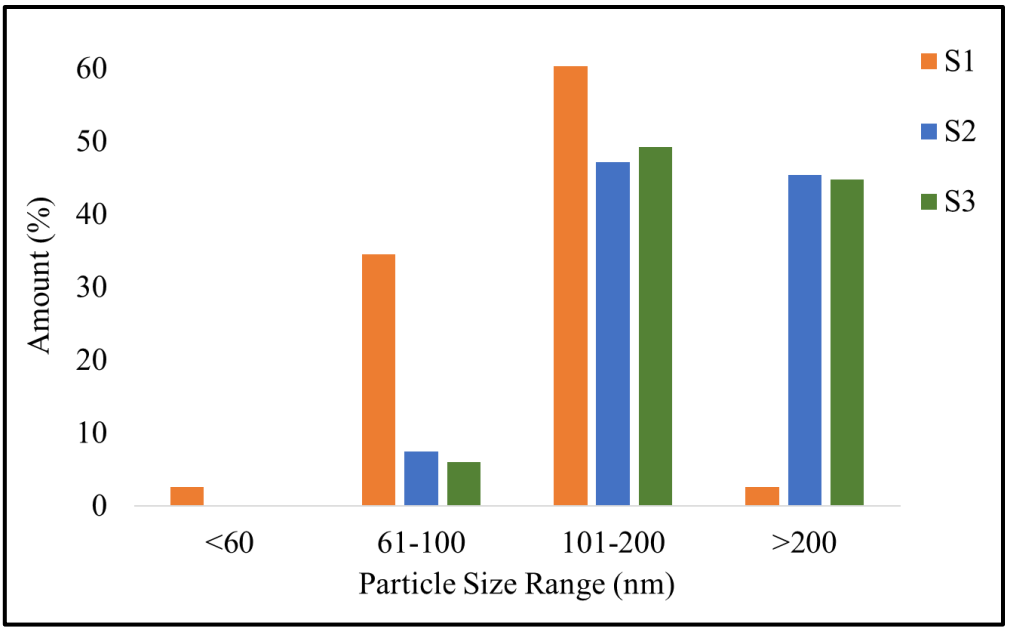

Figure 5.2 Particle size distribution of three E171 samples

5.3.1.2. E171 Samples

Figure 5.3 A through C depicts the SEM images of the TiO_2 particles extracted from coffee creamer, donuts, and chewing gum respectively whereas figure 5.4 shows the particle size distribution. The SEM revealed that approximately 41%, 8%, and 69% TiO_2 particles from coffee creamer, Donuts, and chewing gum respectively were nanosized. The mean particle size for these samples was found to be 114, 195, and 97 nm. Additionally, particles from coffee creamer showed similar particle size distribution and mean particle size as observed in E171 S1 and Donuts as S3. The data obtained from the chewing gum shell is very alarming as the TiO_2 content of the chewing gum is approximately 0.5% of the weight[7] or approximately 7.5 mg per piece of chewing gum. The presence of close to 70% of nanosized particles could pose a significant health risk to its primary consumer market of kids, teenagers, and young adults.

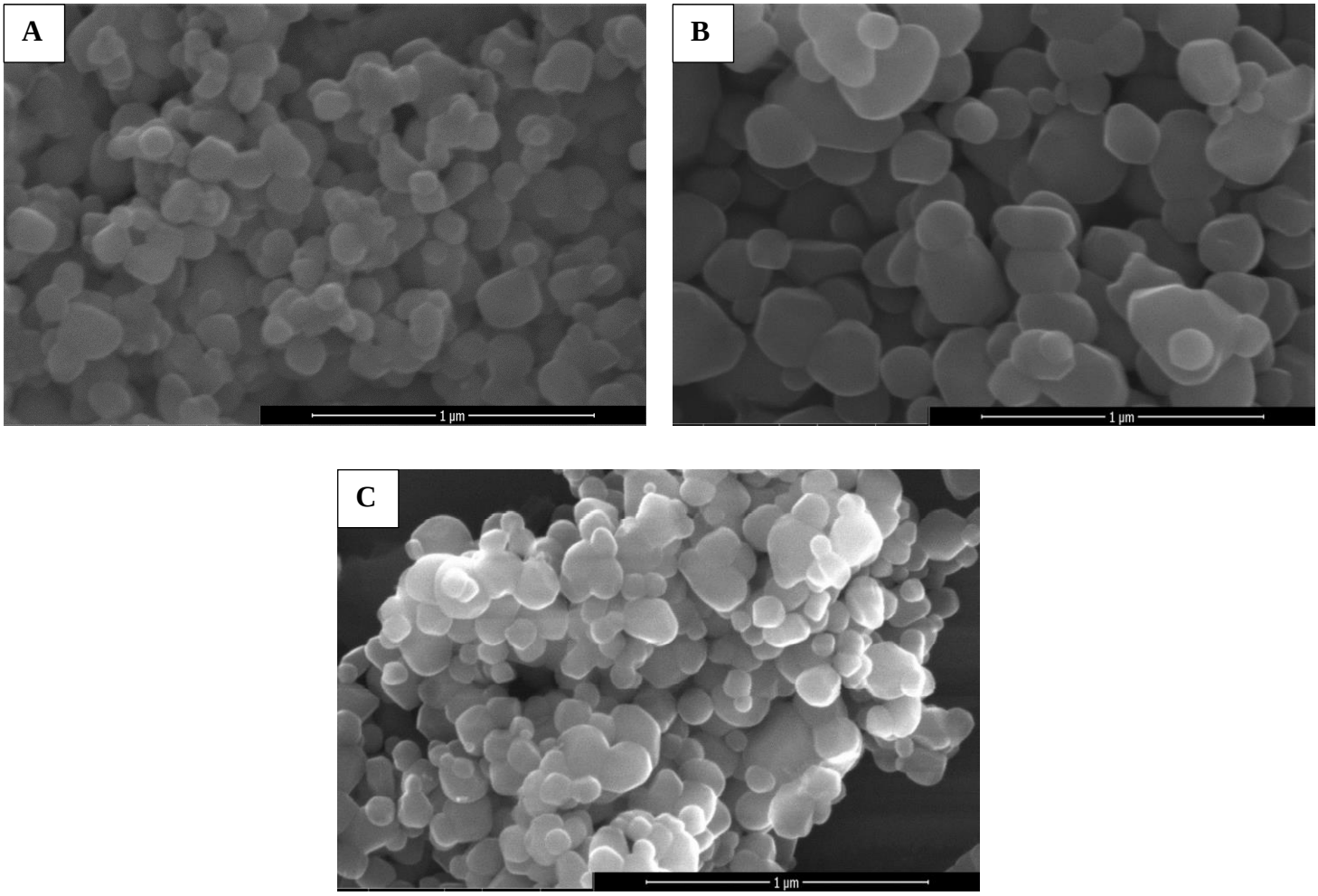

Figure 5.3 Scanning Electron Microscopic Images of (A) Coffee creamer (B) Donuts and (C) Chewing gum

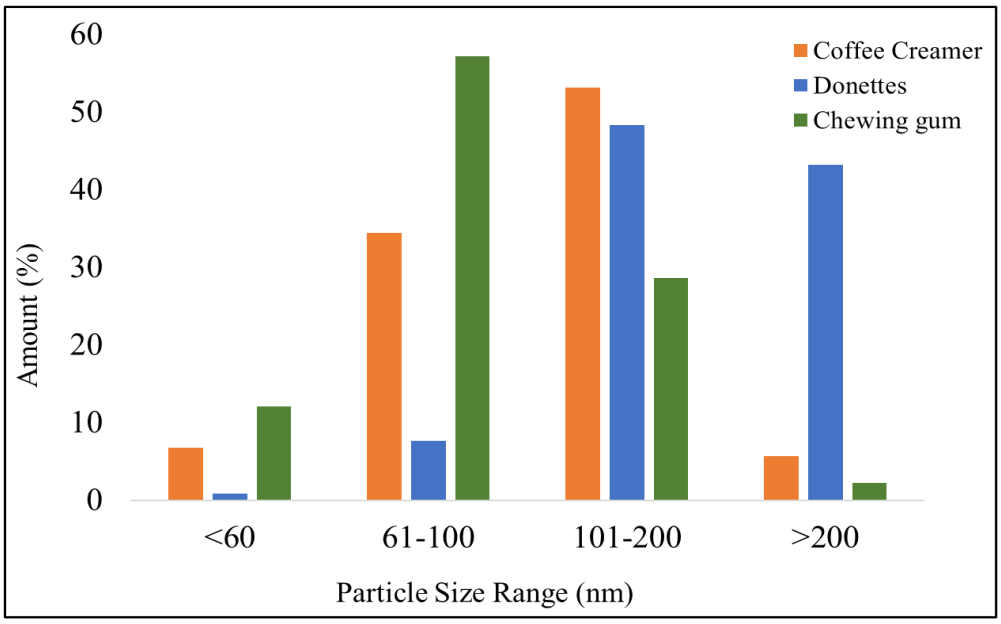

Figure 5.4 Particle size distribution of TiO_2 particles extracted from food samples

5.3.2. SERS Analysis

5.3.2.1. E171 Samples

After obtaining SEM particle size distribution for all three E171 samples, we performed the analysis on the Raman microscope. The results indicated the presence of the characteristic peaks of both TiO_2 anatase and GLN in all the samples except sample S2. S2 generated different peaks than characteristic anatase peaks. Upon investigating we found that those peaks were from the rutile form of TiO_2, which is used as a whitening agent in non-food products, such as sunscreens (Figure 5.5). Since our approach focuses on investigating the particle size of the anatase, S2 was excluded from further analysis.

Table 5.1 shows the R-value of the rest of the four E171 samples. For all four samples, the R-value was higher than the cutoff value of 93 nm, which demonstrates the majority of the particles are bigger the 100 nm. When plotted with the mean size data

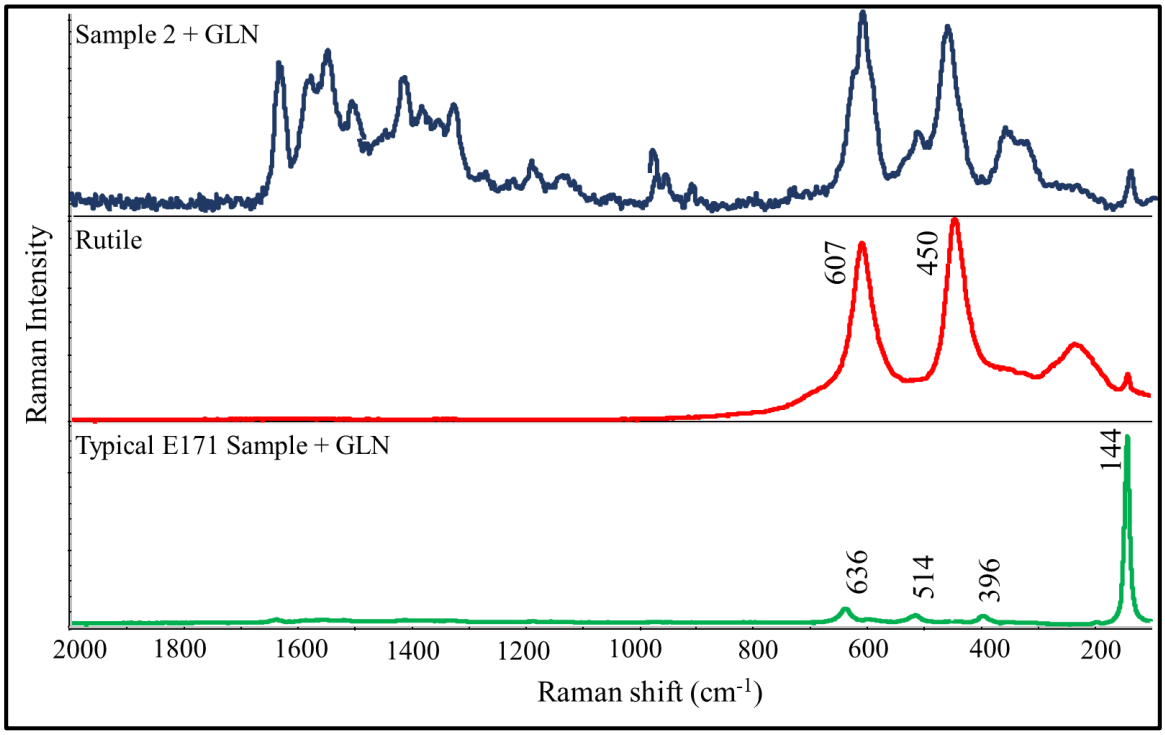

Figure 5.5 SERS analysis if sample 2 showed the presence of rutile form of TiO_2

obtained from SEM, we did not find any strong correlation. However, there is a positive correlation between the

R and the percentage of particles within the 100-200 nm range. The higher percentage of the particles in this range, the larger R. When looking into the nanoparticles, all samples showed the presence of no or very small fraction (≤ 6%) of particles at <65 nm. Up to 34% of particles were found to be in the range of 60 to 100 nm at which SERS data is unavailable as we were not able to source the standards in that range. The result demonstrates the need for more data of the particles between 65 and 100, 100-200, and >200 nm. With these data, it is potential to establish an R standard for quality control of E171 and regulation analysis.

Table 5.1 Mean particle size distribution and R-value for the E171 samples

E171 Samples	Particle Size Distribution Obtained from SEM (%)				R-Value Obtained from SERS Analysis
	≤ 60 nm	61 – 100 nm	101 – 200 nm	> 200 nm	
Sample 1	2.6	34.5	60.3	2.6	93.8
Sample 2	0	7.5	47.1	45.4	NA
Sample 3	0	6.0	49.2	44.7	70.9

5.3.2.2. Food Samples

The R for the TiO_2 particles extracted from the food sample was calculated from the SERS spectra. As seen in Table 5.2 Both coffee creamers and Donuts had almost identical particle size distribution and reported similar R-values. This further validates the performance of the SERS method in complex matrices with varied particle size

distribution. Although there was no significant difference ((P<0.05) was found between the R-values of the foods and their corresponding E171 samples, it is worth noting that both the samples had a slightly higher percentage of NPs, which may have contributed to the marginally lower R-values for food samples. The chewing gum particles reported the R of 32.5 and we were able to validate this data by looking at the particle size distribution. We propitiated the R-value of the particles in the range where we have the standard R available and summed the R fractions obtained. We considered the R of 3.5 for the particles <60 nm, 15.1 for the particles in the range of 61-100 nm and 84.2 for those in between 100-200 and calculated the R using the following formula:

$$R = a(3.5) + b(15.1) + c(84.2) \qquad \text{Equation 5.1}$$

Where, a, b and c are the factions of the particles obtained from the particle size distribution chart. The R calculated from equation 5.1 was 32.5 which matches the R obtained from SERS analysis. The particles in the range of >200 nm were excluded from this calculation due to the unavailability of standards. However, we do not anticipate major increases in the adjusted with the incorporation of >200 nm data because of its very low fraction (0.02) of the entire sample. However, further experiments are required to obtain the R for more standards within the range of 100-200 nm as well as >200 nm.

Table 5.2 Mean particle size distribution and R-value for the TiO_2 particles from food samples

Food Samples	Particle Size Distribution Obtained from SEM (%)				R-value Obtained from SERS Analysis
	≤ 60 nm	61 – 100 nm	101 – 200 nm	> 200 nm	
Coffee Creamer	6.8	34.5	53.1	5.6	86.9
Donuts	0.8	7.6	48.3	43.2	63.1
Chewing gum	12.1	57.1	28.6	2.2	32.5

5.3.3. Raman Mapping

5.3.3.1. E171 Samples

We obtained the Raman maps of samples S1 and S3 and analyzed using the analysis protocol developed in section 4.3.3. Sample S2 was not further analyzed as the initial analysis revealed its crystal type as rutile. Figure 5.6 shows the Raman maps of S1 and S3 at 0.04, 0.004, and 0.0004 g/L concentrations. Using ImageJ software, the % map area covered by particles was analyzed and fit into the models developed in section 4.3.3 to estimate the particle size. Maps of 0.04 and 0.0004 g/L concentrations were used to determine average particle size. The map area obtained at 0.0004 g/L was fit into equation 5.1 and the Raman intensity at 0.04 g/L was fit into equation 5.2.

$$y = 31.517x - 8.7103 \quad \text{Equation 5.2}$$

$$y = 134.39x - 720.78 \quad \text{Equation 5.3}$$

Where in equation 5.2, x is % map area occupied by particles at 0.0004 g/L concentration and y is the estimated particle size. In equation 5.3, y is the Raman intensity obtained at 0.04 g/L concentration and x is the estimated particle size. Table 5.3 compares the estimated particle size obtained through Raman mapping with the mean particle size obtained from SEM. The average particle size estimated from both map area and Raman intensity closely matched with the mean size obtained from SEM analysis and showed no statistical difference ($p \geq 0.05$). Thus, using the Raman mapping technique, we were able to accurately predict the average particle size of the E171 sample containing a broad range of particle size distribution.

Besides, we also utilized Raman mapping and the map area to differentiate the nanoparticles from the microparticles. As discussed in section 4.3.3 of the previous chapter, a linear relationship can be established between the Raman intensity and the particle size at saturation concentration such as 0.04 g/L which can cover the entire filter area uniformly. Using the linear relationship, the Raman intensity of approximately 23300 for the TiO_2 peak at 144 cm^{-1} for 93 nm particles can be established as a cut-off to differentiate the nanoparticles. Therefore, we set the intensity threshold bard to the cut-off intensity to differentiate the area occupied by NPs and producing lower intensity as blue and area occupied by larger particles with higher Raman intensity as red (figure 5.7). We calculated the map area covered by the larger particles using ImageJ software and deducted from the total area covered by the particles (which is ~100%) to obtain the area covered by the NPs. As seen in Table 5.4, the map area for the NPs correlated with the amount of NPs obtained from SEM analysis for sample 1. However, we did not see such a correlation for sample 3 because it contained a very small amount of NPs (~4%). This amount was small enough so

that the lower intensity signals produced by NPs were masked by the higher intensity signals from larger particles. Detecting such a low amount of NPs could be a limitation of this approach however, further study is required to systematically determine the limit of detection.

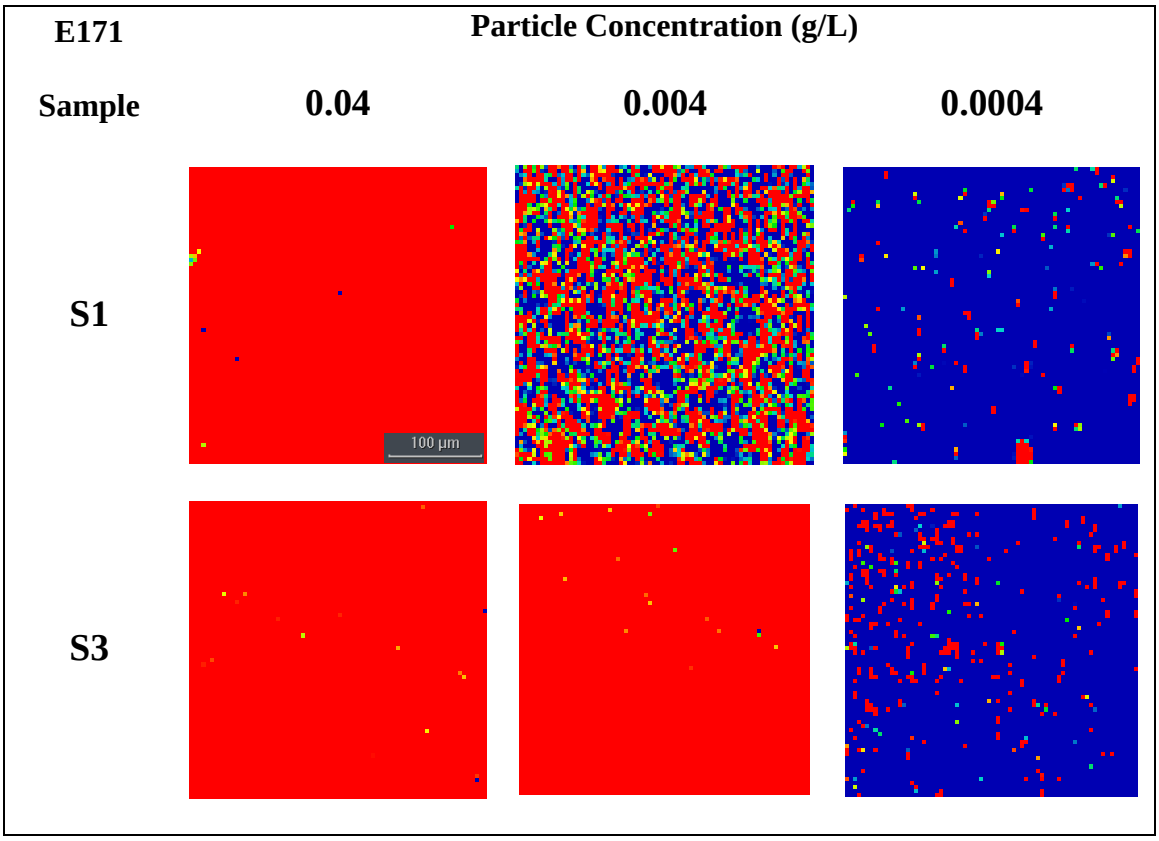

Figure 5.6 Raman maps of two E171 samples at 0.04, 0.004 and 0.0004 g/L concentrations.

Table 5.3 Estimated average particle size for E171 sample shows no significant different compared to the mean size from TEM analysis. Similar alphabet in a raw mean no significant difference (p≥0.05)

E171 Samples	Mean Particle Size from SEM (nm)	Raman Mapping data at 0.0004 g/L		Raman Mapping data at 0.04 g/L	
		Area Covered by Particles (%)	Estimated Particle Size (nm)	Raman Intensity	Estimated Particle Size (nm)
S1	117±5[a]	3.6	113.2±17 [a]	15293	119.2±0.4 [a]
S3	205±19 [b]	7.1	213.5±17 [A]	29350	223.8±15 [b]

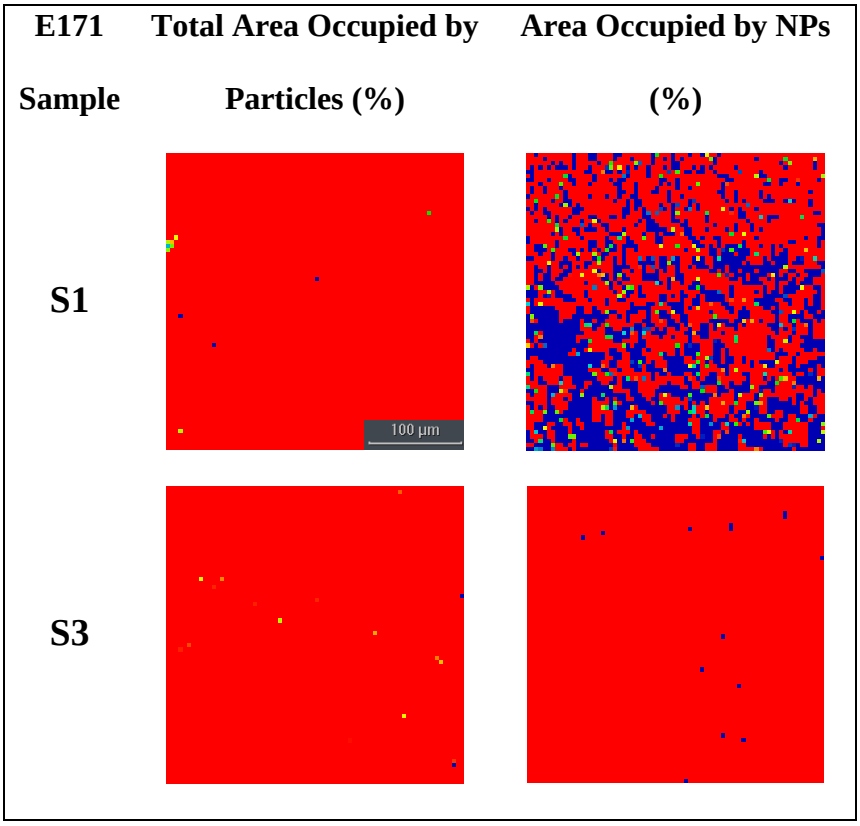

Figure 5.7 Total area occupied by particles vs area occupied by NPs at 0.04 g/L concentration. Blue pixels in the threshold map represents NPs whereas red pixels represents larger particles

Table 5.4 Estimation of the amount of NPs in E171 samples. Different alphabets in a raw mean significant difference between the values ($p<0.05$).

E171 Samples	SEM Analysis	Raman Mapping		
	≤ 100 nm (%)	Total Map area Occupied by Particles (%)	Area Occupied by Larger Particles (%)	Area Occupied by NPs (%)
S 1	37.1±7.5[a]	99.9	64.1	35.9±2.0[a]
S 3	6.0±.5.8[b]	99.9	99.8	0.1±0.0[c]

5.3.3.2. Food Samples

Raman mapping for the particles extracted from the food sample was conducted the similar was as E171. Figure 5.7 represents the maps obtained at approximately adjusted 0.04, 0.004, and 0.0004 g/L concentrations. The ImageJ analysis of the 0.04 and 0.0004 g/L maps was conducted similarly as described in section 5.3.3.1. Table 5.5 represents the average particle size analyzed from % map area covered by particles at 0.0004 g/L as well as from Raman intensity at 0.04 g/L. The results showed no significant difference in the average particle size obtained from SEM and Raman mapping for both Donuts and chewing gum samples. However, the coffee creamer data from Raman mapping was found to be significantly lower than the SEM results. One of the potential reasons for that may be attributed to either the estimated concentration based on the literature review or the lower particle recovery from the digestion process. The data obtained from the literature was published in 2012 and there may have been a change in the manufacturer formula of coffee creamer. The map area occupied by particles is concentration-dependent as lesser particles occupy the lesser surface area. In addition, both the mass of the particles as well as the size

of the particles contribute to the Raman intensity therefore, the lower concentration may result in lesser mass under the lesser spot resulting in lower Raman intensity. Moreover, particle loss may also have occurred during the extraction and washing stages. Therefore, further study is required to determine the accurate quantification and recovery of the particles from digestion using ICP-MS to optimize the results.

Furthermore, we evaluated the Raman maps at 0.04 g/L concentration to estimate the amount of NPs by adjusting the intensity threshold as discussed in section 5.3.3.1. Figure 5.8 indicates the threshold adjusted maps where blue pixels represent NPs and red pixels represent larger particles. We found that the map area obtained after the intensity threshold had a positive correlation with the %NPs present in the sample (Table 5.6). We did not find any significant difference in the % map area derived from thresholding the 0.04 g/L map and the amount of NPs determined from SEM analysis ($P \geq 0.05$). Therefore, the Raman mapping approach showed similar performance in the TiO_2 particles extracted from complex food matrices.

Thus, this data shows that the Raman mapping approach can accurately determine the average size of the TiO_2 particles as well as estimate the amount of NPs present. Raman mapping technique can be utilized as a rapid, easy, and economical approach compared with the electron microscopic method.

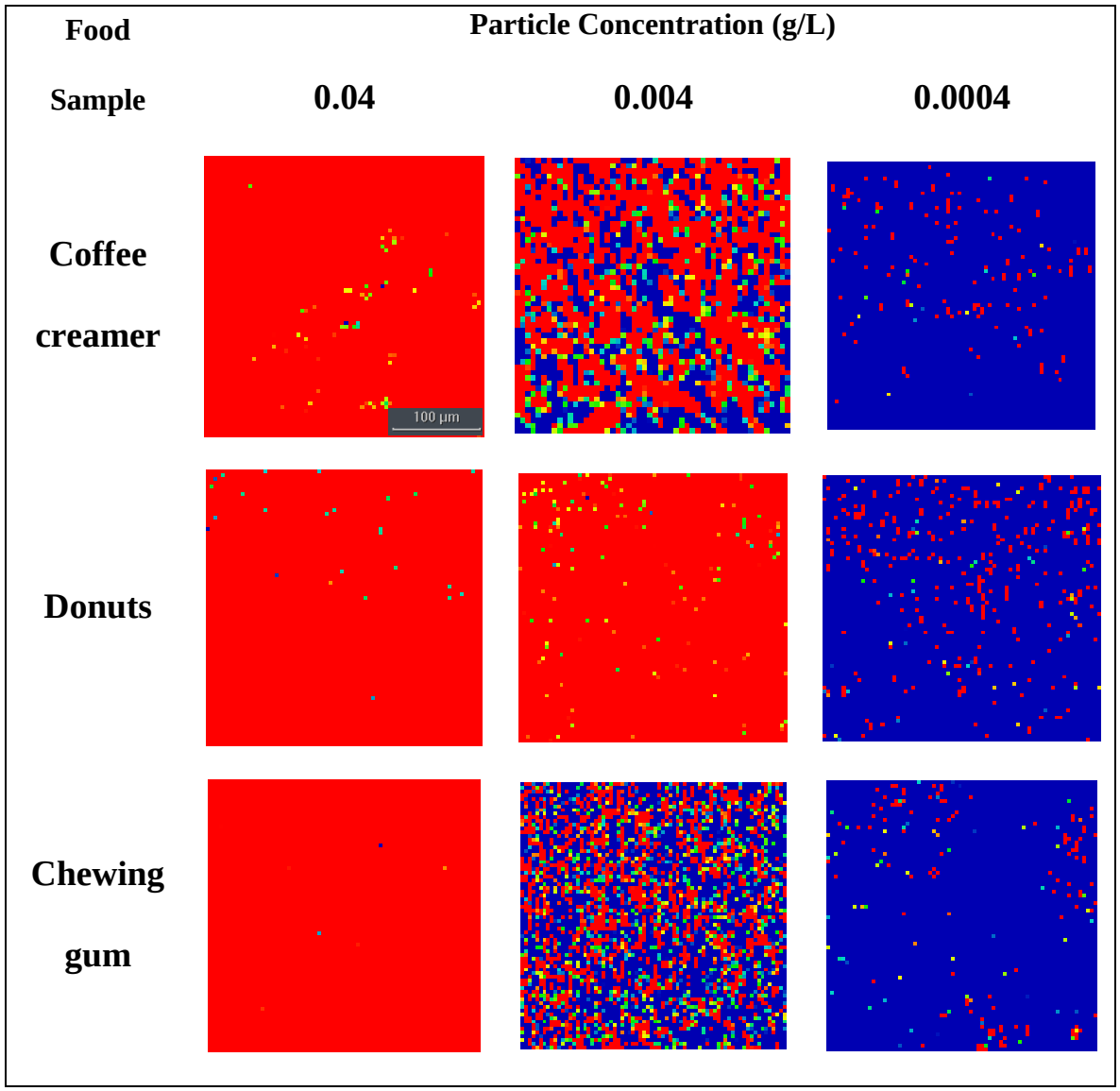

Figure 5.7 Raman maps of TiO_2 particles from food samples at 0.04, 0.004 and 0.0004 g/L concentrations.

Table 5.5 Estimated average particle size for TiO_2 particles in food. Different alphabet in a raw indicates significant difference in the values($p<0.05$).

Food Samples	Mean Particle Size from SEM (nm)	Raman Mapping data at 0.0004 g/L		Raman Mapping data at 0.04 g/L	
		Area Covered by Particles (%)	Estimated Particle Size (nm)	Raman Intensity	Estimated Particle Size (nm)
Coffee creamer	114±3[a]	3.2	90.0±2 [b]	11579	91.5±7.4 [b]
Donuts	195±12[c]	6.8	206.7±1.0 [b]	23673	186.6±6.5 [c]
Chewing gum	97±4[b]	3.4	98.4±3.4[b]	10925	86.7±4.4[b]

Table 5.6 Estimation of the amount of NPs in TiO_2 particles from food samples. Similar alphabet in a raw mean no significant difference ($p\geq0.05$)

Food Samples	SEM Analysis	Raman Mapping		
	≤ 100 nm (%)	Total Map area Occupied by Particles (%)	Area Occupied by Larger Particles (%)	Area Occupied by NPs (%)
Coffee creamer	41.2±4.9[a]	99.9	65.5	34.5±5.2[a]
Donuts	8.5±2.1[b]	100.0	91.4	9.6±2.0[b]
Chewing gum	69.2±5.9 [c]	99.9	28.6	71.4±2.9[c]

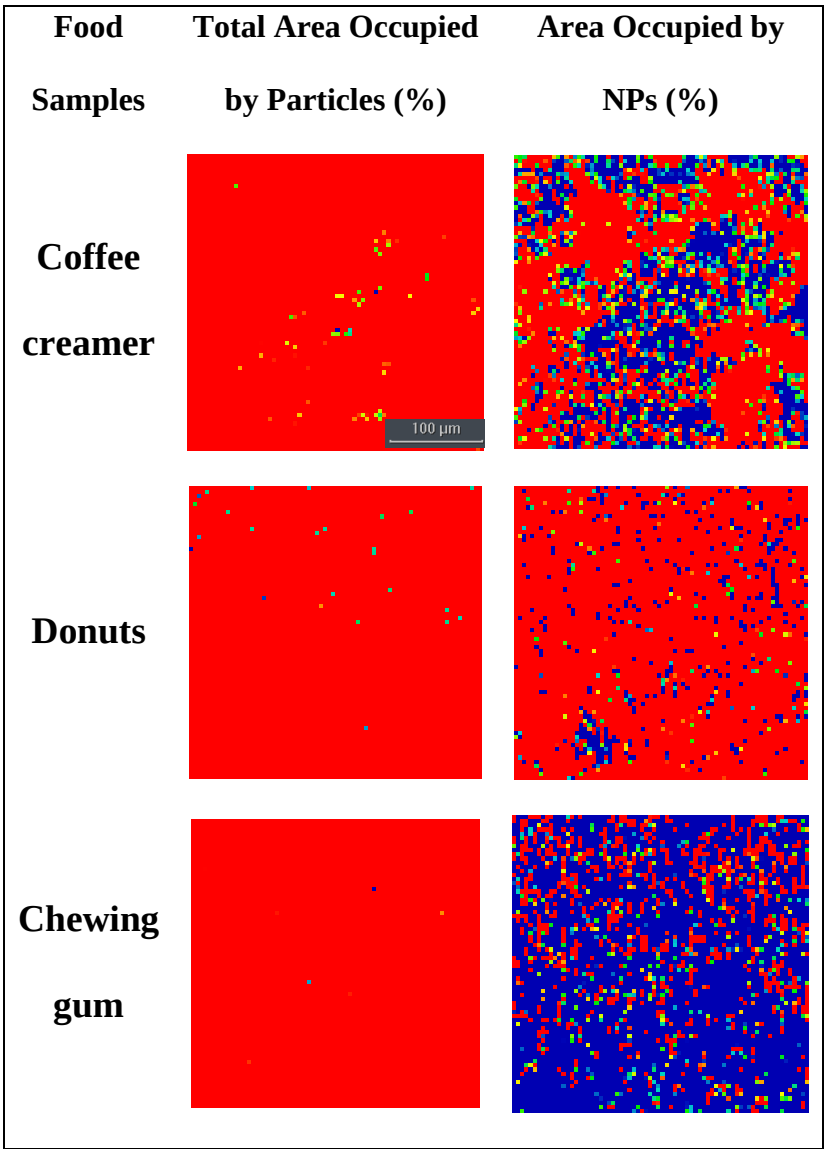

Figure 5.8 Total area occupied by particles vs area occupied by NPs at 0.04 g/L concentration. Blue pixels in the threshold map represents NPs whereas red pixels represents larger particles

5.4. Conclusion

In this chapter, we evaluated the application of SERS and Raman mapping approach developed in the analysis of the TiO_2 particles from E171 and food samples. In conclusion, the found that using the SERS approach, a positive correlation with the R can be potentially established to determine the mean particle size of the sample. However, a lack of R for standards between 65 and 200 nm range limited the accuracy of the method. Therefore, more accurate models can be developed by establishing the R for various particle size samples in addition to the ones analyzed in this study. Moreover, We found that Raman mapping techniques were successful in predicting the mean particle size as well as the amount of NPs from the samples Mean particle size of the samples was predicted by using the Raman intensity and map area models. Additionally, the amount of NPs was determined by establishing the correlation with the map area obtained by adjusting the Raman intensity threshold based on the cut-of intensity for the 93 nm particles. In all, we exhibited the potential and application of both SERS and Raman mapping in the analysis of TiO_2-NPs from the ingredient TiO_2 as well as commercial foods samples.

CHAPTER 6

SUMMARY AND OUTLOOK

In this dissertation, we evaluated the potential of Raman spectroscopic method for the analysis of TiO_2-NPs. We successfully developed SERS and Raman mapping methods and demonstrated its application in the analysis of TIO_2-NPs from ingredient TiO_2 (E171) as well as the TiO_2 extracted from food samples. We first showed that Raman spectroscopic techniques are the rapid, efficient, sensitive, and economic tool that can be used for the quality control of the TiO_2 as well as food products. In the SERS based method, we proved that the R-value obtained from the peak intensity ratios of the TiO_2 peak at 144 cm^{-1} as to GLN peak at 1639 cm^{-1} is preliminarily dependent on particle size, which can be determined to estimate the average particle size of the sample. We then developed a Raman mapping based approach to estimate the mean particle size as well as the amount of NPs. Here we established a positive correlation between both Raman intensity and the map area occupied by particles with particle size. From there we used the Raman intensity of 93 nm particles to adjust the threshold in the Raman map to determine the amount of NPs.

We then validated both of these methods by applying them to real-world samples with a broad range of particle size distribution such as ingredient TiO_2 samples and TiO_2 extracted from foods. We proved that the mapping method was able to accurately determine the average particle size for the E171 samples as well as for the particles extracted from food. In addition, using the mapping technique we successfully predicted the % of nanosized particles from the samples analyzed. The SERS method was also successful in determining the average particle size however, due to the lack of standards

data, no accurate correlation was possible. Table 6.1 summarizes the advantages and limitations of both methods.

Table 6.1 Advantages and limitations of SERS based, and Raman mapping based approaches

Approach	Capabilities & Advantages	Limitation
SERS based	• Utilizes R-value obtained from TiO_2 and ligand peak intensities to predict particle size • R is independent of concentration and particle agglomeration • Can determine the mean particle size of the sample • Sensitive at a minimum of 0.0004 g/L concentration and 30 nm particle size	• The method is ligand depended and a ligand with a strong SERS signal is required • Matrix interferences and change in the surface chemistry of the TiO_2 particles hinders the binding ability of the ligand • R for many different particle size standards need to be generated
Raman Mapping based	• Mean particle size can be estimated using the map area occupied by particles as well as Raman intensity of TiO_2 particles • The amount of NPs can be estimated by applying the Raman intensity of 93 nm particles as a cut-off • Label-free method • Can detect particles up to 5 nm	• Concentration depended on method • Uniform particle dispersion is required

The future work around this research can focus on obtaining more data of R on additional standards in the range of 60 to 100 nm, 100 and 200 nm, and >200 nm. Which will help understand the SERS mechanism of TiO_2 particle in a better way which in turn will develop more accurate methods for TiO_2-NPs analysis. Additionally, ligands with stronger binding affinity and stronger SERS single can further enhance the performance and sensitivity of the method. In the present study, we showed the linear correlation of the R within the mix of 93 nm and 40 nm particles at different proportions, but more of such models need to be built with standards of different particle sizes to further improve the accuracy. Moreover, additional experiments should also be conducted to further validate the methods in more food samples. Forthcoming studies may also focus on determining the limit of detection of the mapping method in a heterogeneous system. Furthermore, this research only focused on the analysis of anatase polymorph of TiO_2 however, rutile analysis should also be explored using the methods developed here. With the identification of LoD, and the rutile analysis method, the mapping method can then be further applied to evaluate TiO_2-NPs from environmental systems.

As the recent research suggests potential toxicity of TiO_2-NPs for humans, consumer acceptance of E171 is negatively impacted because E171 contains TiO_2-NPs. As it is challenging for the food industry to find an economic, stable, and effective white colorant, it is important to control the size of the E171 during the production and application. A rapid analytical method for the analysis of TiO_2will facilitates the quality control of E171 and regulation surveillance, making E171 and food containing E171 safer and more acceptable for the consumers.

BIBLIOGRAPHY

1. Themis Matsoukas, Tapan Desai, Kangtaek Lee. Engineered nanoparticles and their applications. *Journal of Nanomaterials*. 2015;2015:1-2. http://dx.doi.org/10.1155/2015/651273. doi: 10.1155/2015/651273.

2. Hou J, Wang C, Wang X, et al. Toxicity and mechanisms of action of titanium dioxide nanoparticles in living organisms. *Journal of Environmental Sciences*. 2019;75:40-53. https://www.sciencedirect.com/science/article/pii/S100107421733694X. doi: 10.1016/j.jes.2018.06.010.

3. Dan P, Sundararajan V, Ganeshkumar H, et al. Evaluation of hydroxyapatite nanoparticles - induced in vivo toxicity in drosophila melanogaster. *Applied Surface Science*. 2019;484:568-577. https://www.sciencedirect.com/science/article/pii/S0169433219311122. doi: 10.1016/j.apsusc.2019.04.120.

4. Ajdary M, Moosavi MA, Rahmati M, et al. Health concerns of various nanoparticles: A review of their in vitro and in vivo toxicity. *Nanomaterials (Basel, Switzerland)*. 2018;8(9):634. https://www.ncbi.nlm.nih.gov/pubmed/30134524. doi: 10.3390/nano8090634.

5. Brohi RD, Wang L, Talpur HS, et al. Toxicity of nanoparticles on the reproductive system in animal models: A review. *Frontiers in pharmacology*. 2017;8:606. https://www.ncbi.nlm.nih.gov/pubmed/28928662. doi: 10.3389/fphar.2017.00606.

6. Xu F. Review of analytical studies on TiO_2 nanoparticles and particle aggregation, coagulation, flocculation, sedimentation, stabilization. *Chemosphere*. 2018;212:662. doi: 10.1016/j.chemosphere.2018.08.108.

7. Weir A, Westerhoff P, Fabricius L, Hristovski K, von Goetz N. Titanium dioxide nanoparticles in food and personal care products. *Environmental Science & Technology*. 2012;46(4):2242-2250. http://dx.doi.org/10.1021/es204168d. doi: 10.1021/es204168d.

8. Schonburn Z. The quest for the next billion-dollar color. https://www.bloomberg.com/features/2018-quest-for-billion-dollar-red/. Updated 2018. Accessed Oct 17, 2019.

9. Peters RJB, Bemmel Gv, Herrera-Rivera Z, et al. Characterization of titanium dioxide nanoparticles in food products: Analytical methods to define nanoparticles. *Environmental Science & Technology*. 2014.48(11):6391-6400. https://doi.org/10.1021/es500436x

10. Bettini S, Boutet-Robinet E, Cartier C, et al. Food-grade TiO_2 impairs intestinal and systemic immune homeostasis, initiates preneoplastic lesions and promotes aberrant crypt

development in the rat colon. *Scientific Reports*. 2017;7(1):40373. https://search.proquest.com/docview/1899492458. doi: 10.1038/srep40373.

11. Jia X, Jia X, Wang S, et al. The potential liver, brain, and embryo toxicity of titanium dioxide nanoparticles on mice. *Nanoscale Res Lett*. 2017;12(1):1-14. https://www.ncbi.nlm.nih.gov/pubmed/28774157. doi: 10.1186/s11671-017-2242-2.

12. Rizk MZ, Ali SA, Hamed MA, El-Rigal NS, Aly HF, Salah HH. Toxicity of titanium dioxide nanoparticles: Effect of dose and time on biochemical disturbance, oxidative stress and genotoxicity in mice. *Biomedicine & Pharmacotherapy*. 2017;90:466-472. https://www.clinicalkey.es/playcontent/1-s2.0-S0753332217300896. doi: 10.1016/j.biopha.2017.03.089.

13. Jovanović B, Jovanović N, Cvetković VJ, et al. The effects of a human food additive, titanium dioxide nanoparticles E171, on drosophila melanogaster - a 20 generation dietary exposure experiment. *Scientific reports*. 2018;8(1):17922-12. https://www.ncbi.nlm.nih.gov/pubmed/30560898. doi: 10.1038/s41598-018-36174-w.

14. Raja G, Kim S, Yoon D, Yoon C, Kim S. 1 H NMR based metabolomics studies of the toxicity of titanium dioxide nanoparticles in zebrafish (danio rerio). *Bulletin of the Korean Chemical Society*. 2018;39(1):33-39. doi: 10.1002/bkcs.11336.

15. Srinivasan M, Venkatesan M, Arumugam V, et al. Green synthesis and characterization of titanium dioxide nanoparticles (TiO_2 NPs) using sesbania grandiflora and evaluation of toxicity in zebrafish embryos. *Process Biochemistry*. 2019;80:197-202. https://www.sciencedirect.com/science/article/pii/S1359511318319652. doi: 10.1016/j.procbio.2019.02.010.

16. Wu Q, Yan Wei, Liu Chunsheng, Hung T, Li G. Parental transfer of titanium dioxide nanoparticle aggravated MCLR-induced developmental toxicity in zebrafish offspring. *Environmental Science: Nano*. 2018;5(12):2952-2965.

17. Chen Z, Zhou D, Zhou S, Jia G. Gender difference in hepatic toxicity of titanium dioxide nanoparticles after subchronic oral exposure in Sprague-Dawley rats. *Journal of Applied Toxicology*. 2019;39(5):807-819. https://onlinelibrary.wiley.com/doi/abs/10.1002/jat.3769. doi: 10.1002/jat.3769.

18. El-behairy D, Diaa Eldin N, Elbadry E, Mohamed A, Farrag I. Hepato-renal toxicity of titanium dioxide nanoparticles and the protective effects of moringa oleifera leaves extract and vitamin E in male albino rats. *The Egyptian Journal of Hospital Medicine*. 2019:2261. doi: 10.1111/rda.13387.

19. Morgan A, Ibrahim M, Noshy P. Reproductive toxicity provoked by titanium dioxide nanoparticles and the ameliorative role of tiron in adult male rats. *Biochemical and Biophysical Research Communications*. 2017;486(2):595-600. doi: 10.1016/j.bbrc.2017.03.098.

20. Sayes CM, Wahi R, Kurian PA, et al. Correlating nanoscale titania structure with toxicity: A cytotoxicity and inflammatory response study with human dermal fibroblasts and human lung epithelial cells. *Toxicological sciences : an official journal of the Society of Toxicology*. 2006;92(1):174-185. https://www.ncbi.nlm.nih.gov/pubmed/16613837. doi: 10.1093/toxsci/kfj197.

21. Baan R, Straif K, Grosse Y. Carcinogenicity of carbon black, titanium dioxide, and talc. (vol 7, pg 295, 2006). *LANCET ONCOLOGY*. 2006;7(5):365. http://kipublications.ki.se/Default.aspx?queryparsed=id:13740287.

22. European Food Safety Authority. EFSA statement on the review o f the risks related to the exposure to the food additive titanium dioxide (E 171) performed by the french agency for food, environmental and occupational health and safety (ANSES). *European Food Safety Authority*. 2019.

23. Wu S, Zhang S, Gong Y, Shi L, Zhou B. Identification and quantification of titanium nanoparticles in surface water: A case study in lake taihu, china. *Journal of Hazardous Materials*. 2020;382:121045. https://www.sciencedirect.com/science/article/pii/S0304389419309999. doi: 10.1016/j.jhazmat.2019.121045.

24. Shah SNA, Shah Z, Hussain M, Khan M. Hazardous effects of titanium dioxide nanoparticles in ecosystem. *Bioinorganic chemistry and applications*. 2017;2017:4101735-12. https://www.ncbi.nlm.nih.gov/pubmed/28373829. doi: 10.1155/2017/4101735.

25. Zheng D, Wang N, Wang X, et al. Effects of the interaction of TiO_2 nanoparticles with bisphenol A on their physicochemical properties and in vitro toxicity. *Journal of hazardous materials*. 2012;199-200:426-432. https://www.ncbi.nlm.nih.gov/pubmed/22138173. doi: 10.1016/j.jhazmat.2011.11.040.

26. Cho EJ, Holback H, Liu KC, Abouelmagd SA, Park J, Yeo Y. Nanoparticle characterization: State of the art, challenges, and emerging technologies. *Molecular Pharmaceutics*. 2013;10(6):2093-2110. http://dx.doi.org/10.1021/mp300697h. doi: 10.1021/mp300697h.

27. Hoo C, Starostin N, West P, Mecartney M. A comparison of atomic force microscopy (AFM) and dynamic light scattering (DLS) methods to characterize nanoparticle size distributions. *J Nanopart Res*. 2008;10(S1):89-96. https://search.proquest.com/docview/1112829707. doi: 10.1007/s11051-008-9435-7.

28. Zhao B, Yang T, Zhang Z, Hickey ME, He L. A triple functional approach to simultaneously determine the type, concentration, and size of titanium dioxide particles. *Environmental Science & Technology*. 2018;52(5):2863-2869. http://dx.doi.org/10.1021/acs.est.7b05403. doi: 10.1021/acs.est.7b05403.

29. Jeevanandam J, Barhoum A, Chan YS, Dufresne A, Danquah MK. Review on nanoparticles and nanostructured materials: History, sources, toxicity and regulations. *Beilstein journal of nanotechnology*. 2018;9(1):1050-1074. https://www.ncbi.nlm.nih.gov/pubmed/29719757. doi: 10.3762/bjnano.9.98.

30. International Organization for Standardization. ISO/TS/80004-1:2015 nanotechnologies - vocabulary - part 1: Core terms. *International Organization for Standardization*. 2015.

31. FDA. Guidance for industry: Considering whether a food and drug administration-regulated product involves the application of nanotechnology; availability. *U.S. Food and Drug Administration*. 2014:36534.

32. EPA. Technical fact sheet – nanomaterials. *United States Environment Protection Agency*. 2017.

33. EU. Legislation. *Official Journal of the European Union*. 2011;54:1-40.

34. BSI. Terminology for nanomaterials. *British Standards Institution*. 2007.

35. Anu Mary Ealia S, Saravanakumar MP. A review on the classification, characterisation, synthesis of nanoparticles and their application. *IOP Conference Series: Materials Science and Engineering*. 2017;263:32019. doi: 10.1088/1757-899X/263/3/032019.

36. Sahay R, Reddy V, Ramakrishna S. Synthesis and applications of multifunctional composite nanomaterials. *Int J Mech Mater Eng*. 2014;9(1):1-13. https://search.proquest.com/docview/1653028106. doi: 10.1186/s40712-014-0025-4.

37. Feynman RP. There's plenty of room at the bottom. *American Physical Society*. Feb 1960.

38. Christian P, Von der Kammer F, Baalousha M, Hofmann T. Nanoparticles: Structure, properties, preparation and behaviour in environmental media. *Ecotoxicology*. 2008;17(5):326-343. https://www.ncbi.nlm.nih.gov/pubmed/18459043. doi: 10.1007/s10646-008-0213-1.

39. Guo D, Xie G, Luo J. Mechanical properties of nanoparticles: Basics and applications. *Journal of Physics D: Applied Physics*. 2014;47(1):13001. doi: 10.1088/0022-3727/47/1/013001.

40. Hochella J, Michael F, Mogk DW, Ranville J, et al. Natural, incidental, and engineered nanomaterials and their impacts on the earth system. *Science (New York, N.Y.)*. 2019;363(6434):1414. https://www.ncbi.nlm.nih.gov/pubmed/30923195. doi: 10.1126/science.aau8299.

41. de Almeida L, Terumi Fujimura A, Del Cistia ML, et al. Nanotechnological strategies for treatment of Leishmaniasis—A review. *Journal of biomedical nanotechnology*. 2017;13(2):117-133. https://www.ncbi.nlm.nih.gov/pubmed/29376626. doi: 10.1166/jbn.2017.2349.

42. Khan I, Khan I, Saeed K. Nanoparticles: Properties, applications and toxicities. *Arabian Journal of Chemistry*. 2019;12(7):908-931. https://www.sciencedirect.com/science/article/pii/S1878535217300990. doi: 10.1016/j.arabjc.2017.05.011.

43. Shen Z, Nieh M, Li Y. Decorating nanoparticle surface for targeted drug delivery: Opportunities and challenges. *Polymers*. 2016;8(3):83. https://www.ncbi.nlm.nih.gov/pubmed/30979183. doi: 10.3390/polym8030083.

44. Srivastava V, Gusain D, Sharma YC. Critical review on the toxicity of some widely used engineered nanoparticles. *Industrial & Engineering Chemistry Research*. 1900;54(24):6209-6233. http://dx.doi.org/10.1021/acs.iecr.5b01610. doi: 10.1021/acs.iecr.5b01610.

45. Wood L. Global nanotechnology market 2018-2024: Market is expected to exceed US$ 125 billion. https://www.prnewswire.com/news-releases/global-nanotechnology-market-2018-2024-market-is-expected-to-exceed-us-125-billion-300641054.html. Updated 2018. Accessed Oct 10, 2019.

46. Zhang T, Zhang Y, Ding Z, et al. Transcriptional responses and mechanisms of copper nanoparticle toxicology on zebrafish embryos. *Journal of Hazardous Materials*. 2018;344:1057-1068. https://www.sciencedirect.com/science/article/pii/S0304389417308610. doi: 10.1016/j.jhazmat.2017.11.039.

47. Cao Y, Gong Y, Liao W, et al. A review of cardiovascular toxicity of TiO_2, ZnO and ag nanoparticles (NPs). *Biometals*. 2018;31(4):457-476. https://search.proquest.com/docview/2036911359. doi: 10.1007/s10534-018-0113-7.

48. Du J, Tang J, Xu S, et al. A review on silver nanoparticles-induced ecotoxicity and the underlying toxicity mechanisms. *Regulatory Toxicology and Pharmacology*. 2018;98:231-239. https://www.sciencedirect.com/science/article/pii/S0273230018302149. doi: 10.1016/j.yrtph.2018.08.003.

49. Yu Z, Wang W, Kong F, Lin M, Mustapha A. Cellulose nanofibril/silver nanoparticle composite as an active food packaging system and its toxicity to human colon cells. *International Journal of Biological Macromolecules*. 2019;129:887-894. https://www.sciencedirect.com/science/article/pii/S0141813018359725. doi: 10.1016/j.ijbiomac.2019.02.084.

50. Bahadar H, Maqbool F, Niaz K, Abdollahi M. Toxicity of nanoparticles and an overview of current experimental models. *Iranian biomedical journal*. 2016;20(1):1-11. https://www.ncbi.nlm.nih.gov/pubmed/26286636. doi: 10.7508/ibj.2016.01.001.

51. Zhu M, Feng W, Wang B, et al. Comparative study of pulmonary responses to nano- and submicron-sized ferric oxide in rats. *Toxicology*. 2008;247(2-3):102-111.

52. Huang Y, Huang C, Aronstam RS, Chen D. Oxidative stress, calcium homeostasis, and altered gene expression in human lung epithelial cells exposed to ZnO nanoparticles. *Toxicology in Vitro*. 2010;24(1):45-55. https://www.sciencedirect.com/science/article/pii/S088723330900263X. doi: 10.1016/j.tiv.2009.09.007.

53. Khalili Fard J, Jafari S, Eghbal MA. A review of molecular mechanisms involved in toxicity of nanoparticles. *Advanced pharmaceutical bulletin*. 2015;5(4):447-454. https://www.ncbi.nlm.nih.gov/pubmed/26819915. doi: 10.15171/apb.2015.061.

54. Jiang J, Oberdorster G, Elder A, Gelein R, Mercer P, Biswas P. Does nanoparticle activity depend upon size and crystal phase? *Nanotoxicology*. 2009;2(1):33-42.

55. Huang Y, Cambre M, Lee H. The toxicity of nanoparticles depends on multiple molecular and physicochemical mechanisms. *International journal of molecular sciences*. 2017;18(12):2702. https://www.ncbi.nlm.nih.gov/pubmed/29236059. doi: 10.3390/ijms18122702.

56. Iavicoli I, Leso V, Bergamaschi A. Toxicological effects of titanium dioxide nanoparticles: A review of in vivo studies. . 2012. http://hdl.handle.net/10807/3389. doi: 10.1155/2012/964381.

57. Di Paola A, Bellardita M, Palmisano L. Brookite, the least known TiO_2 photocatalyst. *Catalysts*. 2013;3(1):36-73. https://search.proquest.com/docview/1523916232. doi: 10.3390/catal3010036.

58. Diebold U. Structure and properties of TiO 2 surfaces: A brief review. *Applied Physics A: Materials Science & Processing*. 2003;76(5):681-687. doi: 10.1007/s00339-002-2004-5.

59. Ali I, Suhail M, Alothman ZA, Alwarthan A. Recent advances in syntheses, properties and applications of TiO_2 nanostructures. *RSC Advances*. 2018;8(53):30125-30147. doi: 10.1039/C8RA06517A.

60. FDA. Code of federal regulations. *Code of federal regulations*. 2018.

61. Noman M, Noman M, Ashraf M, Ashraf M, Ali A, Ali A. Synthesis and applications of nano-TiO_2: A review. *Environ Sci Pollut Res*. 2019;26(4):3262-3291. https://search.proquest.com/docview/2155929187. doi: 10.1007/s11356-018-3884-z.

62. Haider A, Jameel Z, Al-Hussaini I. Review on: Titanium dioxide applications. *Technologies and Materials for Renewable Energy, Environment and Sustainability*. 2019(157):17-29.

63. CCOHS. Titanium dioxide classified as possibly carcinogenic to humans. . 2006.

64. Yang Y, Doudrick K, Bi X, et al. Characterization of food-grade titanium dioxide: The presence of nanosized particles. *Environmental Science & Technology*. 2014;48(11):6391-6400. http://dx.doi.org/10.1021/es500436x. doi: 10.1021/es500436x.

65. Shi H, Magaye R, Castranova V, Zhao J. Titanium dioxide nanoparticles: A review of current toxicological data. *Particle and fibre toxicology*. 2013;10(1):15. https://www.ncbi.nlm.nih.gov/pubmed/23587290. doi: 10.1186/1743-8977-10-15.

66. Winkler HC, Notter T, Meyer U, Naegeli H. Critical review of the safety assessment of titanium dioxide additives in food. *Journal of nanobiotechnology*. 2018;16(1):51. https://www.ncbi.nlm.nih.gov/pubmed/29859103. doi: 10.3929/ethz-b-000268946.

67. Audran X. France bans titanium dioxide in food products by january 2020. *USDA Foreign Agricultural Service*. 2019.

68. Mahaye N, Thwala M, Cowan DA, Musee N. Genotoxicity of metal based engineered nanoparticles in aquatic organisms: A review. *Mutation Research-Reviews in Mutation Research*. 2017;773:134-160. https://www.sciencedirect.com/science/article/pii/S1383574216301569. doi: 10.1016/j.mrrev.2017.05.004.

69. Lee S, Bi X, Reed RB, Ranville JF, Herckes P, Westerhoff P. Nanoparticle size detection limits by single particle ICP-MS for 40 elements. *Environmental Science & Technology*. 2014;48(17):10291-10300. http://dx.doi.org/10.1021/es502422v. doi: 10.1021/es502422v.

70. Bocca B, Caimi S, Senofonte O, Alimonti A, Petrucci F. ICP-MS based methods to characterize nanoparticles of TiO_2 and ZnO in sunscreens with focus on regulatory and safety issues. *Science of the Total Environment*. 2018;630:922-930. https://www.sciencedirect.com/science/article/pii/S0048969718305588. doi: 10.1016/j.scitotenv.2018.02.166.

71. Candás-Zapico S, Kutscher DJ, Montes-Bayón M, Bettmer J. Single particle analysis of TiO_2 in candy products using triple quadrupole ICP-MS. *Talanta*. 2018;180:309-315. https://www.sciencedirect.com/science/article/pii/S0039914017312432. doi: 10.1016/j.talanta.2017.12.041.

72. Vidmar J, Milačič R, Ščančar J. Sizing and simultaneous quantification of nanoscale titanium dioxide and a dissolved titanium form by single particle inductively coupled plasma mass spectrometry. *Microchemical Journal*. 2017;132:391-400.

https://www.sciencedirect.com/science/article/pii/S0026265X16303034. doi: 10.1016/j.microc.2017.02.030.

73. Lim J, Bae D, Fong A. Titanium dioxide in food products: Quantitative analysis using ICP-MS and raman spectroscopy. *Journal of Agricultural and Food Chemistry*. 2018;66(51):13533-13540. http://dx.doi.org/10.1021/acs.jafc.8b06571. doi: 10.1021/acs.jafc.8b06571.

74. De la Calle I, Menta M, Séby F. Current trends and challenges in sample preparation for metallic nanoparticles analysis in daily products and environmental samples: A review. *Spectrochimica Acta Part B: Atomic Spectroscopy*. 2016;125:66-96. https://www.sciencedirect.com/science/article/pii/S0584854716302142. doi: 10.1016/j.sab.2016.09.007.

75. Williams SKR, Runyon JR, Ashames AA. Field-flow fractionation: Addressing the nano challenge. *Analytical chemistry*. 2011;83(3):634-642. https://www.ncbi.nlm.nih.gov/pubmed/21090634. doi: 10.1021/ac101759z.

76. Meermann B, Nischwitz V. ICP-MS for the analysis at the nanoscale – a tutorial review. *Journal of Analytical Atomic Spectrometry*. 2018;33(9):1432-1468. https://www.openaire.eu/search/publication?articleId=od3364::0494de3945e9d76b6800c9c3d5a3b54d. doi: 10.1039/C8JA00037A.

77. Naicker PK, Cummings PT, Zhang H, Banfield JF. Characterization of titanium dioxide nanoparticles using molecular dynamics simulations. *The Journal of Physical Chemistry B*. 2005;109(32):15243-15249. http://dx.doi.org/10.1021/jp050963q. doi: 10.1021/jp050963q.

78. Raman CV. A change of wave-length in light scattering. *Nature*. 1928;121(3051):619.

79. Gordon KC, McGoverin CM. Raman mapping of pharmaceuticals. *International Journal of Pharmaceutics*. 2011;417(1):151-162. https://www.sciencedirect.com/science/article/pii/S0378517310009713. doi: 10.1016/j.ijpharm.2010.12.030.

80. Buttler HJ, Ashton L, Bird B, et al. Using raman spectroscopy to characterize biological materials. *Nature Protocols*. 2016;11(4):664-687.

81. Fleischmann M, Hendra PJ, McQuillan AJ. Raman spectra of pyridzne adsorbed at a silver electrode. *Chemical Physics Letters*. 1974;26(2):163-166.

82. Schlücker S. Surface-Enhanced raman spectroscopy: Concepts and chemical applications. *Angewandte Chemie International Edition*. 2014;53(19):4756-4795. https://onlinelibrary.wiley.com/doi/abs/10.1002/anie.201205748. doi: 10.1002/anie.201205748.

83. Cailletaud J, De Bleye C, Dumont E, et al. Critical review of surface-enhanced raman spectroscopy applications in the pharmaceutical field. *Journal of Pharmaceutical and Biomedical Analysis*. 2018;147:458-472. https://www.sciencedirect.com/science/article/pii/S0731708517311378. doi: 10.1016/j.jpba.2017.06.056.

84. Lombardi JR, Birke RL, Lu T, Xu J. Charge-transfer theory of surface enhanced raman spectroscopy: Herzberg–Teller contributions. *The Journal of Chemical Physics*. 1986;84(8):4174-4180. doi: 10.1063/1.450037.

85. Dieringer JA, McFarland AD, Shah NC, et al. Surface enhanced raman spectroscopy: New materials, concepts, characterization tools, and applications. *Faraday discussions*. 2006;132:9. https://www.ncbi.nlm.nih.gov/pubmed/16833104.

86. Zhang Z. *Investigate the interactions between silver nanoparticles and leafy vegetables using surface-enhanced raman spectroscopic mapping technique.* University of Massachusetts Amherst; 2019.

87. Craig AP, Franca AS, Irudayaraj J. Surface-enhanced raman spectroscopy applied to food safety. *Annual Review of Food Science and Technology*. 2013;4(1):369-380. https://www.ncbi.nlm.nih.gov/pubmed/23297774. doi: 10.1146/annurev-food-022811-101227.

88. Li L, Hutter T, Steiner U, Mahajan S. Single molecule SERS and detection of biomolecules with a single gold nanoparticle on a mirror junction. *Analyst*. 2013;138:4574-4578.

89. Perets EA, Indrasekara, A. S. D. S., Kurmis A, Atlasevich N, Fabris L, Arslanoglu J. Carboxy-terminated immuno-SERS tags overcome non-specific aggregation for the robust detection and localization of organic media in artworks. *Analyst*. 2015;140:5971-5980.

90. Chen H, Wang C, Zhang Z, He L. Combining headspace solid-phase microextraction and surface-enhanced raman spectroscopy to detect the pesticide fonofos in apple juice. *Journal of food protection*. 2018;81(7):1087-1092. https://www.ncbi.nlm.nih.gov/pubmed/29897273. doi: 10.4315/0362-028X.JFP-17-505.

91. Gao S, Pearson B, He L. Mapping bacteria on filter membranes, an innovative SERS approach. *Journal of Microbiological Methods*. 2018;147:69-75. https://www.sciencedirect.com/science/article/pii/S0167701218301957. doi: 10.1016/j.mimet.2018.03.005.

92. Zhang Z, Han X, Wang Z, et al. A live bacteria SERS platform for the in situ monitoring of nitric oxide release from a single MRSA. *Chemical communications (Cambridge, England)*. 2018;54(51):7022-7025. https://www.ncbi.nlm.nih.gov/pubmed/29873354. doi: 10.1039/C8CC02855A.

93. Wang CM, Roy PK, Juluri BK, Chattopadhyay S. A SERS tattoo for in situ, ex situ, and multiplexed detection of toxic food additives. *Sensors & Actuators: B. Chemical*. 2018;261:218-225. https://www.sciencedirect.com/science/article/pii/S092540051830162X. doi: 10.1016/j.snb.2018.01.146.

94. Jiang Y, Sun D, Pu H, Wei W. Surface enhanced raman spectroscopy (SERS): A novel reliable technique for rapid detection of common harmful chemical residues. *Trends in food science & technology*. 2015;75:10-22.

95. Yang T, Wang P, Gao H, He L. Surface-enhanced raman spectroscopy: A tool for all classes of food contaminants. *Reference Module in Food Science*. 2017.

96. Lin S, Reppert J, Hu Q, et al. Uptake, translocation, and transmission of carbon nanomaterials in rice plants. *Small*. 2009;5(10):1128-1132. https://onlinelibrary.wiley.com/doi/abs/10.1002/smll.200801556. doi: 10.1002/smll.200801556.

97. Li Y, Church JS. Raman spectroscopy in the analysis of food and pharmaceutical nanomaterials. *Journal of Food and Drug Analysis*. 2014;22(1):29-48. https://www.sciencedirect.com/science/article/pii/S1021949814000040. doi: 10.1016/j.jfda.2014.01.003.

98. Guo H, Xing B, Hamlet LC, Chica A, He L. Surface-enhanced raman scattering detection of silver nanoparticles in environmental and biological samples. *Science of the Total Environment*. 2016;554-555:246-252. https://www.sciencedirect.com/science/article/pii/S0048969716302947. doi: 10.1016/j.scitotenv.2016.02.084.

99. Wei C, Li M, Zhao X. Surface-enhanced raman scattering (SERS) with silver nano substrates synthesized by microwave for rapid detection of foodborne pathogens. *Frontiers in microbiology*. 2018;9:2857. https://www.ncbi.nlm.nih.gov/pubmed/30619101. doi: 10.3389/fmicb.2018.02857.

100. Pang S, Yang T, He L. Review of surface enhanced raman spectroscopic (SERS) detection of synthetic chemical pesticides. *Trends in Analytical Chemistry*. 2016;85:73-82. https://www.sciencedirect.com/science/article/pii/S0165993616300218. doi: 10.1016/j.trac.2016.06.017.

101. Dies H, Siampani M, Escobedo C, Docoslis A. Direct detection of toxic contaminants in minimally processed food products using dendritic surface-enhanced raman scattering substrates. *Sensors (Basel, Switzerland)*. 2018;18(8):2726. https://www.ncbi.nlm.nih.gov/pubmed/30126248. doi: 10.3390/s18082726.

102. Alyami A, Quinn AJ, Iacopino D. Flexible and transparent surface enhanced raman scattering (SERS)-active ag NPs/PDMS composites for in-situ detection of food

contaminants. *Talanta*. 2019;201:58-64. https://www.sciencedirect.com/science/article/pii/S0039914019303832. doi: 10.1016/j.talanta.2019.03.115.

103. Mosier-Boss PA. Review of SERS substrates for chemical sensing. *Nanomaterials (Basel, Switzerland)*. 2017;7(6):142. https://www.ncbi.nlm.nih.gov/pubmed/28594385. doi: 10.3390/nano7060142.

104. Israelsen ND, Hanson C, Vargis E. Nanoparticle properties and synthesis effects on surface-enhanced raman scattering enhancement factor: An introduction. *TheScientificWorldJournal*. 2015;2015:124582-12. https://www.ncbi.nlm.nih.gov/pubmed/25884017. doi: 10.1155/2015/124582.

105. Frank O, Zukalova M, Laskova B, Kurti J, Koltani J, Kavan L. Raman spectra of titanium dioxide (anatase, rutile) with identified oxygen isotopes (16,17,18). *Physical Chemistry Chemical Physics*. 2012;14:4567–14572.

106. Baia M, Melinte G, Barbu-Tudoran L, et al. Highly porous nanocomposites based on TiO_2-noble metal particles for sensitive detection of water pollutants by SERS. *Journal of Physics: Conference Series*. 2011;304:012059. http://iopscience.iop.org/1742-6596/304/1/012059. doi: 10.1088/1742-6596/304/1/012059.

107. Wang Y, Yan C, Chen L, Zhang Y, Yang J. Controllable charge transfer in ag-TiO_2 composite structure for SERS application. *Nanomaterials (Basel, Switzerland)*. 2017;7(7):159. https://www.ncbi.nlm.nih.gov/pubmed/28657599. doi: 10.3390/nano7070159.

108. Skoupá V, Jeništová A, Setnička V, Matějka P. Role of TiO_2 nanoparticles and UV irradiation in the enhancement of SERS spectra to improve levamisole and cocaine detection on au substrates. *Langmuir*. 2019;35(13):4540-4547. https://search.proquest.com/docview/2188979680. doi: 10.1021/acs.langmuir.9b00358.

109. Yang L, Gong M, Jiang X, et al. Investigation on SERS of different phase structure TiO_2 nanoparticles. *Journal of Raman Spectroscopy*. 2015;46(3):287-292. https://onlinelibrary.wiley.com/doi/abs/10.1002/jrs.4645. doi: 10.1002/jrs.4645.

110. Fan M, Andrade GFS, Brolo AG. A review on the fabrication of substrates for surface enhanced raman spectroscopy and their applications in analytical chemistry. *Analytica Chimica Acta*. 2011;693(1):7-25. https://www.sciencedirect.com/science/article/pii/S0003267011003151. doi: 10.1016/j.aca.2011.03.002.

111. Gao H, Xing B, White J, Mukharjee A, He L. Ultra-sensitive determination of silver nanoparticles by surface-enhanced raman spectroscopy (SERS) after hydrophobizationmediated extraction. *Analyst*. 2016;141(18):5261-5264.

112. Guo H, Zhang Z, Xing B, et al. Analysis of silver nanoparticles in antimicrobial products using surface-enhanced raman spectroscopy (SERS). *Environmental Science & Technology*. 1900;49(7):4317-4324. http://dx.doi.org/10.1021/acs.est.5b00370. doi: 10.1021/acs.est.5b00370.

113. Zhang Z, Guo H, Carlisle T, et al. Evaluation of postharvest washing on removal of silver nanoparticles (AgNPs) from spinach leaves. *Journal of Agricultural and Food Chemistry*. 2016;64(37):6916-6922. http://dx.doi.org/10.1021/acs.jafc.6b02705. doi: 10.1021/acs.jafc.6b02705.

114. Gao H, He L, Xing B. Application of surface-enhanced raman spectroscopy in the analysis of nanoparticles in the environment. *Environmental Science: Nano*. 2017;4(11):2093-2107.

115. Nia MH, Rezaei-Tavirani M, Nikoofar AR, et al. Stabilizing and dispersing methods of TiO_2 nanoparticles in biological studies. *Journal of Paramedical Sciences*. 2015;6(2):96-105.

116. Huijun He Yan Cheng Chunping Yang Guangming Zeng Canyao Zhu Zhou Yan. Influences of anion concentration and valence on dispersion and aggregation of titanium dioxide nanoparticles in aqueous solutions. *环境科学学报：英文版*. 2017;54(4):135-141. http://lib.cqvip.com/qk/85265X/201704/671978802.html. doi: 10.1016/j.jes.2016.06.009.

117. Qi J, Ye YY, Wu JJ, Wang HT, Li FT. Dispersion and stability of titanium dioxide nanoparticles in aqueous suspension: Effects of ultrasonication and concentration. *Water science and technology: a journal of the International Association on Water Pollution Research*. 2013;67(1):147-151. https://www.ncbi.nlm.nih.gov/pubmed/23128632. doi: 10.2166/wst.2012.545.

118. T. Mazza, E. Barborini, P. Piseri, et al. Raman spectroscopy characterization of TiO_2 rutile nanocrystals. . 2007. http://hdl.handle.net/2434/24183.

119. Zhao B, Cao X, De La Torre-Roche R, et al. A green, facile, and rapid method for microextraction and raman detection of titanium dioxide nanoparticles from milk powder. *RSC Advances*. 2017;7(35):21380-21388. doi: 10.1039/C7RA02520C.

120. Moskovits M. Surface-enhanced raman spectroscopy: A brief retrospective. *Journal of Raman Spectroscopy*. 2005;36(6-7):485-496. https://onlinelibrary.wiley.com/doi/abs/10.1002/jrs.1362. doi: 10.1002/jrs.1362.

121. Njoki PN, Lim IS, Mott D, et al. Size correlation of optical and spectroscopic properties for gold nanoparticles. *The Journal of Physical Chemistry C*. 2007;111(40):14664-14669. http://dx.doi.org/10.1021/jp074902z. doi: 10.1021/jp074902z.

122. Jiang J, Jiang J, Oberdörster G, Oberdörster G, Biswas P, Biswas P. Characterization of size, surface charge, and agglomeration state of nanoparticle dispersions for toxicological studies. *J Nanopart Res*. 2009;11(1):77-89. https://search.proquest.com/docview/1112745690. doi: 10.1007/s11051-008-9446-4.

123. McNamee CE, Tsujii Y, Matsumoto M. Physicochemical characterization of an anatase TiO_2 surface and the adsorption of a nonionic surfactant: An atomic force microscopy study. *Langmuir*. 2005;21(24):11283-11288. http://dx.doi.org/10.1021/la0517890. doi: 10.1021/la0517890.

124. Pradhan S, Hedberg J, Blomberg E, Wold S, Odnevall Wallinder I. Effect of sonication on particle dispersion, administered dose and metal release of non-functionalized, non-inert metal nanoparticles. *J Nanopart Res*. 2016;18(9):1-14. https://www.ncbi.nlm.nih.gov/pubmed/27774036. doi: 10.1007/s11051-016-3597-5.

125. Vidmar J, Mila i R, Golja V, Novak S, Š an ar J. Optimization of the procedure for efficient dispersion of titanium dioxide nanoparticles in aqueous samples. *Analytical Methods*. 2016;8(5):1194-121. doi: 10.1039/c5ay03305e.

126. Vanden-Hehir S, Tipping WJ, Lee M, Brunton VG, Williams A, Hulme AN. Raman imaging of nanocarriers for drug delivery. *Nanomaterials (Basel, Switzerland)*. 2019;9(3):341. https://www.ncbi.nlm.nih.gov/pubmed/30832394. doi: 10.3390/nano9030341.

127. Jianwei Qin, Moon S. Kim, Kuanglin Chao, Byoung-kwan Cho. Raman chemical imaging technology for food and agricultural applications. 2017;42(3):170-189. http://kiss.kstudy.com/search/detail_page.asp?key=3545423.

128. Ho C, Jean N, Hogan CA, et al. Rapid identification of pathogenic bacteria using raman spectroscopy and deep learning. *Nature Communications*. 2019;10(1):1-8. https://search.proquest.com/docview/2310645629. doi: 10.1038/s41467-019-12898-9.

129. Gao S. *Development of filter-based SERS mapping methods for rapid identification and detection of bacteria*. University of Massachusetts Amherst; 2019.

130. Peng M, Wei X, Yu Q, Yan P, Chen Y, Guo J. Identification of ceftazidime interaction with bacteria in wastewater treatment by raman spectroscopic mapping. *RSC Advances*. 2019;9(56):32744-32752. doi: 10.1039/C9RA06006E.

131. Michael R, Lenferink A, Vrensen, Gijs F. J. M, Gelpi E, Barraquer RI, Otto C. Hyperspectral raman imaging of neuritic plaques and neurofibrillary tangles in brain tissue from alzheimer's disease patients. *Scientific Reports*. 2017;7(1):1-11. https://search.proquest.com/docview/1964556281. doi: 10.1038/s41598-017-16002-3.

132. Kong K, Kendall C, Stone N, Notingher I. Raman spectroscopy for medical diagnostics — from in-vitro biofluid assays to in-vivo cancer detection. *Advanced Drug*

Delivery Reviews. 2015;89:121-134. https://www.sciencedirect.com/science/article/pii/S0169409X15000447. doi: 10.1016/j.addr.2015.03.009.

133. Ardini M, Huang J, Sánchez CS, et al. Live intracellular biorthogonal imaging by surface enhanced raman spectroscopy using alkyne-silver nanoparticles clusters. *Scientific reports*. 2018;8(1):12652-12. https://www.ncbi.nlm.nih.gov/pubmed/30140073. doi: 10.1038/s41598-018-31165-3.

134. Lindquist NC, de Albuquerque, Carlos Diego L, Sobral-Filho RG, Paci I, Brolo AG. High-speed imaging of surface-enhanced raman scattering fluctuations from individual nanoparticles. *Nature Nanotechnology*. 2019;14(10):981-987. doi: 10.1038/s41565-019-0535-6.

135. Tuschel D. The effect of microscope objectives on the raman spectra of crystals. *Spectroscopy*. 2017;32(9).

136. Vandenabeele P. Raman instrumentation. In: Vandenabeele P, ed. *Practical raman spectroscopy an introduction.* John Wiley & Sons Ltd; 2013:61-100.

137. Solís DM, Taboada JM, Obelleiro F, Liz-Marzán LM, García de Abajo, F. Javier. Optimization of nanoparticle-based SERS substrates through large-scale realistic simulations. *ACS Photonics*. 2017;4(2):329-337. http://dx.doi.org/10.1021/acsphotonics.6b00786. doi: 10.1021/acsphotonics.6b00786.

138. Hwang J, Yu J, Kim H, Oh J, Choi S. Food additive titanium dioxide and its fate in commercial foods. Nanomaterials (Basel, Switzerland). 2019;9(8):1175. https://search.datacite.org/works/10.3390/nano9081175. doi: 10.3390/nano9081175.

139. Geiss O, Ponti J, Senaldi C, et al. Characterisation of food grade titania with respect to nanoparticle content in pristine additives and in their related food products. Food additives & contaminants. Part A, Chemistry, analysis, control, exposure & risk assessment. 2019;37(2): 239-253.

https://search.datacite.org/works/10.1080/19440049.2019.1695067. doi: 10.1080/19440049.2019.1695067.

140. Candás-Zapico S, Kutscher DJ, Montes-Bayón M, Bettmer J. Single particle analysis of TiO_2 in candy products using triple quadrupole ICP-MS. Talanta. 2018;180:309-315. http://dx.doi.org/10.1016/j.talanta.2017.12.041. doi: 10.1016/j.talanta.2017.12.041.

141. Rompelberg C, Heringa MB, van Donkersgoed G, et al. Oral intake of added titanium dioxide and its nanofraction from food products, food supplements and toothpaste by the Dutch population. Nanotoxicology. 2016;10(10):1404-

1414. https://search.datacite.org/works/10.1080/17435390.2016.1222457. doi: 10.1080/17435390.2016.1222457

142. Potocnik J. Recommendations on the definition of nanomaterial. Official Journal of the European Union. 2011(L275):38-40. http://dx.doi.org/10.1055/s-0030-1256238. doi: 10.1055/s-0030-1256238